

7. Status of Advanced Tritium Breeder Development for DEMO in the Broader Approach activities in Japan

Tsuyoshi Hoshino, Fumiaki Oikawa and Takeo Nishitani

*Fusion Research and Development Directorate, Japan Atomic Energy Agency,
4002, Oarai, Higashi Ibaraki, Ibaraki, 311-1393, Japan*

DEMO reactors require “⁶Li-enriched ceramic tritium breeders” which have high tritium breeding ratios (TBRs) in the blanket designs of both EU and JA. Both parties have been promoting the development of fabrication technologies of Li₂TiO₃ pebbles and of Li₄SiO₄ pebbles including the reprocessing. However, the fabrication techniques of tritium breeders pebbles have not been established for large quantities. Therefore, these parties launch a collaborative project on scaleable and reliable production routes of advanced tritium breeders.

In addition, this project aims to develop fabrication techniques allowing effective reprocessing of ⁶Li. The development of the production and ⁶Li reprocessing techniques includes preliminary fabrication tests of breeder pebbles, reprocessing of lithium, and suitable out-of-pile characterizations.

The R&D on the fabrication technologies of the advanced tritium breeders and the characterization of developed materials has been started between the EU and Japan in the DEMO R&D of the International Fusion Energy Research Centre (IFERC) project as a part of the Broader Approach activities from 2007 to 2016. The equipment for production of advanced breeder pebbles is planned will be installed in the DEMO R&D building at Rokkasho, Japan. The design work in this facility was carried out. The specifications of the pebble production apparatuses and related equipment in this facility were fixed, and the basic data of these apparatuses was obtained. In this design work, the preliminary investigations of the dissolution and purification process of tritium breeders were carried out.

From the results of the preliminary investigations, lithium resources of 90% above were recovered by the aqueous dissolving methods using HNO₃ and H₂O₂. The removal efficiency of ⁶⁰Co by the addition in the dissolved solutions of lithium ceramics were 97-99.9% above using activated carbon impregnated with 8-hydroxyquinolinol. In this report, preparation status of the equipments and preliminary investigation results will be present.

Corresponding Author:

Fumiaki Oikawa
fumiaki.oikawa@jaea.go.jp
Fusion Research and Development Directorate, Japan Atomic Energy Agency
4002, Oarai, Higashi Ibaraki, Ibaraki, 311-1393, Japan
+81-29-266-7417(Tel), +81-29-266-7741(Fax)

Status of Advanced Tritium Breeder Development in the Broader Approach activities in Japan

Tsuyoshi HOSHINO, Fumiaki OIKAWA and Takeo NISHITANI
Japan Atomic Energy Agency

©2008 JAEA 

Introduction

DEMO reactors require “ ^6Li -enriched ceramic tritium breeders” which have high tritium breeding ratios (TBRs) in the blanket designs of both EU and JA. Both parties have been promoting the **development of fabrication technologies of Li_2TiO_3 pebbles** and of Li_4SiO_4 pebbles including the reprocessing.

However, the fabrication techniques of tritium breeders pebbles have not been established for large quantities. Therefore, these parties launch a **collaborative project on scaleable and reliable production routes of advanced tritium breeders**.

In addition, this project aims to develop fabrication techniques allowing **effective reprocessing** of ^6Li .

Introduction (cont.)

The R&D on the fabrication technologies of the advanced tritium breeders and the characterization of developed materials have been started between the EU and JA in the DEMO R&D of the [International Fusion Energy Research Centre \(IFERC\)](#) project as a part of the [Broader Approach](#) activities from 2007 to 2016.

This study consists of main two tasks.

Task-1 : Preparation of test [equipment](#) at the Rokkasho site

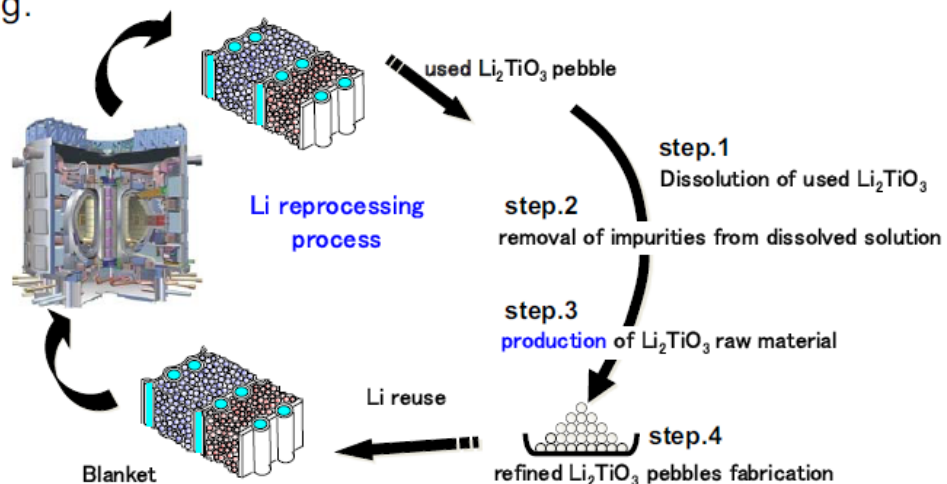
Task-2 : [Production](#) of advanced breeder pebbles and the [characterization](#) of the pebbles on physical, chemical, mechanical and other properties.

Studies on [reprocessing and re-use](#) of tritium breeder materials.

Objective

Tritium breeder is one of the most important functional materials in the DEMO blanket. R&D is planned on the fabrication technologies of the tritium breeder materials and on the [characterization](#) of developed materials as a DEMO R&D activity.

Therefore, [detail design works of the equipment](#) for [production](#) of advanced breeder pebbles carried out for the design of the DEMO R&D building.



Schedule of JA

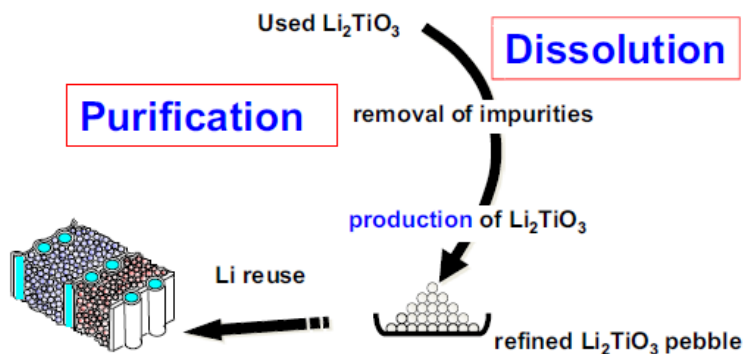
* Phase-1: Preparation Phase

* Phase-2: Full-scale R&D and Summary Phase

Items	Year	2007	2008	2009	2010	2011	2012	2013	2014	2015	2016	
		← Phase-1 →			← Phase-2 →							
Preparation of Test Equipment (Task-1)	- Assessment	█										
	- Preparation of Equipment		█	█	█	█						
Fabrication and Characterization (Task-2)	Pebble Fabrication (Task-2-1)		█	█	█	█	█	█	█	█	█	
	Characterization (Task-2-2)		█	█	█	█	█	█	█	█	█	
	Reprocessing Studies (Task-2-3)		█	█	█	█	█	█	█	█	█	

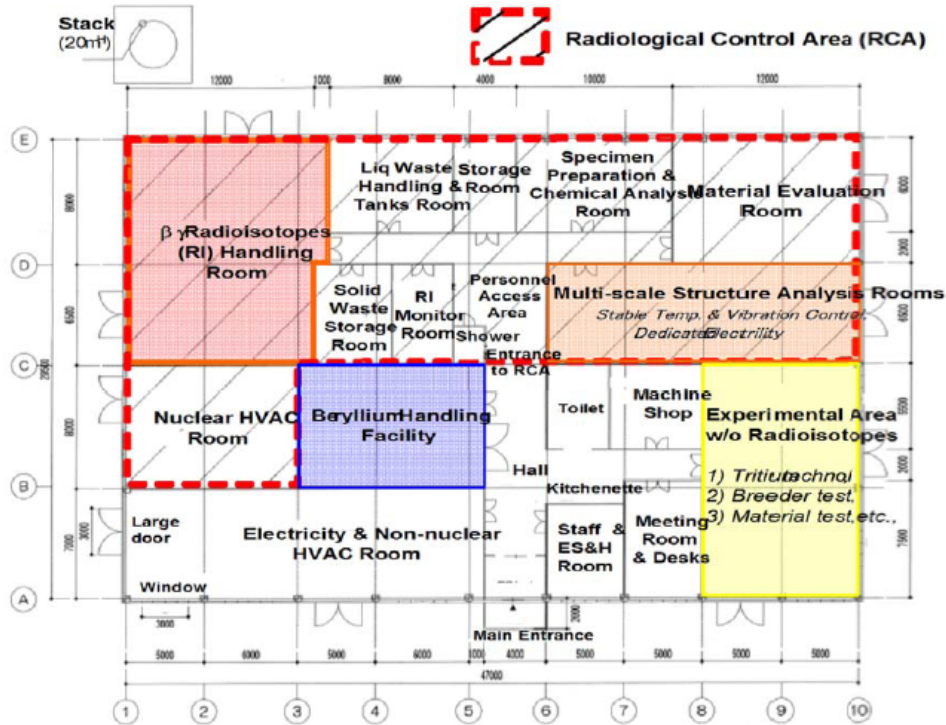
Status

- 1) Preparation of equipment:
 - Preparatory design was carried out, prior to fabrication of the breeder pebble fabrication apparatus and related equipment;
- 2) Preliminary investigations to examine the specifications of the equipment was carried out:
 - in particular, for the dissolution and purification processes.



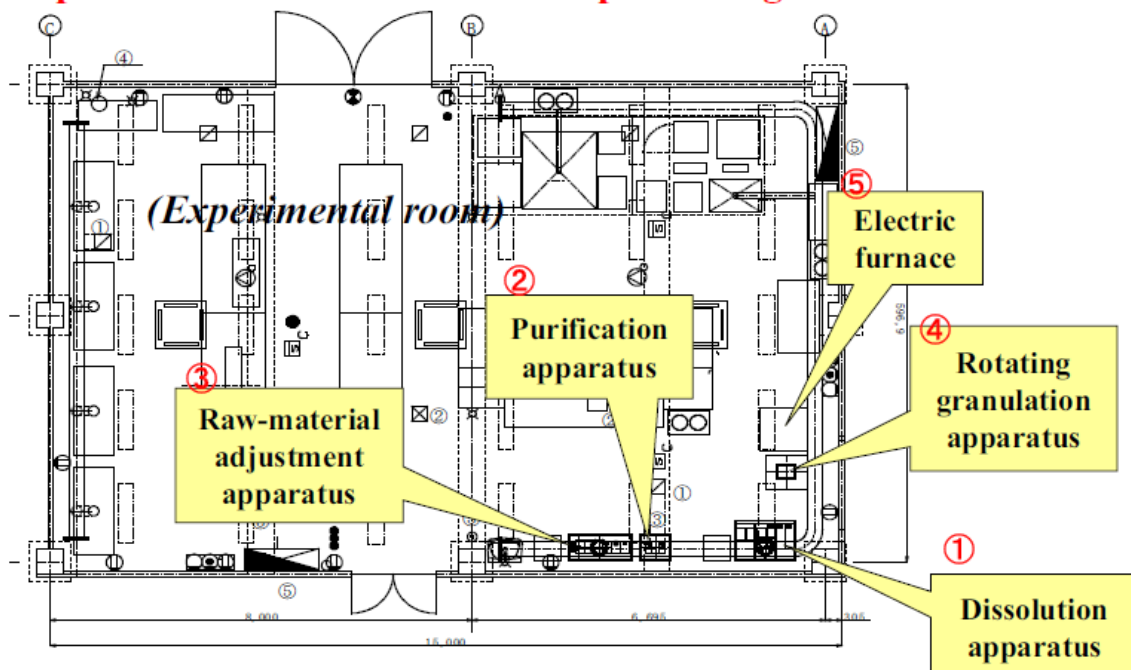
DEMO R&D building

[Conceptual arrangement in 2008]

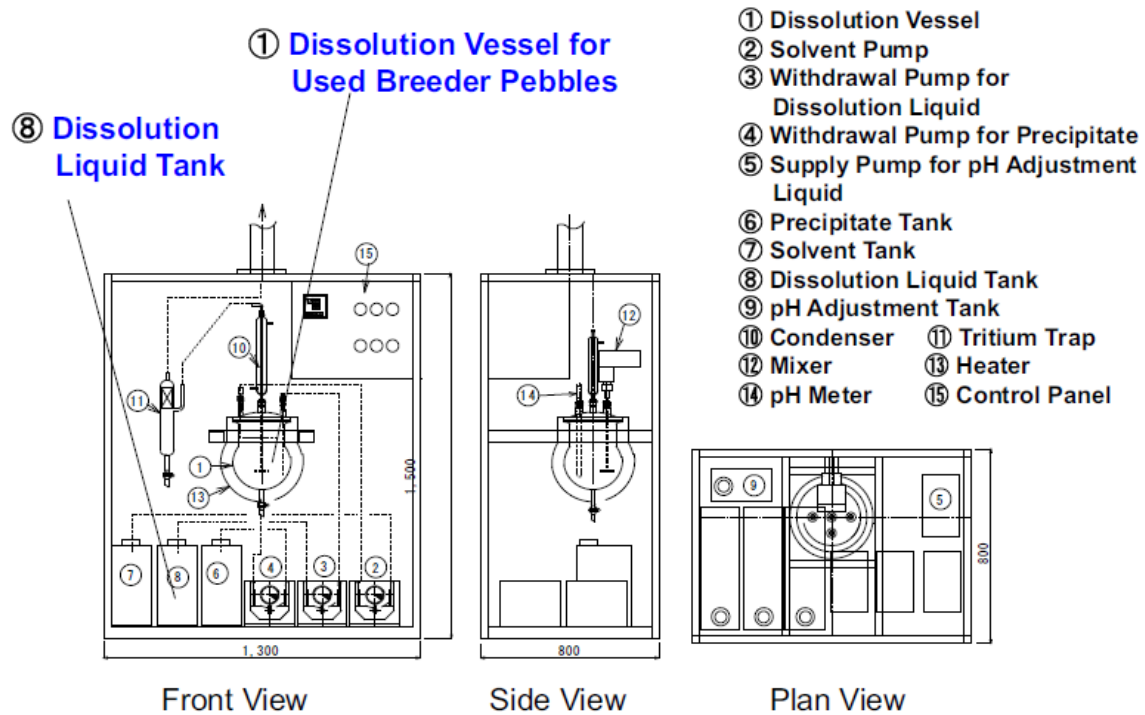


Plan View of the Experimental Room for Breeder R&D

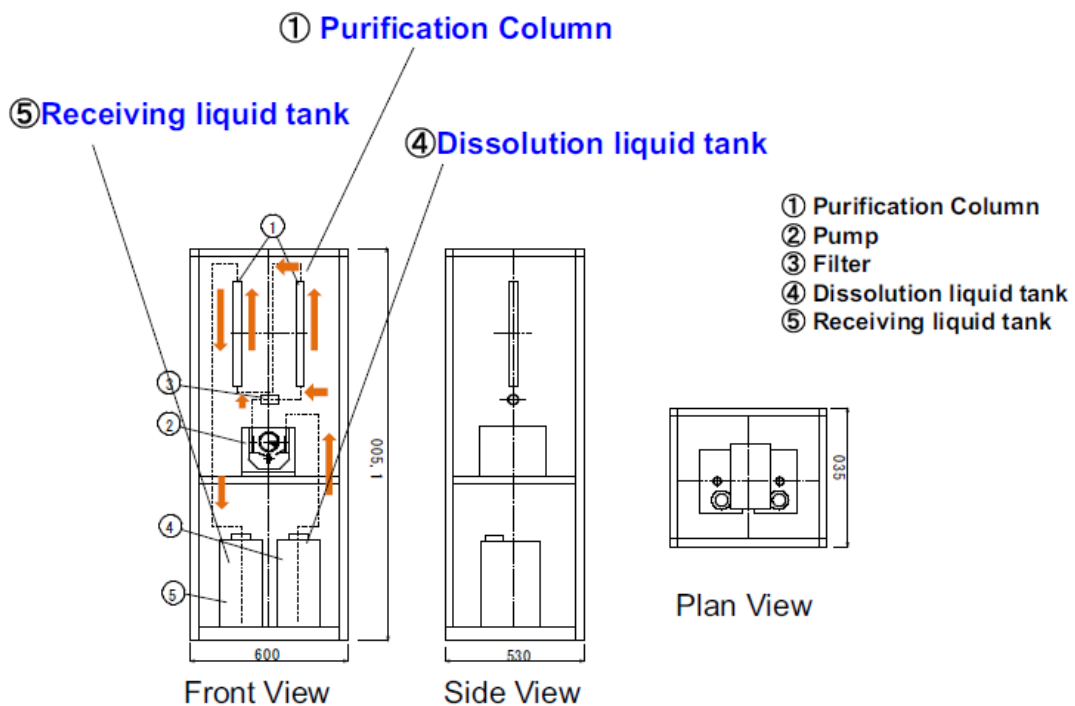
Specification of fabrication and processing devices were fixed.



Conceptual Design of Dissolution Apparatus



Conceptual Design of Purification Apparatus



Preliminary Investigations (Dissolution, Purification)

Dissolution



Li₂O
(Solvent: HNO₃)



Li₂TiO₃
(Solvent: H₂O₂ + HNO₃)

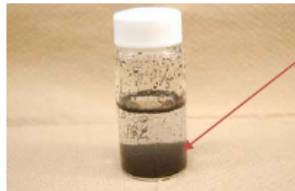
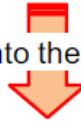


Li₄SiO₄
(Solvent: HNO₃)

- 1) Li₂O and Li₄SiO₄ were dissolved completely by HNO₃.
- 2) Li₂TO₃ was very difficult to dissolve only by HNO₃.
- 3) In the case of Li₂TiO₃, creamy white precipitates (titanium oxide) were observed using H₂O₂ and HNO₃ solvent.

Purification

⁶⁰Co added into the solutions for purification test



Activated carbon impregnated with 8-hydroxyquinolinol was selected as absorption of ⁶⁰Co.

- 4) ⁶⁰Co in the solution adsorbed with activated carbon impregnated with 8-oxyquinolinol.

Results of Preliminary Investigations

Li ceramics	Dissolving condition	Dissolving yields of Li	Removal efficiency of impurity; ⁶⁰ Co
Li ₂ O	HNO ₃ at RT	96-100%	99.8%
Li ₂ TiO ₃	H ₂ O ₂ + HNO ₃ at RT	91 ± 3%	99.9%
Li ₄ SiO ₄	HNO ₃ In boiling	93 ± 4%	97.6%

- 1) Lithium resources of 90% above were recovered by the aqueous dissolving methods using HNO₃ and HNO₃+H₂O₂.
- 2) Removal efficiency of ⁶⁰Co by the addition in the dissolved solutions of lithium ceramics were 97-99.9% above using activated carbon impregnated with 8-oxyquinolinol.

Conclusions

- 1) Design of breeder pebble fabrication apparatus and related equipment was carried out.
- 2) Preliminary investigations on the dissolution and purification steps of the pebble fabrication process were carried out.



- 1) Implementation of **equipment preparation** for breeder pebble fabrication and characterization will be started.
- 2) Preceding studies will be started in the following three tasks:
 - 2-1) **Production** of advanced breeder pebbles.
 - 2-2) **Characterization** of the developed materials.
 - 2-3) Studies related to **reprocessing and re-use**.

Acknowledgement

This study has been prepared as an account of work assigned to the Japanese Implementing Agency under the Procurement Number IFERC-T5PA01-JA within the "Broader Approach Agreement" between the Government of Japan and the European Atomic Energy Community.

8. Evaluation of the First Cycles of the High Dose Li-ceramic Irradiation in HFR

A.V. Fedorov, A.J. Magielsen, J.B.J. Hegeman

NRG, Petten, The Netherlands

As a part of the European programme for the development of the Helium Cooled Pebble Bed a high dose irradiation experiment HICU is in progress. HICU is an acronym for **H**igh neutron fluence **I**rradiation of pebble **st**a**C**ks for **f**usion. The objective of the HICU project is to investigate the impact of neutron spectrum and influence of constraint conditions on the thermo-mechanical behaviour of ceramic breeder pebble beds. The Cd-shielding is used to tailor the neutron spectrum in order to achieve the DEMO relevant dpa/He ratio.

Two types of Li-ceramic pebbles are irradiated: orthosilicate, Li_4SiO_4 (OSi) and metatitanate, Li_2TiO_3 (MTi). The OSi pebbles are supplied by FZK, Germany, the MTi pebbles are supplied partly by JEARI and CEA Saclay. In total 45 pebble beds are under irradiation. The pebbles are contained in platinum tubes. The irradiation temperatures are chosen in the range of 600 °C to 850°C.

The irradiation has started in February 2008 and is scheduled to continue for approximately 4 years. This work presents the analysis of the in-pile data acquired in the first cycles of the irradiation.

Corresponding Author:

A.V. Fedorov

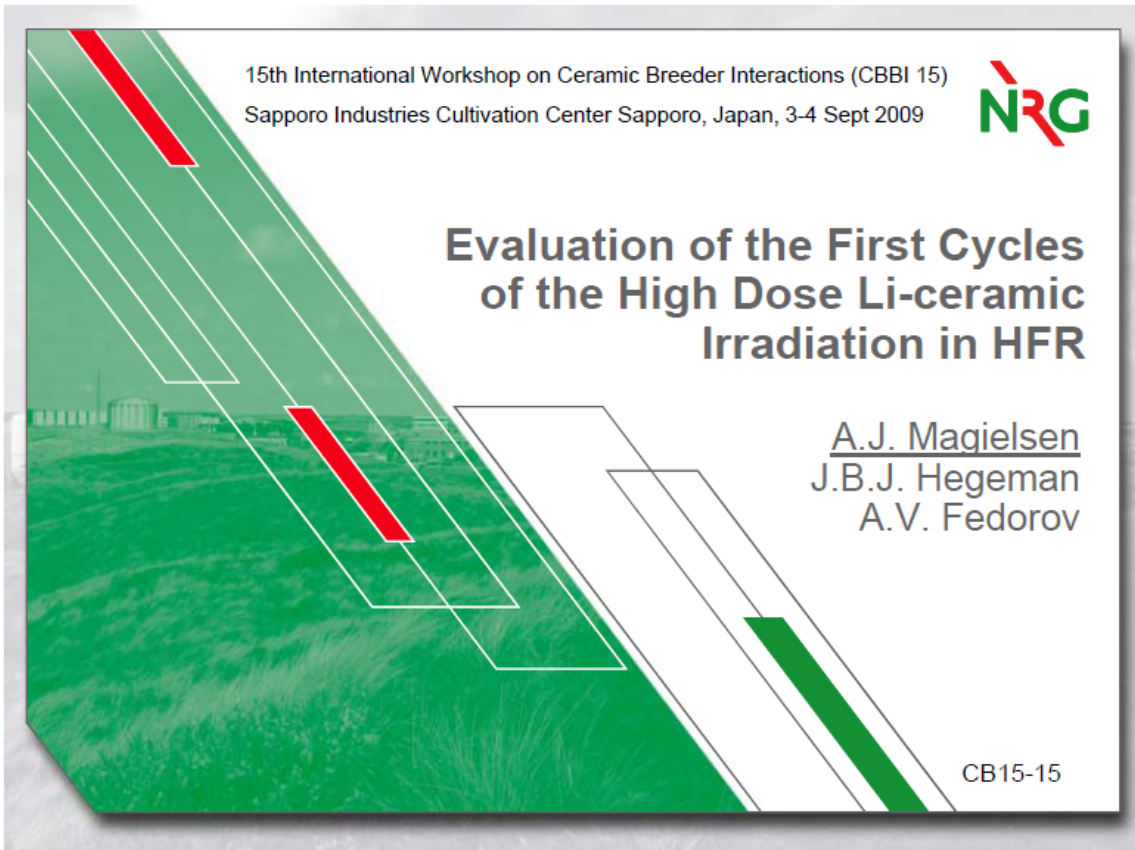
fedorov@nrg.eu

The Nuclear Research & consultancy Group (NRG)

Petten, North Holland, 1755 ZG Petten, The Netherlands

T +31 (0) 224 568034

F +31 (0) 224 568608



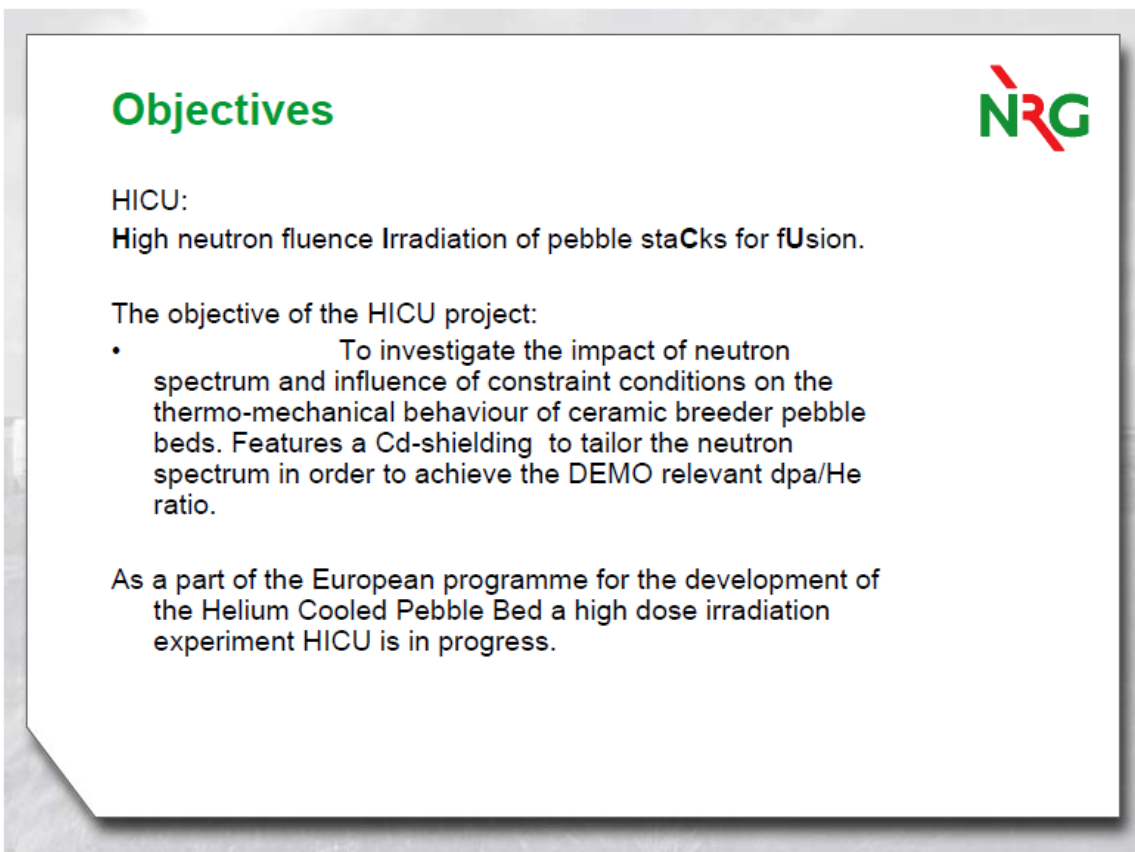
15th International Workshop on Ceramic Breeder Interactions (CBBI 15)
Sapporo Industries Cultivation Center Sapporo, Japan, 3-4 Sept 2009

NRG

Evaluation of the First Cycles of the High Dose Li-ceramic Irradiation in HFR

A.J. Magielsen
J.B.J. Hegeman
A.V. Fedorov

CB15-15



Objectives

NRG

HICU:
High neutron fluence Irradiation of pebble staCks for fUision.

The objective of the HICU project:

- To investigate the impact of neutron spectrum and influence of constraint conditions on the thermo-mechanical behaviour of ceramic breeder pebble beds. Features a Cd-shielding to tailor the neutron spectrum in order to achieve the DEMO relevant dpa/He ratio.

As a part of the European programme for the development of the Helium Cooled Pebble Bed a high dose irradiation experiment HICU is in progress.

Irradiation parameters



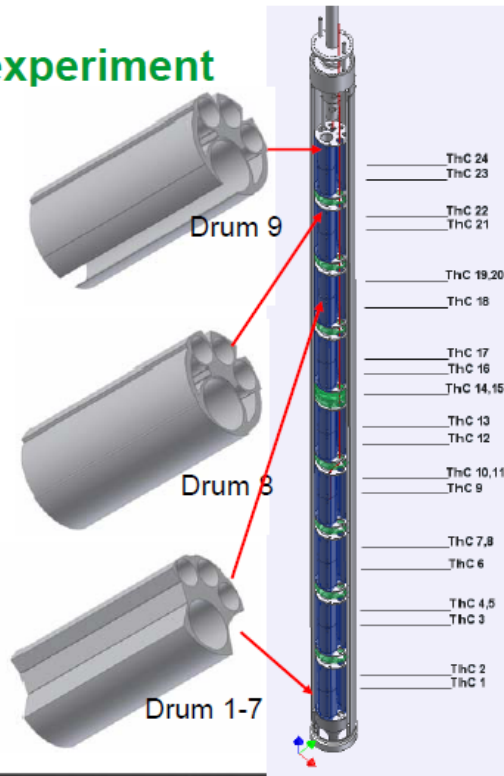
Lithium isotope compositions and spectrum tailoring measures are chosen so as to obtain in DEMO relevant dpa/burnup-ratios (~6 dpa/%) as well as (using higher ^6Li -enrichment) - DEMO relevant burn-ups (10-15 %).

The test matrix includes:

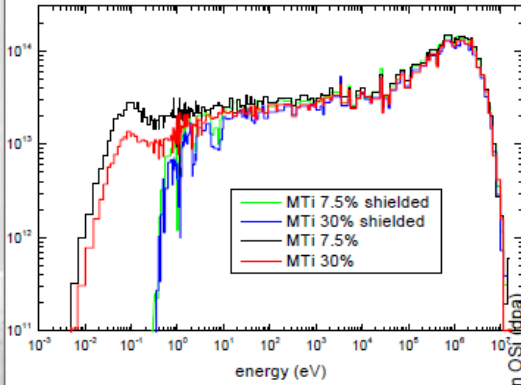
- OSi, various ^6Li enrichments, Annealed and as-received
- MTi, various ^6Li enrichments, pebbles sizes, porosity, grain sizes
- JP Mti, 31 % enriched in ^6Li , various TiO_2 levels

	HICU
Fluence ($E > 0.1 \text{ MeV } 10^{26} \text{ n/m}^2$)	1.5
Fluence ($E > 1 \text{ MeV } 10^{26} \text{ n/m}^2$)	0.7
^6Li enrichments Li_4SiO_4 (%)	0.06, 7.5, 20
^6Li enrichments Li_2TiO_3 (%)	0.06, 11, 30
^6Li Burnup (%)	0.74 - 13
Neutron damage (dpa)	20-25
Temperatures ($^{\circ}\text{C}$)	600-650 750-800

Design of HICU experiment

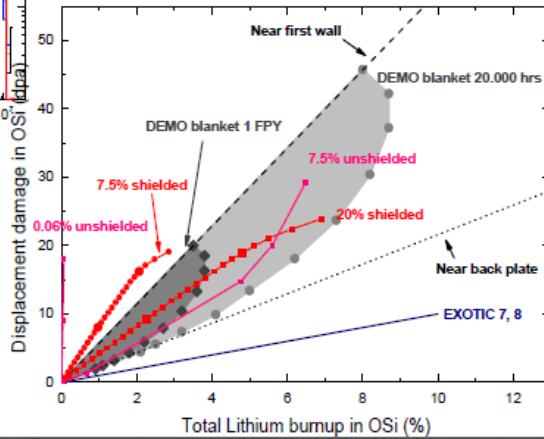


Tailoring of neutron spectrum

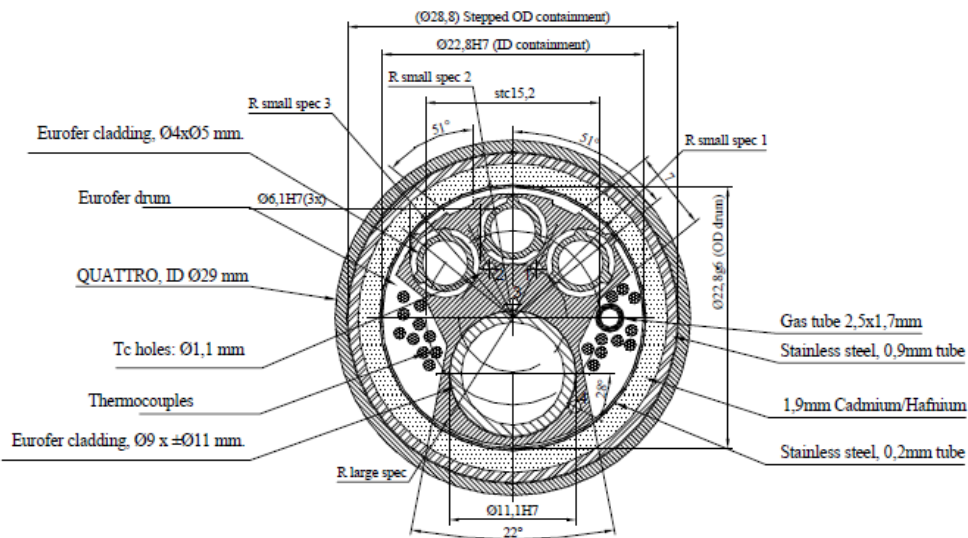


USE OF Cd SHIELD

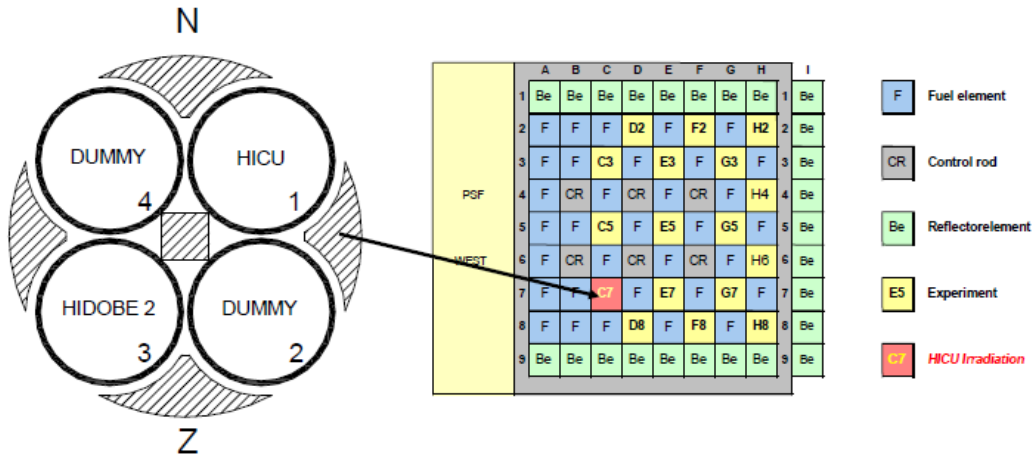
Objective: Absorption of thermal neutrons to tailor spectrum and reduce n, α reaction to achieve DEMO relevant dpa/burnup ratio



Cross section drum 1-7



In core loading of experiment

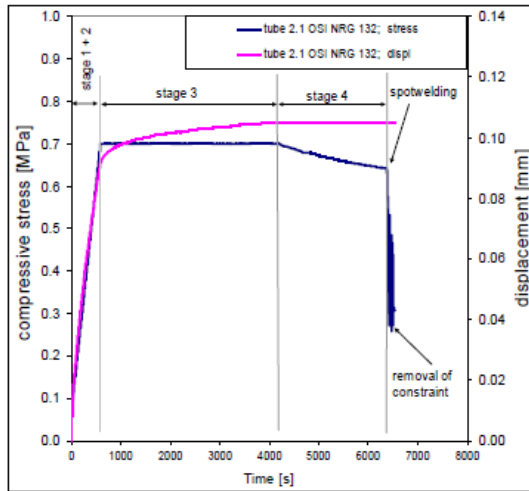


HICU Test Matrix



Material	Supplier	NRG-ID	High Constraint		Low Constraint		Total
			High T	Low T	High T	Low T	
OSI-20	OSI	20 EU-FZK NRG-126	2		1	1	4
OSI-7.5	OSI	7.5 EU-FZK NRG-125	2	1	1	1	5
OSI-7.5+	OSI	7.5 EU-FZK NRG-129	1				1
OSI-0.06	OSI	0.06 EU-FZK NRG-124			1	1	2
			5	1	3	3	12
MTI-30	MTi	30 EU-CEA NRG-120	2		1	1	4
MTI-11	MTi	11 EU-CEA NRG-119	2	1	1	1	5
MTI-0.06	MTi	0.06 EU-CEA NRG-118			1	1	2
MTI-ref	Mti	7.5 EU-CEA NRG-121			1	1	2
MTI-ref+	MTi	7.5 EU-CEA NRG-122	1		1		2
MTI-ref++	MTi	7.5 EU-CEA NRG-123			1	1	2
MTI-ref+++	MTi	7.5 EU-CEA NRG-130	1	1			2
MTI-ref++++	MTi	30 EU-CEA NRG-131			1	1	2
			6	2	7	6	21
MTI-31	MTi	31 JAERI NRG-115	1		1	1	3
MTI-31-5%	Mti-5%	31 JAERI NRG-116	1	1	1	1	4
MTI-31-10%	Mti-10%	31 JAERI NRG-117	1		1	1	3
MTI-7.5	Mti	7.5 JAERI NRG-127			1		1
			3	1	4	3	11
be-disk	EU-Be						
be-peb	EU-Be	Be			1		
					1	0	1
Total			14	4	15	12	45

Pebble bed packing of large drums to define thermomechanical loads



NRG-117 mti-31-10% (above)
tube 2.5 NRG-124 osi-0.06

Pre-stressing of tube 2.1, showing stress and displacement as function of time

Changes on locations of the ceramic pebble stacks

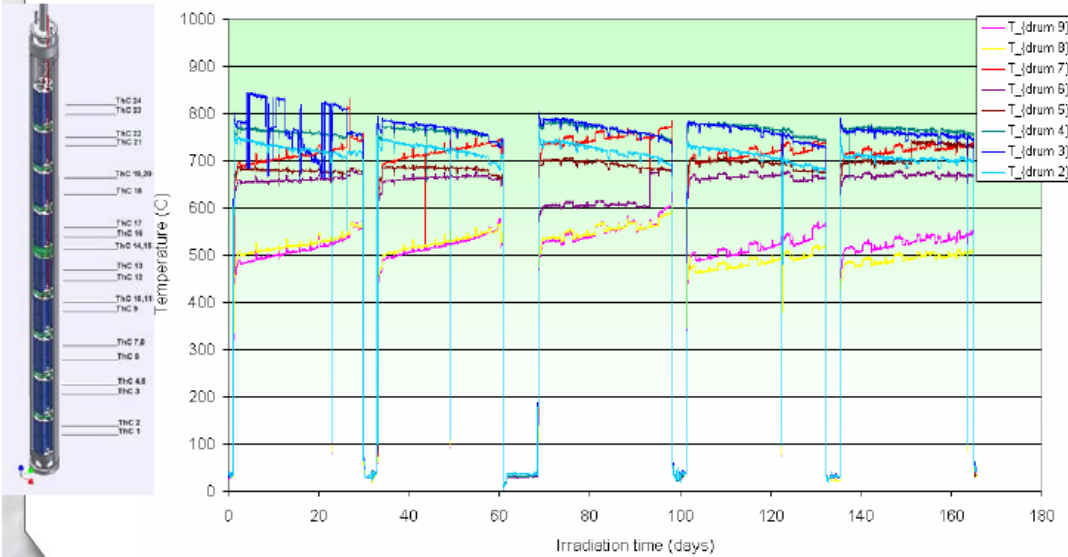


		5.1	mti-ref+++	NRG-130 EU-CEA	800-850	9.4
DRUM 5	1	5.2	osi-7.5+	NRG-129 EU-FZK	800-850	12.3
		5.3	osi-20	NRG-126 EU-FZK	800-850	24.9
		5.4	mti-30	NRG-120 EU-CEA	800-850	28.3
		4.3	mti-30	NRG-120 EU-CEA	800-850	34.7
DRUM 6	1	6.1	osi-7.5	NRG-125 EU-FZK	800-850	13.0
		6.2	osi-7.5	NRG-125 EU-FZK	800-850	13.0
		6.3	be-peb	0 EU-Be	800-850	0.0
		4.4	mti-0.06	NRG-118 EU-CEA	800-850	1.4
DRUM 7	1	6.5	osi-0.06	NRG-124 EU-FZK	800-850	3.7
		7.1	mti-11	NRG-119 EU-CEA	800-850	12.8
		7.2	mti-11	NRG-119 EU-CEA	800-850	12.2
		7.3	mti-ref	NRG-121 EU-CEA	800-850	9.8
		7.4	mti-11	NRG-119 EU-CEA	800-850	13.0
DRUM 8	1	7.5	mti-7.5	NRG-127 JAERI	800-850	8.8
		8.1	osi-20	NRG-126 EU-FZK	800-850	20.6
		8.2	osi-20	NRG-126 EU-FZK	800-850	19.4
		9.4	mti-ref++	NRG-123 EU-CEA	650	6.8
		8.4	osi-7.5	NRG-125 EU-FZK	650	11.7
DRUM 9	1	8.5	osi-0.06	NRG-124 EU-FZK	650	3.2
		3.2	mti-31-5%	NRG-116 JAERI	800-850	24.7
		3.1	mti-31	NRG-115 JAERI	800-850	19.6
		8.3	mti-ref+++	NRG-131 EU-CEA	650	27.3
		9.5	osi-20	NRG-126 EU-FZK	650	22.5
		2.3	mti-30	NRG-120 EU-CEA	650	21.9

Absolute in-pile temperature levels



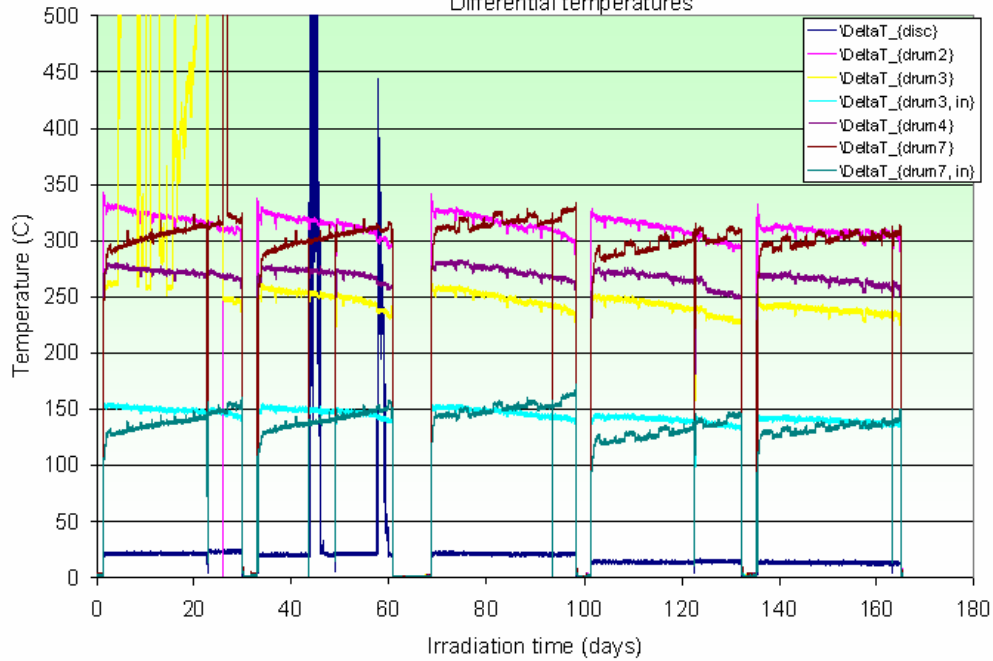
Irradiation from Feb 2008 to July 2008



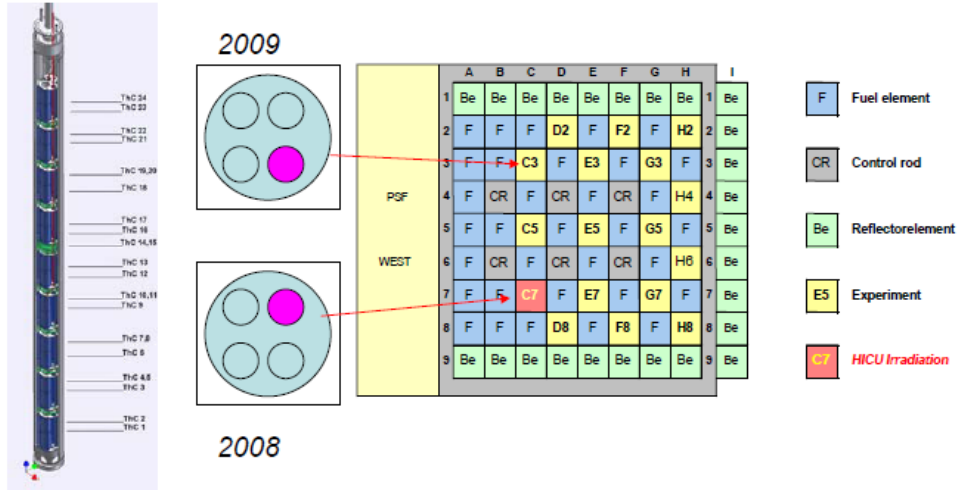
In pile Temperature differences (2008)



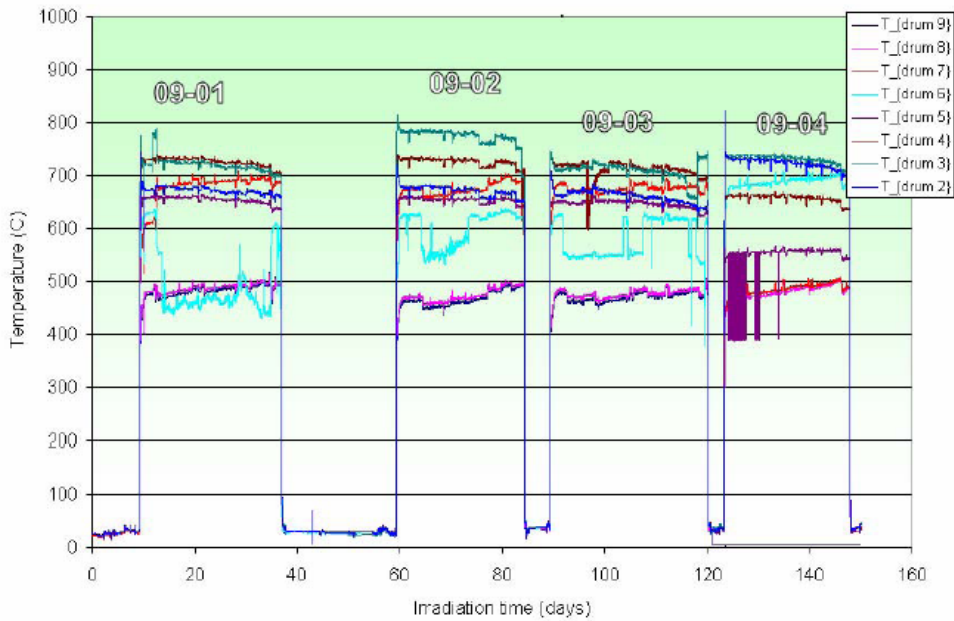
Differential temperatures



In core loading after 2008



Irradiation in 2009



Outlook for further irradiation cycles



Current situation on HFR:

A shut down of HFR for investigation and repair of primary coolant system was performed from half 2008 until begin 2009

The authorities examined together with NRG the possibility to continue operation under defined conditions and survey

NRG can continue the operation under these defined conditions (leak detection system/if no other reactors can take over isotope production)

Repair scheduled for March 2010 then shut down of HFR for five months

Post Irradiation Examination at NRG



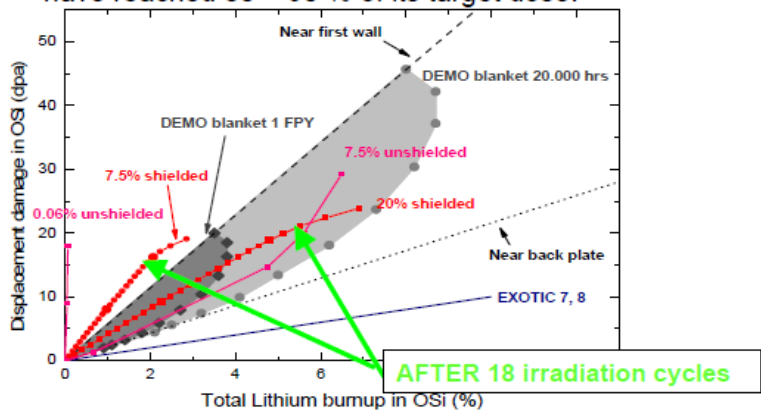
Bed structure	dimensional changes visual+SEM inspection resin impregnation + ceramography pebble-bed thermo-mechanics ? X-ray tomography ?
Pebbles	composition, microstructure swelling, crush load?, annealing studies T-inventory and release Lithium burnup

Outlook for HICU



Additional 6 irradiation cycles for HICU until repair, total of 18 cycles

Before repair of the HFR primary coolant specimens in HICU have reached 80 – 90 % of its target dose.



Outlook for Post Irradiation planning



Option 1:

PIE can be started in 2011 for 100 % target dose (higher uncertainty because of repair HFR)

Option 2:

PIE can be started in 2010 for 80-90 % target dose (lower uncertainty because HICU will be finished before repair)

In any case:

Valuable and very relevant data will come available to the Test blanket materials community

9. IR analysis of the behavior of hydrogen isotopes thermally absorbed in ternary Li oxides

*Kisaburo Azuma, Takuji Oda and Satoru Tanaka
Department of Nuclear Engineering and Management, The University of Tokyo,
Hongo 7-3-1, Bunkyo-ku, Tokyo 113-8656, Japan, azuma@flanker.q.t.u-tokyo.ac.jp*

Abstract

In order to deepen understanding on the behavior of hydrogen isotopes in solid breeding material, infrared absorption of O-D stretching mode and migration energies of hydrogen was analyzed in LiNbO₃. Deuterium was introduced into samples by means of thermal absorption in D₂O atmosphere at 1073 K. DFT calculation indicates that H⁺ diffuses via interstitial sites as well as Li substitutional sites.

Keywords: LiNbO₃, hydrogen isotopes, diffusion, FT-IR, TDS, DFT

1. Introduction

Ternary Li oxides are candidate solid breeding materials for a fusion reactor. Because the blanket system is required to release tritium quickly, it is necessary to understand the behavior of hydrogen isotopes in the breeding material. In general, defects influence hydrogen isotope behavior. For example, the various existing states of deuterium are observed in LiAlO₂ irradiated by D₂⁺ ion [1]. However, the interaction between hydrogen isotope and defects in ternary Li oxides is not understood sufficiently.

We have recently conducted IR absorption analyses of LiTaO₃/LiNbO₃ after 300 keV D⁺ irradiation to clarify the existing states of hydrogen isotopes interacting with radiation defects [2]. Two O-D stretching vibration peaks of -OD[•] in the bulk were observed and the one at 2615 cm⁻¹ was attributed to -OD[•] affected by Ta/Nb defect.

In the present study, the behavior of deuterium thermally absorbed in LiNbO₃ was analyzed through IR spectra recorded during constant-rate heating. Because the sample has no radiated defect, influence of radiation defects can be examined by comparison with results of the previous irradiation experiments.

We also focused on sites of hydrogen in bulk and its migration barrier in order to achieve insight into diffusion mechanism of deuterium. In Li₂O, it has been reported that Li vacancy trapping stabilizes a hydrogen atom [3]. Accordingly, potential energies and migration energies of hydrogen at a Li substitutional site or an interstitial site were calculated using plane-wave pseudopotential DFT method.

2. Experimental and calculation conditions

2.1. Infrared spectroscopy

Single crystal of LiTaO₃ and LiNbO₃ (10×10×0.5 mm³, (001) orientation) was used for investigation. A sample was placed in a silica tube so that the infrared light passes it perpendicularly. The tube can be evacuated by a turbo molecular pump and can be heated up to 1273 K by heating furnace. Fig. 1 shows a schematic drawing of the equipment. For thermal absorption of deuterium, the sample was kept at 1073 K under 100 Pa of D₂O for 90 min. After the thermal absorption, it was cooled down to room temperature for 2 h.

Then, IR spectra were recorded during constant-rate heating (3 K min⁻¹ up to 973 K) under a controlled atmosphere (vacuum or 100 Pa of H₂O).

The number of scans was set to 500 in order to achieve an adequate signal-to-noise ratio within a reasonable measurement time. Since spectra observed by this way have information on the bulk more than the surface, detected O-D stretching vibrations were attributed to -OD[•] in the bulk.

2.2. DFT calculation

All calculations were performed using spin-restricted PAW pseudopotential DFT method with the VASP code. PBE functional of the generalized gradient approximation (GGA) was used. When we applied the cut-off energy of 400 eV, energy for migration barrier converged within 0.01 eV. The Monkhorst-Pack scheme was used for the

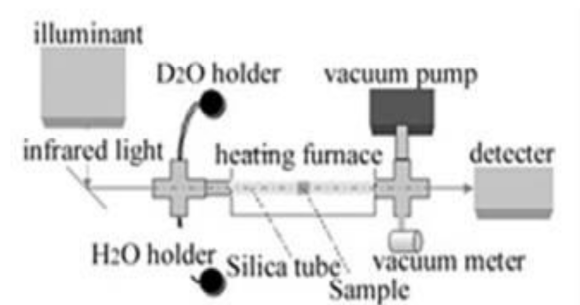


Fig. 1. Schematic drawing of the IR absorption analysis system

Brillouin-zone sampling (2×2×1). According to the cut-off energy and the size of the unit cell, the mesh size for fast Fourier transformation was determined automatically using VASP code to achieve an exact representation of the charge density at the given cut-off energy.

Elastic band method, which can search the saddle point existing between given initial and final configurations, was used to analyze hydrogen migration. The migration barrier was calculated by subtracting the energy of the saddle point from that of stable site.

3. Results and discussion

3.1. IR analysis on the behavior of deuterium in LiNbO₃

Fig. 2 shows the IR spectra of LiNbO₃ crystal during heating in a vacuum after the thermal absorption of D₂O. The peak observed at 2560 cm⁻¹ at room temperature shifted to lower wave numbers and its absorbance decreased as the temperature increased. The peak disappeared above 873 K. This O-D stretching vibration peak has been attributed to -OD⁻ of interstitial D⁺ or -OD⁻ interacting with a Li defect in the bulk [4,5].

3.2. Migration energies of H⁺

Potential energies of H⁺ and O-H bond length at Li substitutional sites [S₁],[S₂],[S₃],[S₄] and interstitial sites ([I], [I']) are shown in Table 1. H⁺ at site [S₁],[S₂],[S₃],and [S₄] bonds the first, second, third, and fourth nearest oxygen atom to a Li vacancy, respectively. Site [I] and [I'] are the first and second most stable site in interstitial sites [6]. These energies are represented as the difference of potential energies between the most stable site [S₁] and a corresponding site.

Table 1 shows that potential energies of H⁺ at Li substitutional sites are lower than that at interstitial sites. However, H⁺ at the site [S₃] is unstable and migrates to interstitial site, which has no activation energy. As the distance between Li vacancy and H⁺ at Li substitutional site is smaller, the H⁺ at its site is more stable.

Congruent lithium niobate, experimentally studied crystals, have a composition that is significantly short of lithium ([Li]/[Nb]=0.945). This suggests that most of H⁺ exists at Li substitutional site, especially [S₁].

Migration energies for H⁺ at Li substitutional site [S₁] and interstitial site [I] have been calculated. Although there are many possible paths, we concentrate here just on the migration from one [S₁] to another [S₁], and from one [I] to another [I]. The step of former migration is categorized as follows: (1) a jump of H⁺ toward neighboring oxygen and (2) a rotation of O-H bond and a simultaneous jump of lithium toward Li vacancy. Based on this, two paths have been calculated: Path A, which consists of jump to [S₁], rotation to [S₂], and jump to [S₁], and Path B, which consists of jump to [S₄] and rotation to [S₁]. As concerns the H⁺ at [I], the migration energy of jump from [I] to [I'] and rotation from [I'] to [I] are calculated (Path C). These paths are indicated in Fig. 3.

Table 1. Potential energies and O-H length of H⁺ at Li substitutional sites ([S_i]) and interstitial site ([I], [I']).

	Potential energy(eV)	O-H length
S ₁	0.0	0.983
S ₂	0.1	0.998
S ₃	unstable	1.041
S ₄	0.5	1.034
I	0.5	1.003
I'	0.6	1.034

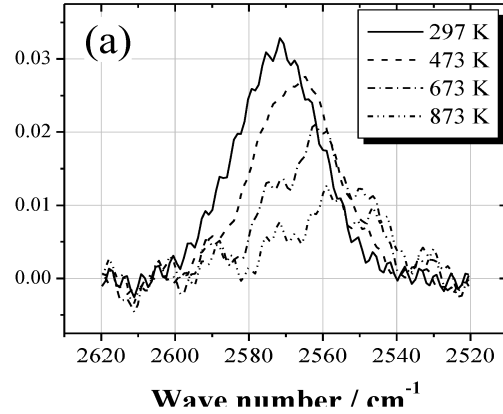


Fig. 2. Infrared absorption spectra of the thermally absorbed crystal during heating in a vacuum.

Table 2. Migration energies of Path A and B for a Li substitutional H⁺, and Path C for an interstitial H⁺.

		Migration energy (eV)
Path A	Jump S ₁ – S ₁	0.9
	Rotation S ₁ – S ₂	1.5
	Jump S ₂ – S ₁	0.3
Path B	Jump S ₁ – S ₄	1.1
	Rotation S ₄ – S ₁	1.7
Path C	Jump I – I'	0.2
	Rotation I' – I	0.5

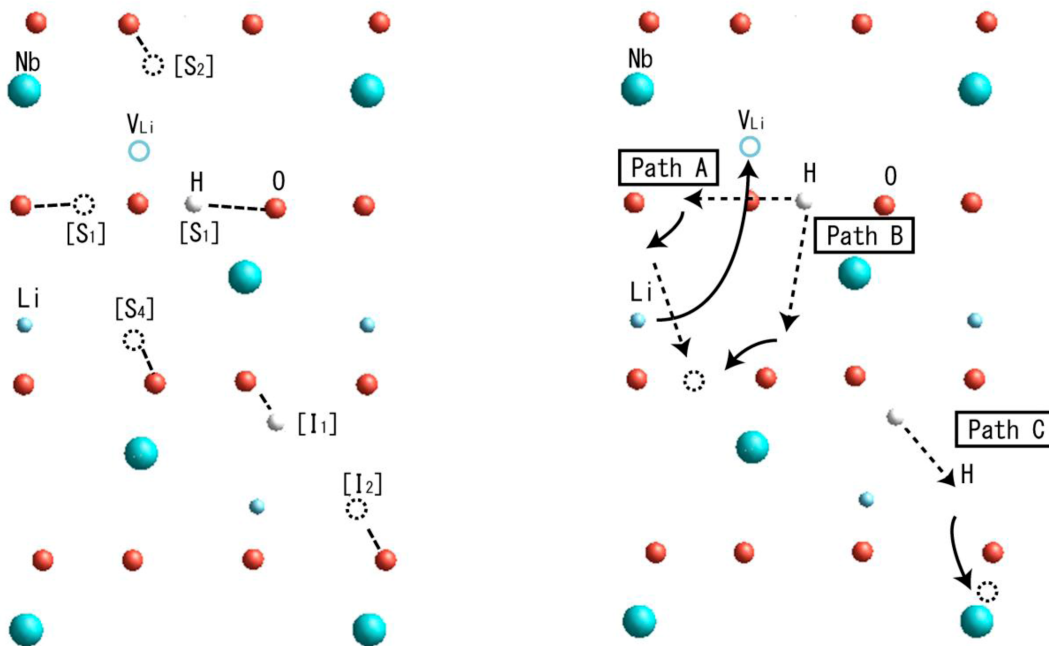


Fig. 3. Schematic diagram of H⁺ sites (left) and migration paths (right).

We show the migration energy for H⁺ diffusion in Table 2. The migration via Path A and B are required for larger energies than via Path C. This result suggests that interstitial H⁺ diffuse faster than substitutional one, and explains the reason activation energy of diffusion evaluated by previous FT-IR report (0.9eV) [7] is lower than migration energy of Li substitutional H⁺ (1.5eV). In Fig. 3, because the energy difference between this H⁺ is small, a part of H⁺ exists as interstitial one at high temperatures. This H⁺ is likely to diffuse via interstitial sites, where migration energy of H⁺ is 0.5eV, until these are trapped by a Li vacancy. Therefore, apparent migration energy observed in previous experimentation is in the 0.5-1.5 eV energy ranges. It should be noted that the H⁺ migration from a Li substitutional site to an interstitial site is affected by Li atom diffusion. The influence of other defects will be studied for future work.

4. Conclusions

IR spectra of LiNbO₃ single crystal during heating were recorded in a vacuum or 100 Pa of H₂O after thermal absorption of D₂O. The observation was compared with ion irradiation experiments.

- ◆ Radiated defects make deuterium have various existing state, but hydrogen atoms diffuse as -OD⁻ states at high temperatures.
- ◆ Li substitutional site is the most stable for H⁺ in LiNbO₃.
- ◆ As migration barrier of an interstitial H⁺ (~0.5 eV) is lower than a Li substitutional site (~1.5 eV), H⁺ diffuses via interstitial sites as well as Li substitutional sites.

References

- [1] T. Luo, T. Oda, Y.Oya, S. Tanaka, J. Nucl. Mater. 372 (2008) 53-58.
- [2] T. Oda, S. Tanaka, AESJ. 2007. Fall Meeting.
- [3] R. Shah, A. D. Vita, M. C. Payne, J. Phys.: Condens. Matter 7 (1995) 6981.
- [4] R. Gonzalez, Y. Chen, J. Phys.: Condens. Matter 14 (2002) R1143.
- [5] T. Luo, T. Oda, S. Tanaka, J. Nucl. Mater. 382 (2008) 46.
- [6] H. H. Nahm, C. H. Park, Appl. Phys. Lett. 78 (2001) 3812.
- [7] R. Gonzalez, Y. Chen, M. Mostoller, Phys. Rev. B 24 (1981) 6862.

**Modeling of tritium behavior in ternary lithium oxides:
in case of lithium niobate**

Kisaburo Azuma¹, Takuji Oda¹, Satoru Tanaka¹

¹ *Department of Nuclear Engineering and Management, The University of Tokyo, Tokyo, Japan*

Ternary Li oxides are candidate solid breeding materials for a fusion reactor. It is important to understand stable existing states and diffusion behavior of hydrogen isotopes bred in solid breeding materials, for estimation of tritium inventory and economic efficiency precisely. In the present work, we studied lithium niobate as a typical example of ternary lithium oxides by means of vibration analysis (quantum mechanical calculation) and molecular simulations (Monte Carlo method). Since many experimental works have been reported for single crystal specimen, simulation results can be directly compared with them. Based on evaluation of existing states and migration behavior of hydrogen isotopes, a model of hydrogen behavior in ternary lithium oxides was constructed.

Two existing sites of hydrogen isotopes are expected in lithium niobate: Li substitutional sites where a hydrogen isotope captured by a lithium vacancy and interstitial sites. Quantum mechanical calculation indicates that a hydrogen atom in a Li substitutional site is more stable than that in interstitial sites. According to vibration analysis, the frequency of O-H stretching vibration in each site is different. As stretching frequency of hydrogen isotopes bonded to the nearest oxygen to lithium vacancy is close to experimental value, it is considered that hydrogen isotopes mainly exist at these substitutional sites.

Calculation by elastic band method for finding minimum energy paths shows that migration barrier of the interstitial site is lower than that of the substitutional site. These results infer that at low temperatures, a hydrogen atom basically exist at the substitutional site; however, at high temperatures, it easily moves to the interstitial site because of little energy difference between those states (0.5 eV), and then diffuse rapidly until retrapped by a lithium vacancie. A model to calculate diffusion coefficient was constructed on the basis of migration energies and paths obtained by the quantum mechanical calculations in atomic scale. In comparison with experimental results, the validity of the model was appraised. The applicability for other ternary lithium oxides including lithium titanate was discussed.

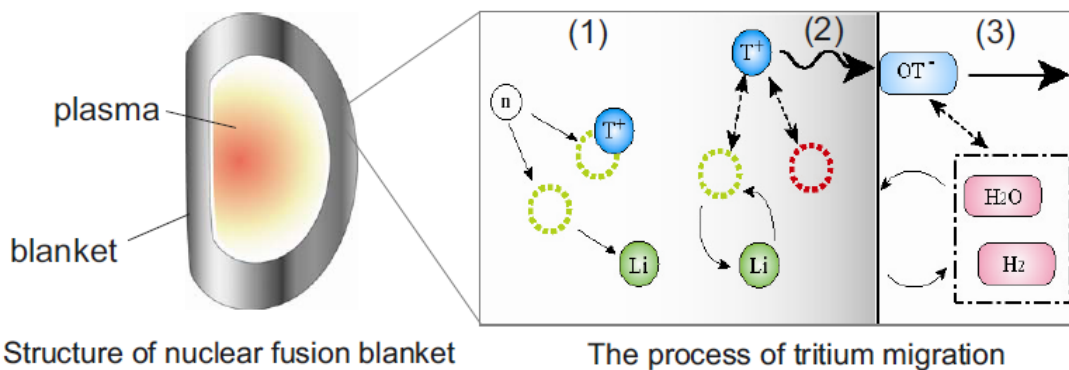
Modeling of tritium behavior in lithium niobate by vibration spectroscopy and molecular simulation

Kisaburo Azuma, Takuji Oda, Satoru Tanaka

Department of Nuclear Engineering and Management,
The University of Tokyo, Tokyo, Japan

Introduction 1/2

The blanket system of fusion reactor is required to breed tritium sufficiently, and to recovery it quickly.



Hydrogen isotope behavior in breeding material:

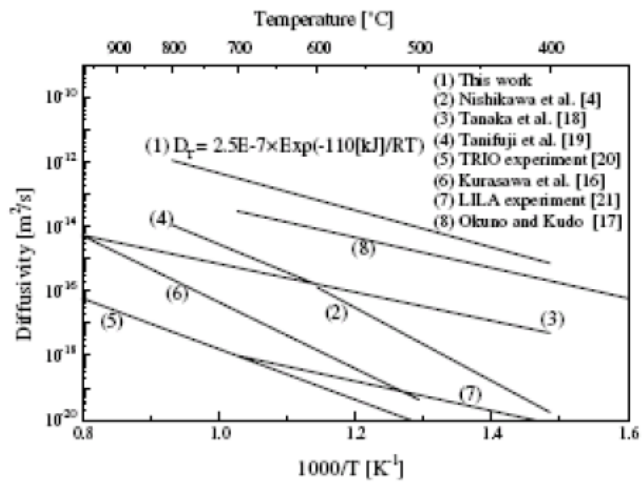
- 1) Tritium generation by neutron irradiation,
- 2) Diffusion in the bulk and grain boundaries,
- 3) Desorption from the surface.

Introduction 2/2

problems

In ternary lithium oxides, several discrepancies of diffusion coefficient for hydrogen isotope have also been observed.

Influence of grain size, trapping by vacancies, or hydrogen concentration?



Diffusivities of tritium in LiAlO₂ reported by different authors [1]

Hydrogen migration processes in the bulk have not been understood adequately.

Understanding this behavior in the material is important in order to optimize the recovery condition for the quick tritium recovery.

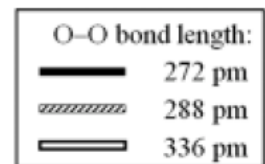
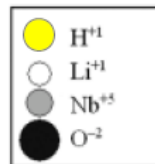
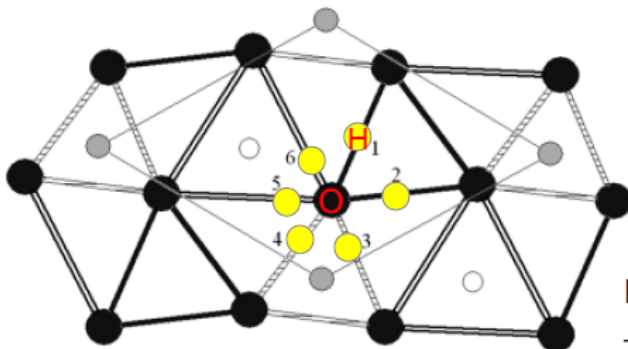
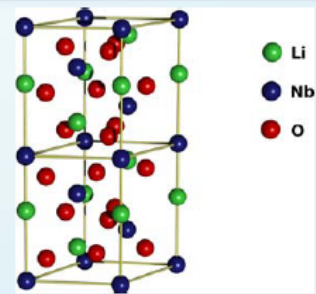
- 3 -

[1]M. Nishikawa, et al., J. Nucl. Mater. 335 (2004) 70-76.

Previous work

Subject material :LiNbO₃.

- Ternary Li oxide
- Many previous works have been reported.
- Single crystal of congruent component has many Li vacancy (≈ 1%). This is useful to investigate the interaction between Li vacancy and hydrogen.



Hydrogen in LiNbO₃ exists as -OH⁻, which is infrared active.

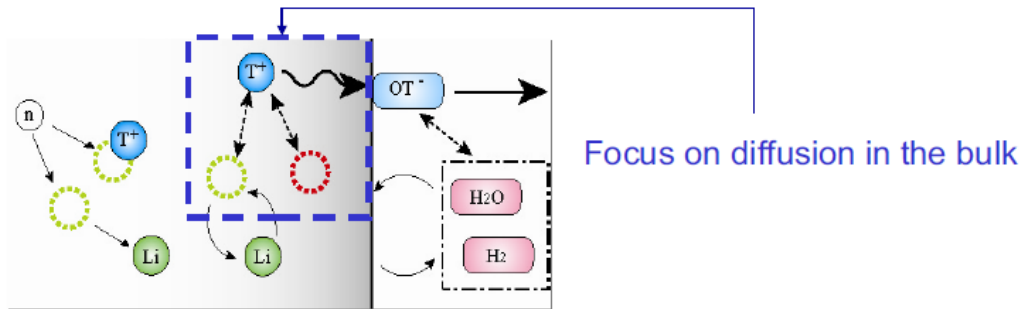
The suggested site of -OH[1].

- 4 -

[1]D.I. Shevtsov et al., Ferroelectrics 341 (2006) 55

Purpose

Construction of the model of hydrogen behavior in ternary lithium oxides, based on evaluation of existing states and migration behavior of hydrogen isotope,



Analysis using Quantum Mechanical Calculations

- 1) hydrogen stability in LiNbO_3
- 2) vibration analysis at the saddle point
- 3) migration barrier of H^+ at each site

- 5 -

Contents

- 1) Searching stable sites for H^+ in LiNbO_3
- 2) Determination of migration path of H^+ at Li substitutional site
- 3) Evaluation of migration barrier of the path of H^+ at Li substitutional site
- 4) Evaluation of migration barrier of the path of H^+ at interstitial site

Conclusion

- 6 -

1) Searching stable sites for H⁺ in LiNbO₃: Method

calculation conditions

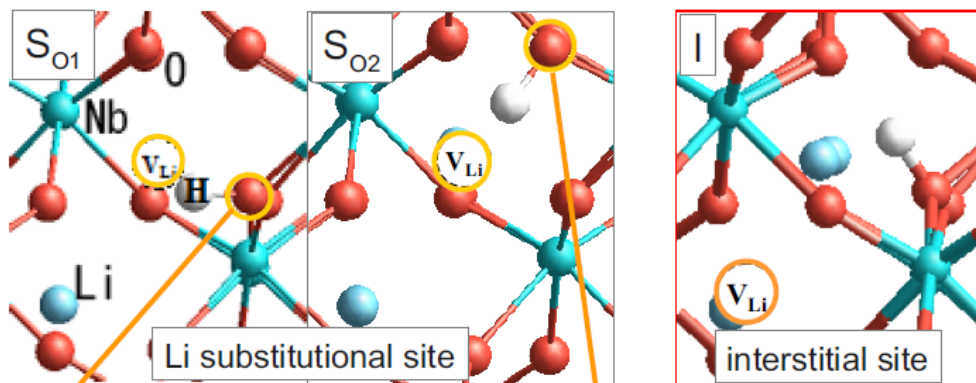
plane-wave pseudopotential DFT (VASP code)

• functional: GGA/PBE

• pseudopotential: PAW

Li substitutional site is thought to be stable site of H⁺ in LiNbO₃.

- Hydrogen at Li substitutional site is stable in Li oxide.
- Many Li vacancies exist in LiNbO₃, which is congruent component. (≈ 1%. This is larger than hydrogen concentration)



Binding to the closest oxygen from Li vacancy

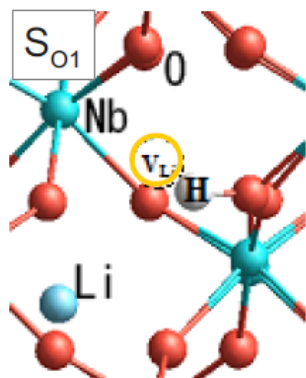
the 2nd closest oxygen

- 7 -

1) Searching stable sites for H⁺ in LiNbO₃: Results

Energy calculation of the structure containing impurity hydrogen.

(Li ₂₃ Nb ₂₄ O ₇₂ H ₁)	Li substitutional				Most stable interstitial site
	S _{O1}	S _{O2}	S _{O3}	S _{O4}	I
V _{Li} -O distance(Å)	2.029	2.221	3.309	3.471	3.879
O-H bond length(Å)	0.983	0.998	1.041	1.034	1.003
energy(eV)	0	+0.1	+0.6	+0.5	+0.5



Binding to same oxygen atom

H⁺ is stabilized by Li vacancy trapping (0.4 eV)

Potential energy of site S_{O3} and S_{O4} are comparable with that of Interstitial site.

Most of hydrogen exist at Li substitutional site S_{O1}, S_{O2}

- 8 -

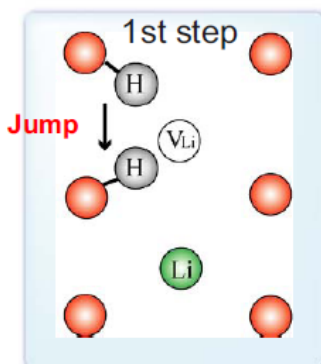
Contents

- 1) Searching stable sites for H^+ in $LiNbO_3$
 - Most of hydrogen exist at Li substitutional site S_{O1}, S_{O2}
- 2) Determination of migration path of H^+ at Li substitutional site
- 3) Evaluation of migration barrier of the path of H^+ at Li substitutional site
- 4) Evaluation of migration barrier of the path of H^+ at interstitial site

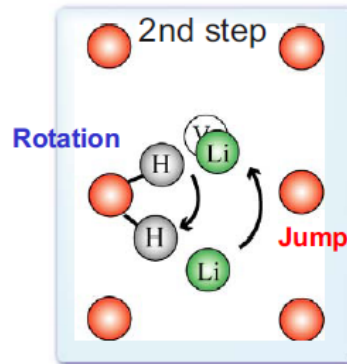
Conclusion

- 9 -

2) Determination of migration path of H^+ at Li substitutional site



Jump of H^+ from Li substitutional site to interstitial site, to bond another O atom.



Rotation of O-H bond axis from interstitial site to another Li substitutional site.

+

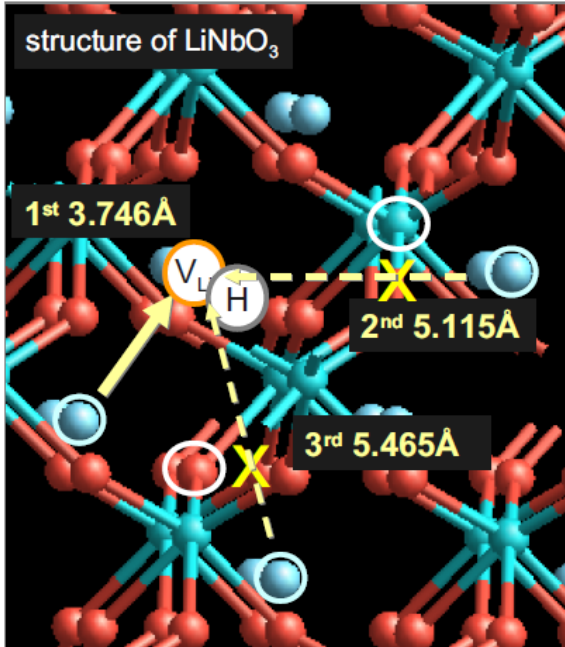
Jump of Li^+ to neighboring Li site (Li-vacancy site)

It is important to find the migration path of H^+ and Li^+ , respectively.

- 10 -

2) Determination of migration path of H⁺ at Li substitutional site : Li⁺ migration

Possible migration path of Li⁺



Distance between Li atoms:

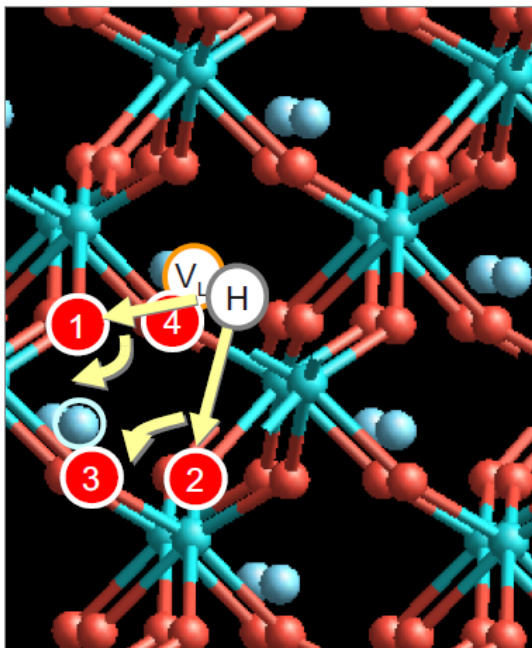
- 3.746 Å (The closest one)
- 5.115 Å (The 2nd closest one)
→ interrupted by Nb atom
- 5.465 Å (The 3rd closest one)
→ interrupted by O atom

Only the closest Li⁺ can migrate to Li vacancy.

- 11 -

2) Determination of migration path of H⁺ at Li substitutional site : H⁺ migration

Possible migration path of H⁺ at Li substitutional site



There are 4 possible path to migrate next Li substitutional site.

- 1) Jump to the 1st closest O atom,
- 2) Jump to the 4th closest O atom,
- 3) Jump to the 3rd closest O atom,
- 4) Jump to the 4th closest O atom,

However, these sites are unstable.

Path 1 and 2 are to be discussed in the following discussion.

- 12 -

Contents

- 1) Searching stable sites for H⁺ in LiNbO₃
 - Most of hydrogen exist at Li substitutional site S_{O1}, S_{O2}
- 2) Determination of migration path of H⁺ at Li substitutional site
 - There are 2 migration paths of H⁺ at Li substitutional site.
- 3) Evaluation of migration barrier of the path of H⁺ at Li substitutional site
- 4) Evaluation of migration barrier of the path of H⁺ at interstitial site

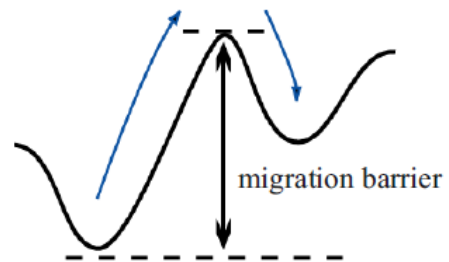
Conclusion

- 13 -

3) Evaluation of migration barrier of the path of H⁺ at Li substitutional site : Method

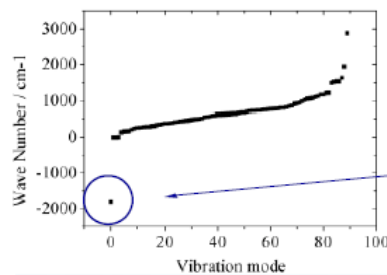
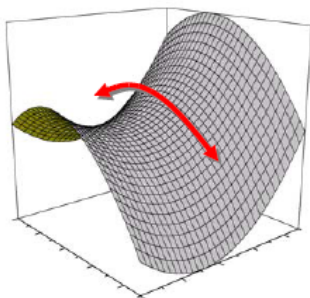
Migration barrier of H⁺ at a certain site in LiNbO₃ was calculated by DFT.

- searching the saddle point of minimum energy path on potential energy curve.
- calculating the migration barrier between the stable state and the transition state.



Vibration analysis is used to confirm whether or not the transition state is a true saddle point.

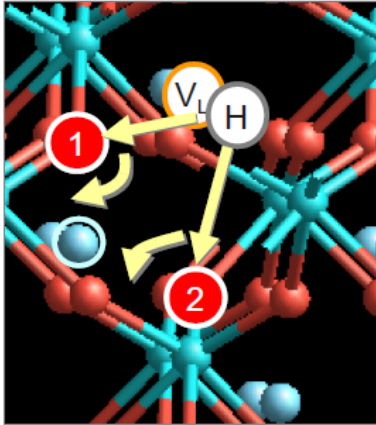
- An imaginary frequency indicates the existence of a vibrational mode that is dynamically unstable.



If the analyzed point is saddle point, it exhibits only one imaginary frequency.

- 14 -

3) Evaluation of migration barrier of the path of H⁺ at Li substitutional site : result



Migration barrier of H⁺ of each path

			Migration barrier (eV)
Path 1	Jump	$S_{O1}-S_{O2}$	0.3
	Rotation	$S_{O1}-S_{O2}$	1.4
Path 2	Jump	$S_{O1}-S_{O4}$	1.1
	Rotation	$S_{O1}-S_{O4}$	1.7
Exp.			0.9 [1]

Experimental value of migration barrier is lower than calculated value of each migration path.

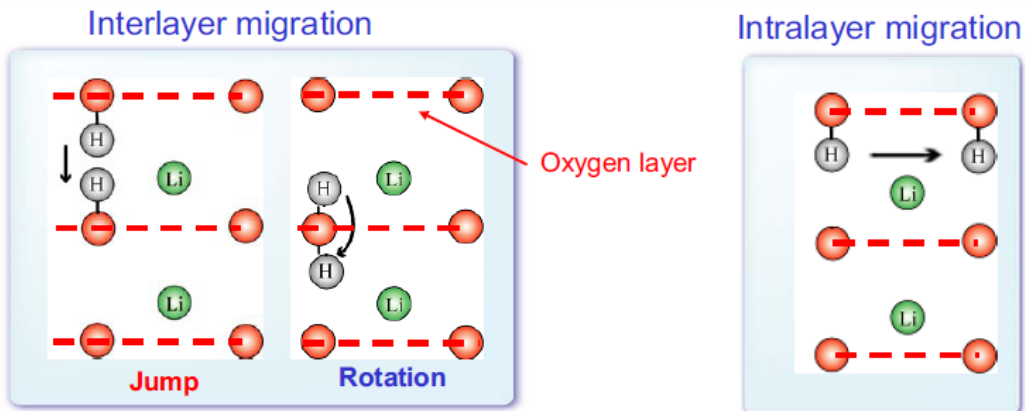
There is another path for the migration of H⁺ from Li substitutional site.

Contents

- 1) Searching stable sites for H⁺ in LiNbO₃
 - Most of hydrogen exist at Li substitutional site S_{O1}, S_{O2}
- 2) Determination of migration path of H⁺ at Li substitutional site
 - There are 2 migration paths of H⁺ at Li substitutional site.
- 3) Evaluation of migration barrier of the path of H⁺ at Li substitutional site
 - Experimental value of migration barrier is lower than migration paths of H⁺ at Li substitutional site.
- 4) Evaluation of migration barrier of the path of H⁺ at interstitial site

Conclusion

4) Evaluation of migration barrier of the path of H⁺ at interstitial site



1st step

Jump of H⁺ from Li interstitial site to interstitial site, to bond another O atom.

2nd step

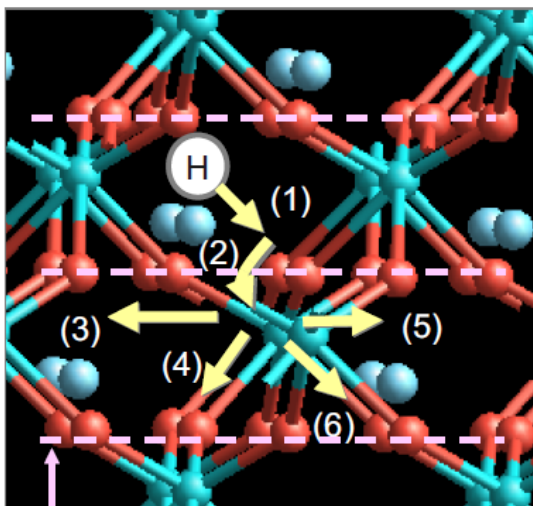
Rotation of O-H bond axis from interstitial site to another Li interstitial site.

Only one step

Jump of H⁺ from Li interstitial site to another interstitial site.

- 17 -

4) Evaluation of migration barrier of the path of H⁺ at interstitial site : result



Oxygen layer

migration barrier of H⁺

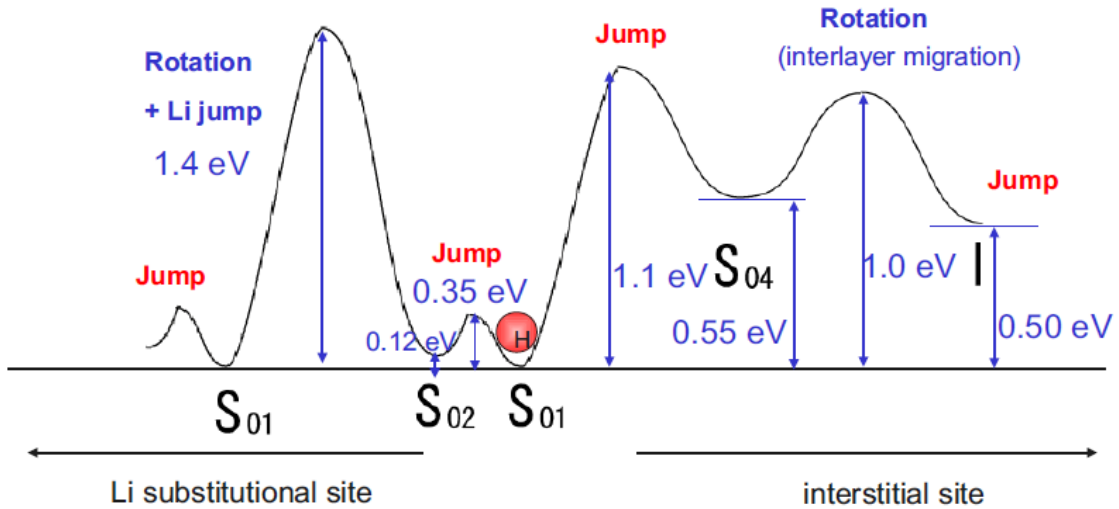
			Migration barrier (eV)
interlayer migration	Jump	(1)	0.1
	Rotation	(2)	0.5
intralayer migration	Jump	(3)	0.9
	Jump	(4)	0.9
	Jump	(5)	0.7
	Jump	(6)	0.7
Exp.			0.9

Migration barrier of H⁺ at interstitial site is lower than that at Li substitution site, and experimental value.

- 18 -

Example of potential energy curve for H⁺ migration

Potential energy curve can be drawn by the energy of each site and migration barrier.



Although most of hydrogen are at Li substitutional site, H⁺ tend to migrate via interstitial sites, rather than Li substitutional sites.

Conclusion

Migration barrier of H⁺ at Li substitutional site and interstitial site in LiNbO₃, has been calculated using plane-wave pseudopotential DFT .

Most of hydrogen are at Li substitutional site.

The migration barrier of H⁺ at Li substitutional site is 1.4~1.7 eV.

The migration barrier of H⁺ at interstitial site is 0.5~0.9 eV.

Because the experimental value is 0.9 eV, H⁺ migrate through both Li substitutional sites and interstitial sites.

Further research is required to assess whether this model is sensible, or not. Diffusion coefficient calculated by Monte Carlo method with that of experimental value will be compared in the future.

10. Modeling of Point Defects on Mechanical Properties in Lithium Aluminate

Hiroki Tsuchihira, Takuji Oda, Satoru Tanaka

The University of Tokyo, 7-3-1 Hongo, Bunkyo-ku, Tokyo 113-8656, Japan

E-mail: masuyama@flanker.q.t.u-tokyo.ac.jp

Abstract

Elastic constants of LiAlO_2 containing point defects were evaluated with molecular dynamics or statics simulation. The point defects were introduced by displacement cascade simulation and random configuration. Through comparison of the results obtained from these two kinds of simulation, it was indicated that aggregation of point defects could lower the elastic constants.

1. Introduction

Elastic properties of ceramic breeder materials are used to predict the response of materials to thermal loads and to calculate the lower bound on the thermal gradient, which may contribute to material fragmentation [1]. A COMPLIMENT experiment [2] showed a reduction of the Young's moduli of LiAlO_2 to about 80% of the initial values after neutron irradiation of 1.8 dpa. However, the origin has not been understood, such as the effects of helium, hydrogen isotopes, vacancy/interstitial clusters, etc. Therefore, it is difficult to make a precise prediction about change of elastic properties in a fusion reactor of the future.

In the present study, we aim to understand the influence of point defects on elastic properties (elastic constants, bulk modulus, Young's modulus and Poisson's ratio) in an atomic scale, which are difficult to examine by experiment. Especially, we focus on elastic constants because the other three properties can be obtained from elastic constants as the following equations:

$$S = C^{-1},$$

$$K = \frac{1}{9}(2C_{11} + 2C_{12} + 4C_{13} + C_{33}),$$

$$Y_x = S_{11}^{-1}, \quad Y_z = S_{33}^{-1} \quad \text{and}$$

$$\sigma_\alpha(\beta) = -S_{\alpha\beta} Y_\beta, \tag{1}$$

where C_{ij} is elastic constants, S elastic compliance, K bulk modulus (of Voigt [3]), Y Young's moduli and σ Poisson's ratio. For the aim, molecular statics (MS) and molecular dynamics (MD) technique were used for gamma lithium aluminate, which is a candidate of solid breeding material and has a relatively simple structure.

The rest of the paper is organized as follows. In section 2, calculation details are presented. The

potential model used in the present study, calculation condition of the displacement cascade simulation and configuration method of the point defects are explained. In section 3, the decrease of C_{11} by displacement cascade is described at first. Then, C_{11} and C_{33} in system containing point defects in various configurations are presented. From the comparison of the two kinds of simulation, the effect of defect aggregation is discussed. The paper is closed by section 4 with concluding remarks.

2. Calculation method

2.1. Potential model

We adopted a pairwise potential model [4] for simplicity, with reliance on high ionicity of LiAlO_2 . Our pairwise potential model between two ions is expressed as

$$U(r) = \frac{q_1 q_2}{r} + \exp(-r) \times \sum_{n=N_0}^{N_0+N-1} \left(a_n \times \frac{1}{r^n} \right), \quad (2)$$

where q_1 and q_2 are effective charges, r [\AA] an interatomic distance, and N_0 , N and a_n [eV \AA^n] the smallest power, the number of inverse polynomial functions, and the coefficient of each term, respectively. The Coulombic term was evaluated using Ewald summation technique [5], while the remaining terms were calculated directly with the cut-off distance of 10 \AA . The results of Mulliken population analysis [6] in the optimized LiAlO_2 structure were adopted as fixed values of ionic charges: +0.7e for Li^+ , -1.1e for O^{2-} and +1.5e for Al^{3+} , respectively. N_0 , N and a_n were determined to reproduce potential energies in various distorted crystal structures, which were evaluated by plane-wave pseudopotential DFT calculation. In consequence, these parameters were obtained as $N_0=4$, $N=6$ and a_n listed in ref. [4].

The formation energy of a Li Frenkel pair evaluated by DFT calculation and MS calculation with the potential model, respectively 2.92 eV and 3.07 eV, showed good agreement. The formation energies of an O and Al Frenkel pair obtained with the potential model were 6.20 eV and 6.60 eV, respectively, which are appropriate as the formation energy in an oxide metal. The reasonable results about the formation energy indicate that the potential model can deal with point defects.

2.2. Displacement cascade simulation

In irradiation simulations with MD, the displacement cascade is triggered by introducing primary knock-on atom (PKA). In the present study, an O atom was displaced with the energy of 5 keV toward $\langle 543 \rangle$, $\langle 453 \rangle$ and $\langle 345 \rangle$ direction in a $30 \times 30 \times 30$ supercell (432,000 atoms) under periodic boundary condition (PBC). The a , b and c lattice constants were 15.4, 15.4 and 18.5 nm, respectively. All cascade simulations were carried out at an initial temperature of 0 K under NVE ensemble using variable time step dependent on the maximum velocity and interaction force in the system. With an assumption of Boltzman distribution, the final temperature of the system became 67 K. All the MD simulations were conducted using the DL_POLY code [7].

2.3. Random configuration of point defects

In order to investigate what kind of point defect has significant influence on elastic constants, a few point defects were incorporated in $3\times 3\times 3$ supercells (432 atoms). Table 1 shows the sort of point defect. These kinds of point defect were put at positions determined randomly. Namely, a vacancy was introduced by removing an atom, and an interstitial atom was taken in by putting an atom at an interstitial site determined randomly. The white balls in Fig. 1 show the interstitial sites in the primitive cell. The concentrations of each defect became 0.23 (1 defect), 0.46 (2 defects) or 0.69% (3 defects). When vacancies or interstitials were incorporated, the total charge was neutralized by applying a uniform background charge.

For comparison with the result of displacement cascade simulation, the systems including a few Frenkel pairs were also investigated. In this case, the elements of Frenkel pairs were determined randomly (no weighting). For example, when the concentration was 0.69%, containing 3 Frenkel pairs in the system, sometimes all of them were Li, in another time they were Li, O and Al.

In all the calculations, elastic constants C_{11} and C_{33} were evaluated after geometry optimization. The calculations were conducted with 100 randomly determined configurations for each kind of defects.

3. Results and discussion

3.1. Displacement cascade simulation

Fig. 2 shows the time dependency of vacancy structure in case that PKA displacement direction was $\langle 345 \rangle$. In the present paper, a vacancy was defined as a site that there was no atom within 0.8 \AA from the ideal atomic positions. The defect structure was not almost changed after 3 ps from the introduction of PKA. Simulations with PKA displacement direction of $\langle 543 \rangle$ and $\langle 453 \rangle$ were also conducted.

Fig. 3 shows the number of defects remained after 3 ps in case that PKA displacement direction was $\langle 345 \rangle$. In Li, both the number of generated defects (the sum of replacement, anti-site and interstitial) and annihilated defects (replacement) were the largest. The both were the smallest in Al, and intermediate in O. Although the number of displaced atoms of Li was about three times larger than that of Al, the number of remaining interstitials of Li and Al were almost equal. This tendency was also seen in case of $\langle 453 \rangle$ and $\langle 543 \rangle$ PKA displacement direction.

Elastic constant C_{11} was evaluated in the unirradiated crystal and the three irradiated structures as Fig. 4. 100% of C_{11} represents the value of the perfect crystal. The value of C_{11} decreased about 10% by the displacement cascades. Fig. 4 also shows the vacancy concentration of the structures. Among the defected structures, the value of C_{11} did not show obvious dependencies on the vacancy concentration. A possible reason for this is the dependency of C_{11} on the defect configuration. In other words, contrary to Fig. 4, the value of C_{11} can take different values depending on the defect configuration even if the defect concentration is equivalent.

3.2. Random configuration of point defects

Figs. 5 (a) – (f) show the effect of point defects on the values of C_{11} and C_{33} . The plots and bars represent the average value and the standard deviation of 100 times calculation, respectively. From Figs.

5 (a) and (b), it is indicated that Al atoms worked to increase C_{11} because C_{11} increased and decreased when the concentration of Al interstitial and Al vacancy increased, respectively. Meanwhile from Figs. 5 (d) and (e), it can be seen that O atoms worked to increase C_{33} . Li atoms did not work so effective.

From the comparison of Figs. 5 (a) – (c), for C_{11} , the result of Frenkel pairs seems like a simple sum of the result of interstitial and vacancy. This indicates that for C_{11} , the effect of the interaction between interstitial atoms and vacancies was smaller than the effect of point defect itself. And from the comparison of Figs. 5 (d) – (f), the same behaviour was also suggested for C_{33} .

3.3. Comparison between the results of the displacement cascade and the random configuration calculation

Fig. 6 shows the dependency of C_{11} on the concentration of Frenkel pairs. In the black plots of Fig. 6, the elements and positions of Frenkel pairs were determined randomly (see section 2.3). The red plots represent the same results as in Fig. 4. Even if the concentration of Frenkel pairs is the same, pairs generated by displacement cascade lowered C_{11} than the random configuration of Frenkel pairs. The Frenkel pairs introduced by displacement cascade were more aggregative than the random configuration. Therefore, it is indicated that aggregation of point defects can lower C_{11} .

4. Conclusions

Elastic constants of LiAlO_2 containing point defects were evaluated with molecular dynamics or statics simulation. The point defects were introduced by displacement cascade simulation and random configuration. By the displacement cascade, the value of C_{11} decreased about 10% by the displacement cascades. Among the defected structures, the value of C_{11} did not show obvious dependencies on the vacancy concentration. A possible reason for this is the dependency of C_{11} on the defect configuration.

From the molecular statics calculation, it was indicated that Al and O atoms respectively work to increase C_{11} and C_{33} . Li atoms did not work so effective. The effect of Frenkel pairs on C_{11} and C_{33} seems a simple sum of the effect of interstitial and vacancy.

From the comparison between displacement cascade and random configuration simulation, it was indicated that aggregation of point defects can decrease C_{11} .

References

- [1] C.E. Johnson et al., ISFNT-2, Karlsruhe, Germany, 3-8 Jun 1991.
- [2] W. Dienst, J. Nucl. Mater. 212-215 (1994) 891-896.
- [3] J.F. Nye, Physical properties of crystals, Oxford University Press, Oxford, 1957.
- [4] H. Tsuchihira et al., accepted by J. Nucl. Mater.
- [5] P.P. Ewald, Ann. Physik 64 (1921) 253-287.
- [6] R.S. Mulliken, J. Chem. Phys. 23 (1955) 1833.
- [7] T.R. Forester et al., DL_POLY User Manual (1995).

Table 1. The sort of point defect.

	Li	O	Al
Vacancy	○	○	○
Interstitial	○	○	○
Frenkel pair	○	○	○

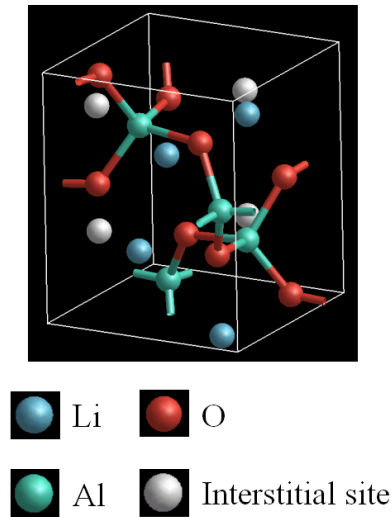


Fig. 1. The primitive cell of LiAlO₂.

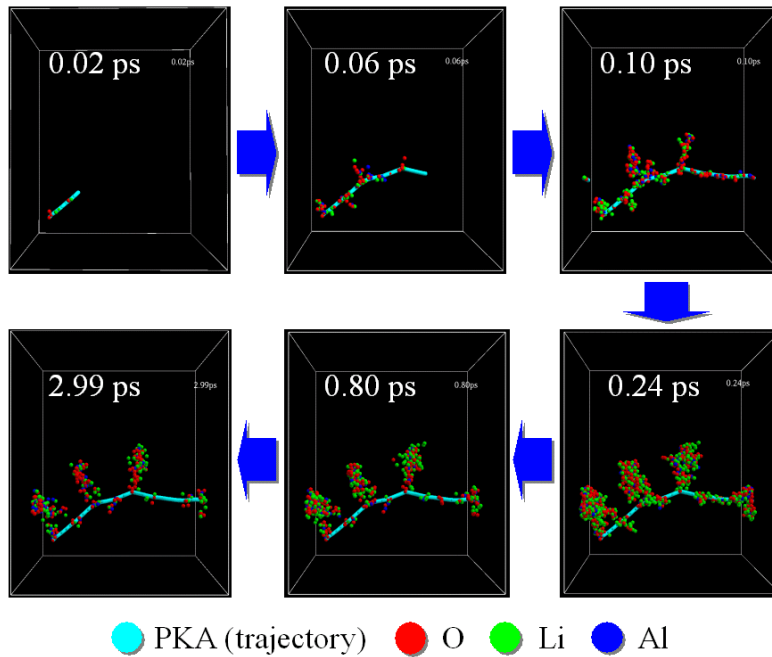


Fig. 2. The time dependency of vacancy structure in case that PKA displacement direction is $\langle 345 \rangle$. $t=0$ is the time PKA was displaced.

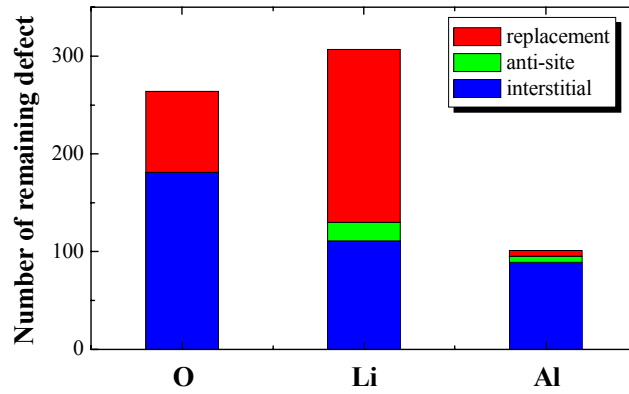


Fig. 3. The number of remaining defects in case that PKA displacement direction is $\langle 345 \rangle$.

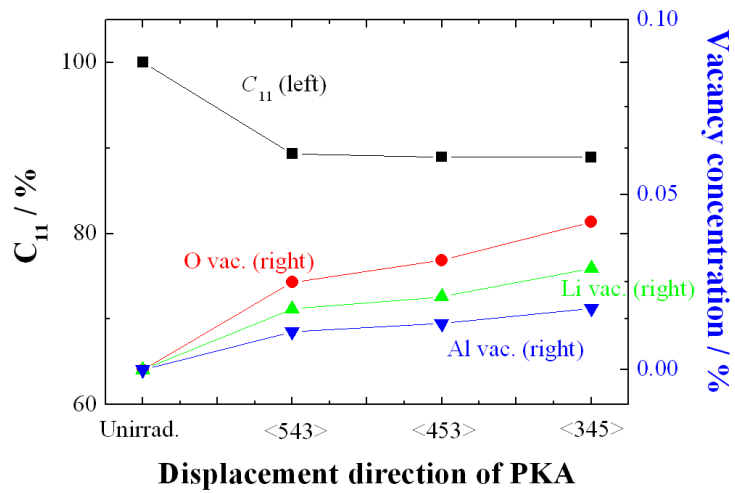
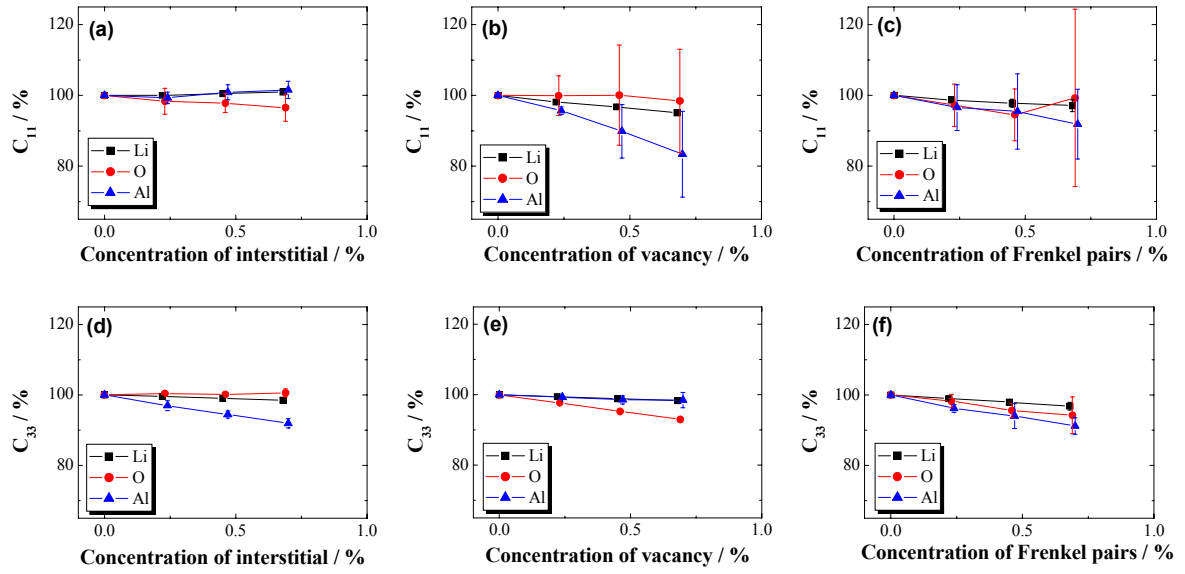


Fig. 4. C_{11} and vacancy concentration evaluated in the unirradiated crystal and the three defected structures.



Figs. 5. The effect of point defects on the values of C_{11} and C_{33}

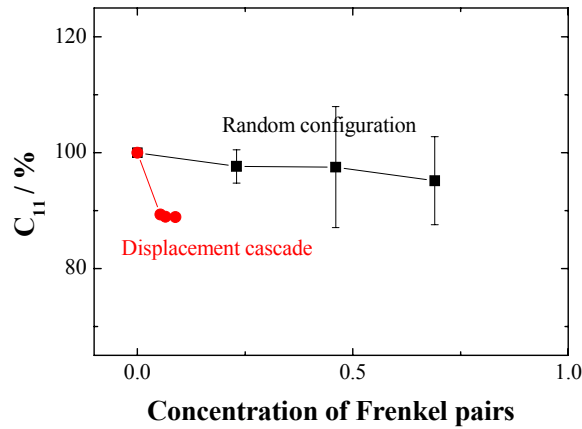


Fig. 6. The dependency of C_{11} on the concentration of Frenkel pairs.

Modeling of Point Defects on Mechanical Properties in Lithium Aluminate

Hiroki Tsuchihira¹, Takuji Oda¹ and Satoru Tanaka¹

¹ *Department of Nuclear Engineering and Management, The University of Tokyo, 7-3-1 Hongo, Bunkyo-ku, Tokyo 113-8565, JAPAN*

Mechanical properties of lithium containing oxides that will be used as solid breeding materials in fusion reactors change during reactor operation, because of formation of irradiation defects by high-energy particle irradiation. Therefore, it is important for retaining material performance to understand the effects of defects on mechanical properties, and then to deal with them appropriately. However, the effects have not been revealed quantitatively.

In the present study, by using computer simulation, we aimed to evaluate and model influence of point defects on mechanical properties (elastic constants, bulk modulus, young's modulus and poisson's ratio) in atomic scale, which are difficult to examine by experiment. For this aim, molecular statics (MS) simulation was performed for gamma lithium aluminate, which is a candidate of solid breeding material and has a relatively simple structure. Interatomic potentials, which are necessary for MS simulation, were constructed by fitting a model function to total energies obtained by ab initio calculation.

Mechanical properties of lithium aluminates of various point-defect concentrations and configurations were evaluated. According to the point-defect concentration, the mechanical properties changed. Moreover, even in the case of the same point-defect concentration, the mechanical properties varied with depending on the point-defect configurations. Influence of point-defect concentration and configuration on mechanical properties in gamma lithium aluminate was quantitatively derived.

Modeling of Point Defects on Mechanical Properties in Lithium Aluminate

*Department of Nuclear Engineering and Management,
The University of Tokyo*

Hiroki Tsuchihira, Takuji Oda, Satoru Tanaka

Background

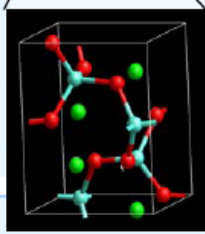
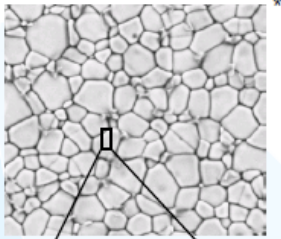
- Elastic properties of ceramic breeder materials are used to predict the response of materials to thermal loads and to calculate the lower bound on the thermal gradient which may contribute to material fragmentation*.
- A COMPLIMENT experiment** showed a reduction of the Young's moduli of LiAlO_2 to about 80% of the initial values after neutron irradiation of 1.8 dpa.
- However, the origin is not understood from the elementary process. Therefore, it is difficult to make a precise prediction about change of elastic properties in a fusion reactor of the future.

* C.E. Johnson et al., ISFNT-2, Karlsruhe, Germany, 3-8 Jun 1991.

** W. Dienst, Journal of Nuclear Materials 212-215 (1994) 891-896.

Purpose of the present research

To understand influence of point defects on elastic properties in LiAlO_2



➤ In order to predict the elastic-property change of a pebble, we have to understand

- ◆ Property of grain itself
- ◆ Effect of grain boundary
- ◆ Behavior as a pebble

➤ In the present research, we focused on the property of grain itself.

* M.O. Orlandi, Mat. Res. 6 (2003)

Contents of the presentation

1. Irradiation simulation with molecular dynamics (MD) technique to introduce point defects.

2. Evaluation of elastic constants based on the obtained structure.

3. Molecular statics (MS) simulation to investigate the effect of each kind of point defect on elastic constants.

4. Comparison between irradiation and MS simulation

Contents of the presentation

1. Irradiation simulation with molecular dynamics (MD) technique to introduce point defects.

- Potential model
- Simulation condition
- Obtained irradiation-defect structure

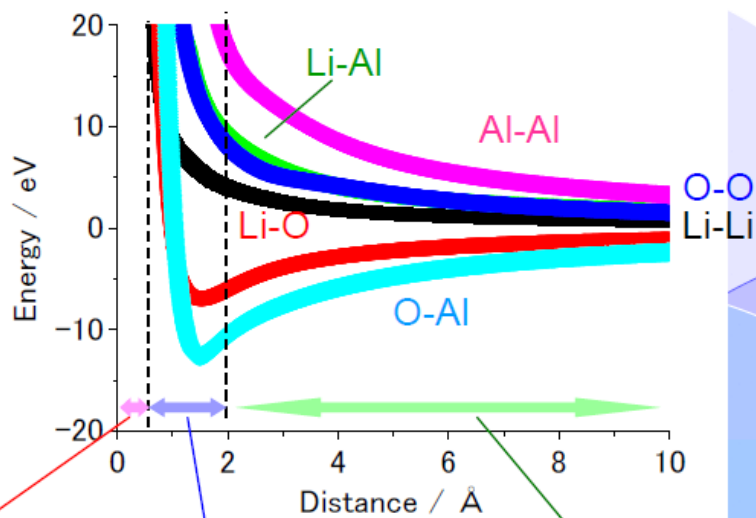
2. Evaluation of elastic constants based on the obtained structure.

3. Molecular statics (MS) simulation to investigate the effect of each kind of point defect on elastic constants.

4. Comparison between irradiation and MS simulation

Adopted potential model

➤ A potential model is necessary for MD and MS simulation



ZBL potential*

Polynomial (interpolation)

Fitting to the energy responses as the LiAlO₂ crystal structure was changed

*Biersack J P and Ziegler J F 1982 Nucl. Instrum. and Meth. 194 93

Evaluation of material properties

Material properties	Properties related to	Calc. method	Calc. code
Lattice constant, Mechanical properties	Structure	MS	GULP
Thermal expansion, Melting point	High-temperature	MD	DL POLY
Formation energy of a frenkel pair	Defect	MS	GULP

		Exp.	DFT	PM
Lattice constant / Å	a	5.17 ^a	5.12	5.12
	c	6.26 ^a	6.18	6.17
Elastic constant / GPa	C ₁₁	173.2 ^b , 161.8 ^c	158.0	128.4
	C ₁₂	26.1 ^b , 74.1 ^c	61.7	76.2
	C ₁₃	48.8 ^b , 73.9 ^c	65.0	88.8
	C ₃₃	176.2 ^b , 194.7 ^c	177.2	203.6
	C ₄₄	64.3 ^c	68.6	50.2
	C ₆₆	35.5 ^c	66.0	54.3
Linear expansion coefficient / 10 ⁻⁶ K ⁻¹	a	15 ^a , 17 ^b	-	13
	c	7 ^a , 10 ^b	-	14
Melting point / K		1953 - 1993 ^a	-	2000
Formation energy of a Li frenkel energy / eV		-	2.92	3.07

^a B. Cockayne et al., J. Cryst. Growth 54 (1981) 546. ^b M.M.C. Chou et al., Appl. Phys. Lett. 88 (2006) 161906.
^c F. Jachmann et al., J. Appl. Phys. 98 (2005) 73501.

Calculation condition of irradiation simulation

➤ In the irradiation simulation with MD, the displacement cascade is triggered by introducing PKA (primary knock-on atom).

System: Li₁₀₈₀₀₀Al₁₀₈₀₀₀O₂₁₆₀₀₀ (30 × 30 × 30 supercell)

PKA (primary knock-on atom) energy : 5 keV

PKA displacement direction: <543>, <453>, <345>

Initial temperature: 0 K

Ensemble: NVE

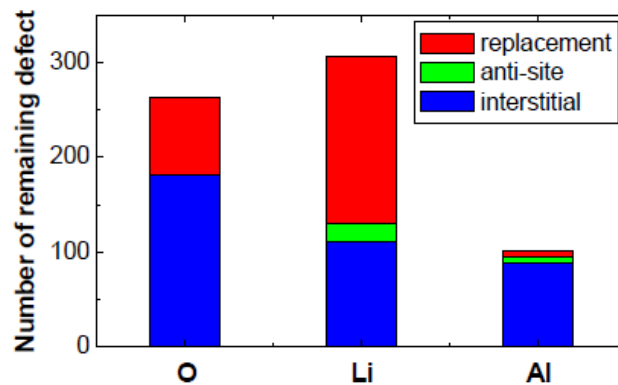
Time dependency of defect structure: <345>, vacancy

● PKA (trajectory)
● O
● Li
● Al

The length of side out h

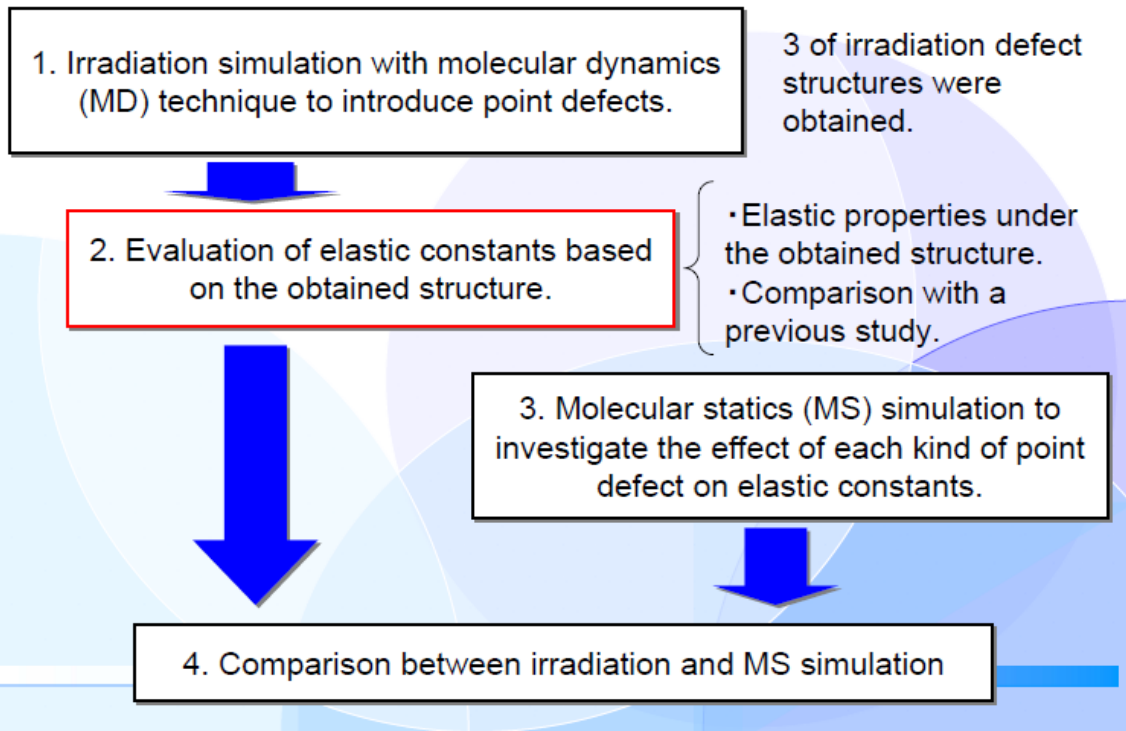
- The defect structure got almost stable after 3 ps from the introduce of PKA.
- Thus, 3 of irradiation defect structures were obtained.

The number of remaining defects: in case of <345>



- Li: Both the number of generation (replacement + anti-site + interstitial) and annihilation (replacement) of defects were the largest.
- Al: The both were the smallest. O: The both were the middle.
- Although the number of displaced atoms of Li were about 3 times larger than that of Al, the number of remaining interstitials of Li and Al were almost equal.
- The above tendencies were also seen in case of <453> and <543>.

Contents of the presentation



Correlation among elastic properties

$$S = C^{-1}$$

$$K = \frac{1}{9}(2C_{11} + 2C_{12} + 4C_{13} + C_{33})$$

$$Y_x = S_{11}^{-1} \quad Y_z = S_{33}^{-1}$$

$$\sigma_\alpha(\beta) = -S_{\alpha\beta}Y_\beta$$

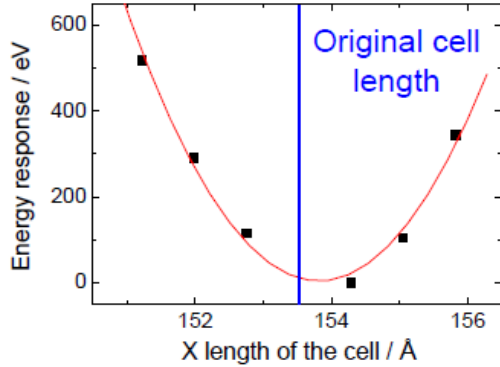
C: Elastic constant
 S: Elastic compliance
 K: Bulk modulus (of Voight)
 Y: Young's moduli
 σ : Poisson's ratio

(Crystallographically, x, y directions of LiAlO_2 are equivalent.)

- K, Y, σ can be obtained from C_{ij} .
- Therefore, we focused on C_{ij} in the present research.

Evaluation of elastic constants in irradiated systems

- C_{11} in irradiated systems were evaluated.



C_{11} was evaluated from the equation:

$$C_{ij} = \frac{1}{V} \left(\frac{\partial^2 U}{\partial \varepsilon_i \partial \varepsilon_j} \right)$$

V: Volume
U: Energy
 ε : strain

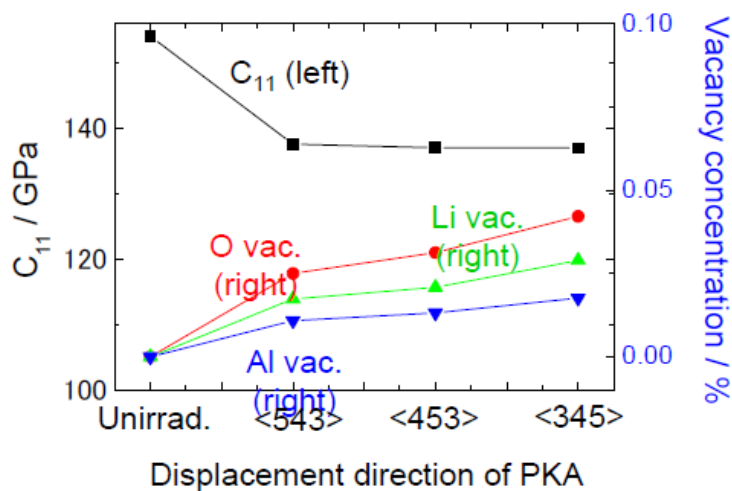
Fig. Cell length vs. energy response in case that PKA displaced toward <345>.

	unirrad.	<543>	<453>	<345>
C_{11} / GPa	154.1	137.6	137.0	137.0

- C_{11} of LiAlO_2 decreased $\sim 10\%$ by the displacement cascades.

Evaluated elastic constants in irradiated systems

- Correlation between C_{11} and vacancy concentration were investigated.



- C_{11} was dependent on the vacancy concentration.
- When the vacancy concentration was increased, C_{11} was lowered.

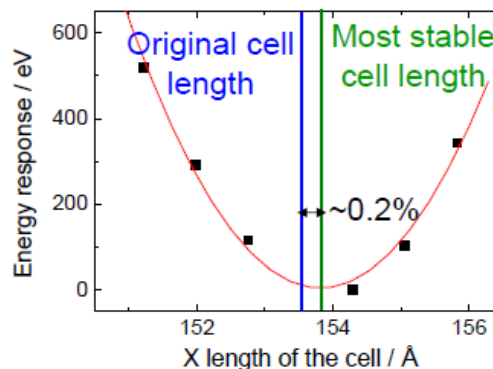
Discussion: comparison with a previous study

	Present study			Previous study*
	<543>	<453>	<345>	
Temperature / K	67 (at the end of simulation)			several hundreds
dpa	0.0084	0.0101	0.0091	1.8
Reduction of elastic property / %	-10.7 (C_{11})	-11.1 (C_{11})	-11.1 (C_{11})	-20 (Young's moduli)

- In spite of the large difference of dpa, the difference of reduction ratios of elastic property between the present and previous studies are not so large.
- In addition to considering the effect of grain boundary, He generation or something like that, it is necessary to count the temperature effect.
- That is, many defects must have been annihilated in the previous study.

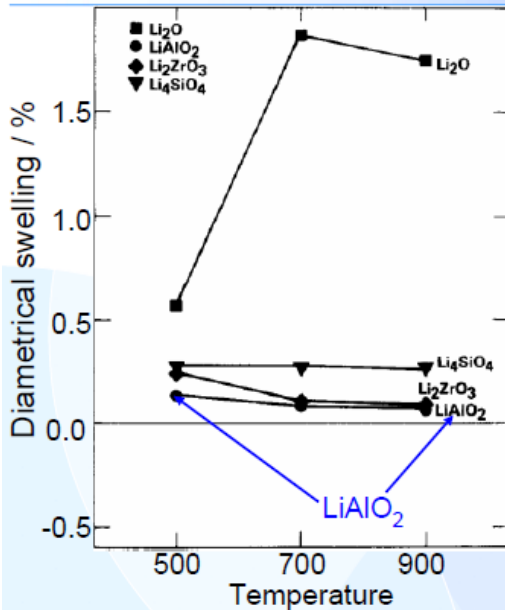
* W. Dienst, Journal of Nuclear Materials 212-215 (1994) 891-896.

Discussion: the effect of swelling



- The irradiation simulation cannot describe the swelling because of using NVE ensemble.
- However, the most stable cell length was quite near ($\Delta \sim 0.2\%$) the original cell length. This fact indicates that the significant swelling does not occur in the condition of the simulation.

Discussion: the effect of swelling

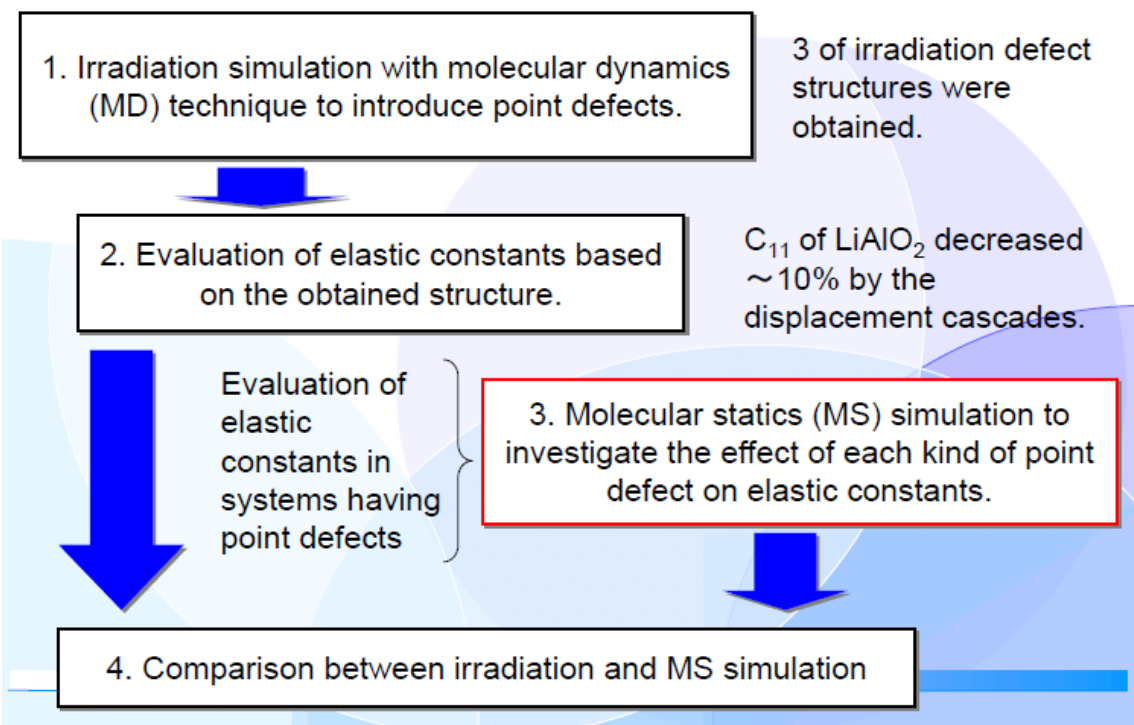


- The swelling of LiAlO₂ by neutron irradiation was small [1].
- Therefore, the influence of the neglect of swelling should be not so large.

Fig. Diametrical swelling of Li₂O, Li₄SiO₄, Li₂ZrO₃ and LiAlO₂ after achieving a burnup of 3×10^{20} captures/cm³ [1].

[1] G.W. Hollenberg, J. Nucl. Mater. 122 & 123 (1984) 896.

Contents of the presentation



Calculation method of elastic constants in systems having point defects

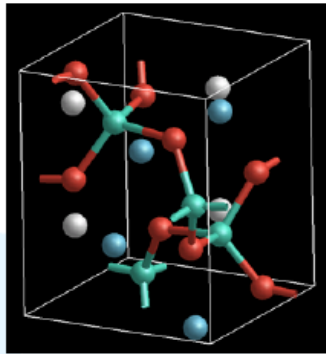


Fig. A primitive cell

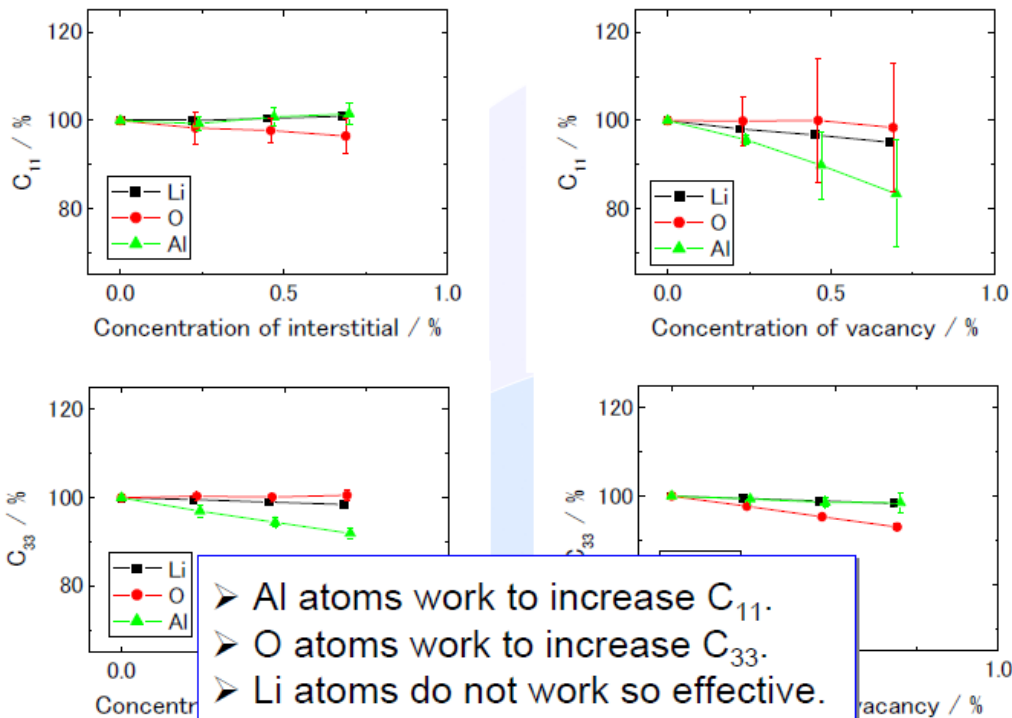
➤ In order to investigate what kind of point defects has significant influence, point defects of 1 ~ 3 were incorporated in $3 \times 3 \times 3$ supercells at random position, without mixture of defects of different element.

Table. The sort of point defects

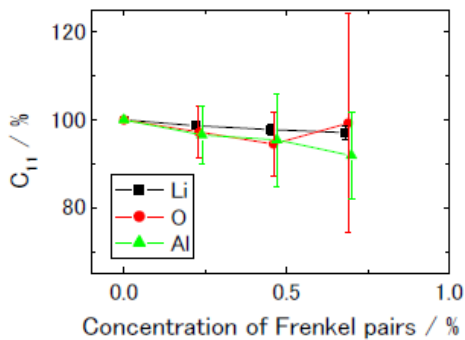
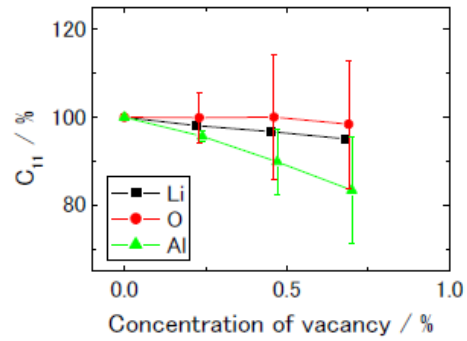
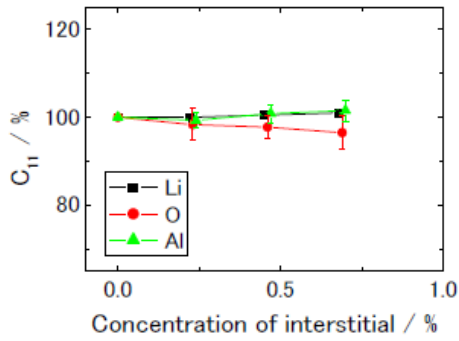
	Li	O	Al
vacancy			
interstitial			
Frenkel pairs			

- The concentrations of each defect were 0.23, 0.46 or 0.69%, respectively.
- The total charge was neutralized by applying a uniform background charge.
- After relaxation, elastic constants C_{11} and C_{33} were evaluated.
- Each calculation was conducted 100 times.

Effect of point defects on C_{11} and C_{33}



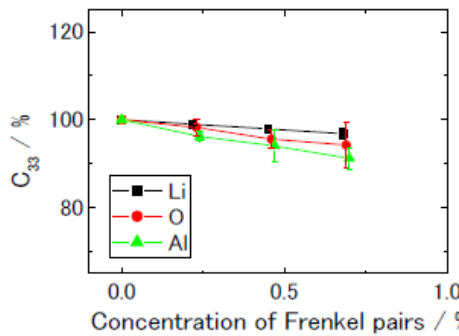
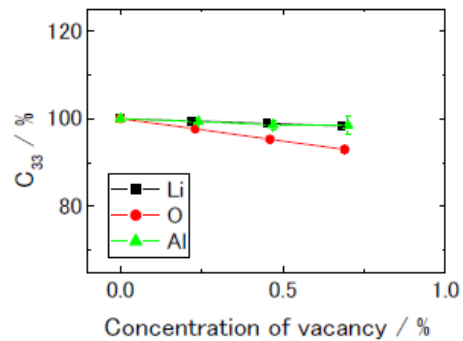
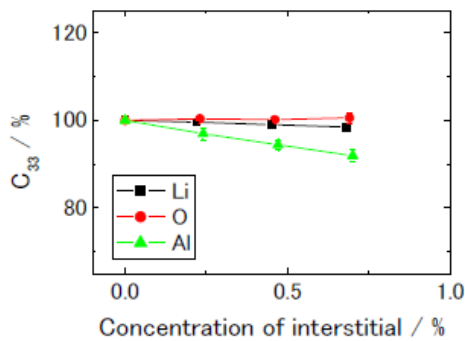
Effect of Frenkel pairs on C_{11}



➤ The result of Frenkel pairs seems like a sum of the result of interstitial and vacancy.

➤ This indicates that for C_{11} , the effect of interstitial – vacancy interaction is smaller than the effect of point defect itself.

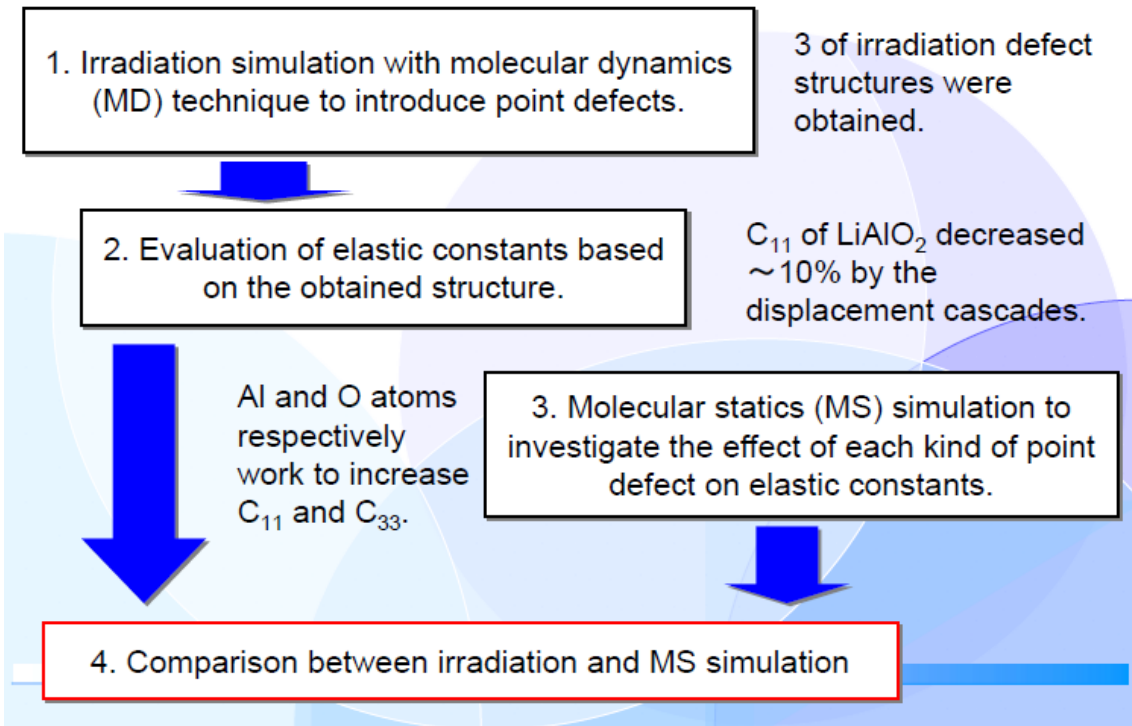
Effect of Frenkel pairs on C_{33}



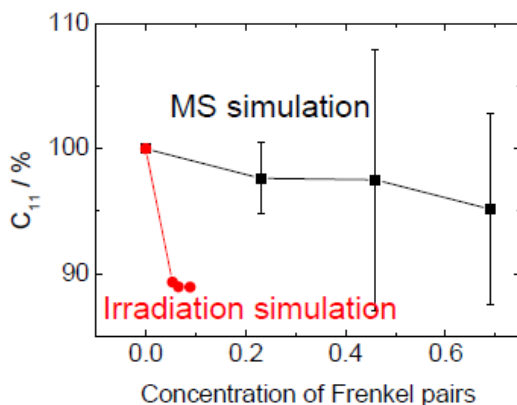
➤ Same as in C_{11} , the result of Frenkel pairs seems a sum of the result of interstitial and vacancy.

➤ This indicates that also for C_{33} , the effect of interstitial – vacancy interaction is smaller than the effect of point defect itself.

Contents of the presentation



Comparison between irradiation and MS simulation



MS simulation:

- The elements of Frenkel pairs were determined randomly (no weighting).
- For example, when the concentration is 0.69%, containing 3 Frenkel pairs in the system, sometimes all of them were Li, in another times they were Li, O and Al.

- Even if the concentration of Frenkel pairs are same, the pairs generated by displacement cascade much lowered C_{11} than the random configuration of Frenkel pairs.
- The Frenkel pairs by displacement cascade is more aggregative than the random configuration. Therefore, it is concluded that aggregation of point defects can lower the elastic property.

Conclusions

From the irradiation simulation:

- C_{11} of LiAlO_2 was lowered by displacement cascades.
- When the vacancy concentration was increased, C_{11} was lowered.
- It was indicated that the significant swelling does not occur in the condition of the simulation.

From the molecular statics calculation:

- Al and O atoms respectively work to increase C_{11} and C_{33} .
- Li atoms work not so effective.
- The effect of Frenkel pairs on C_{11} and C_{33} seems a sum of the effect of interstitial and vacancy.

From the comparison between irradiation and MS simulation:

- It can be said that aggregation of point defects can lower the elastic property.

11. Modeling of tritium behavior in ternary lithium oxides: in case of Li_2TiO_3

Takuji Oda, Satoru Tanaka
The University of Tokyo, 7-3-1 Hongo, Bunkyo-ku, Tokyo 113-8656, Japan
E-mail: oda@flanker.n.t.u-tokyo.ac.jp

Abstract

In order to understand behavior of hydrogen isotopes in Li_2TiO_3 , quantum mechanical calculation based on density functional theory was performed. With focusing on H^+ substitutional for Li^+ in Li_2TiO_3 , the stabilities, migration paths and migration barriers were evaluated. There were several stable sites for the substitutional H^+ in Li_2TiO_3 , and the sites were categorized into three groups by (1) position of Li vacancy and (2) H-O-Ti angle. Migration between two of these three sites was also divided into two types, jump and rotation. The jump has basically a larger barrier than the rotation. Based on obtained atomic-scale information, a kinetic Monte Carlo simulation was conducted to evaluate diffusion coefficients of T. The apparent activation energy for T diffusion was comparable between the present calculation and previous experiment results, although the absolute values were different by one or two orders of magnitude.

Keywords:

Li_2TiO_3 , hydrogen isotopes, tritium, diffusion, quantum mechanical calculation, DFT

1. Introduction

The interaction of hydrogen isotopes with radiation defects is one of the most influential factors determining tritium recovery rate and inventory in the solid breeding material of fusion reactors. This influence would be enhanced during reactor operation, as the concentration of defects increases. Therefore, understanding of the influence of radiation defects is important for establishing a safety and economical fuel cycle.

Among multiple candidates for the tritium breeding material, lithium oxide (Li_2O) has the longest history of researches on the influence of radiation defects on the behavior of hydrogen isotopes [1]. In various radiation defects, Li vacancy and F centers have attracted large attention, because the former are extensively generated via the tritium breeding reaction, and the latter are recognized to strongly affect the stability and the release behavior of tritium [2].

In the previous studies using quantum mechanical calculations, the stability of the hydrogen isotopes interacting with a Li vacancy [3] or an F^0 center [2, 4] has been evaluated. According to the calculation results, the interactions with these defects heighten the stability of hydrogen isotopes, and thus depress the tritium diffusivity and increase the tritium inventory. Moreover, the interaction mechanisms are different between a Li vacancy and an F center: the former seemed to migrate together with an H/D/T atom [3], while the latter seemed to trap it, and then release it by recombination with an O ion [5].

In comparison with Li_2O , knowledge on ternary lithium oxides (Li_2TiO_3 , Li_4SiO_4 , etc), which are promising candidates of tritium breeder at this moment, are limited. It would be due to complicated crystalline structure of these materials, easy variation of crystalline composition and easy inclusion of impurity such as hydroxide and carbonate. Because these points make experiment difficult, researches using computational simulation are essential so as to understand the tritium behavior in ternary lithium oxides.

In the present study, we conducted quantum mechanical calculations for Li_2TiO_3 , based on density functional theory (DFT). Prior to studying the influence of radiation defects on the tritium behavior, the stability, migration path, and migration barrier of hydrogen isotopes substitutional to Li (described as sub-H, hereafter) in Li_2TiO_3 were focused. In Li_2O , sub-H participates in an O-D bond ($-\text{OD}^{\cdot}$), and $-\text{OD}^{\cdot}$ is known as the main chemical state [6]. In addition, it was confirmed by both theoretical calculation [3] and experiment [7] that sub-H is more stable than interstitial H^+ , which is another possible $-\text{OD}^{\cdot}$. Hence, focusing on sub-H would be reasonable as the first step of computational simulation.

2. Method and computational details

First of all, lattice constants were optimized with a primitive cell of Li_2TiO_3 . Then, with fixing lattice constants to the optimized values, a constitutional Li atom was replaced for a H atom, in order to introduce a sub-H. As a system containing a sub-H, $\text{Li}_{15}\text{O}_8\text{Ti}_2\text{H}$ and $\text{Li}_{31}\text{Ti}_{16}\text{O}_{48}\text{H}$ were used under

three-dimensional periodic boundary condition. Because the number of crystallographically different sites is not one for Li, we tested around 10 configurations that would be possible sub-H configurations. Subsequently, migration of sub-H between two of several sub-H sites was evaluated using nudged elastic band method [8], in order to determine migration path and migration barrier of sub-H.

All calculations were performed using VASP code based on DFT and the plane-wave pseudopotential approach. The GGA-PBE functional and ultrasoft pseudopotentials were used: the number of electrons treated explicitly is 3 for Li, 12 for Ti, 6 for O and 1 for H. The k-point sampling and energy cutoff, which are key parameters for convergence of total energy, were determined so as to obtain convergence of around 0.1 eV for relative stabilities and migration barriers of sub-H.

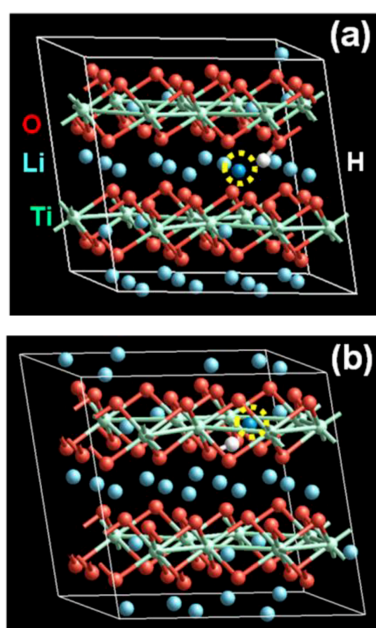
3. Results and discussion

3.1. Configurations and stabilities of sub-H

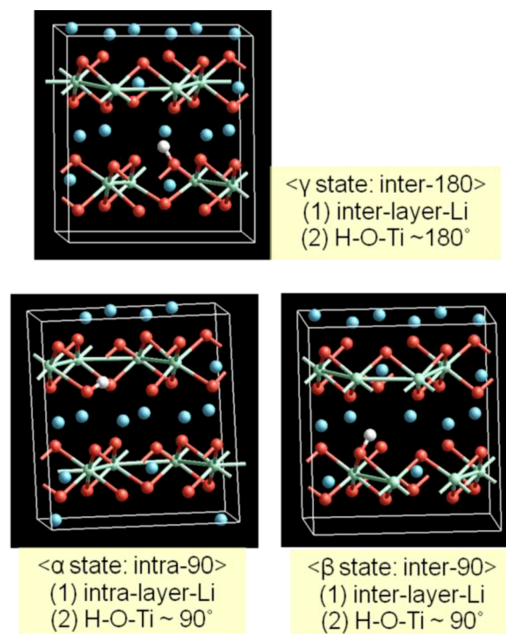
Figs. 1 show two different sites for Li atoms constituting Li_2TiO_3 . In Li_2TiO_3 , constituent Ti and O atoms form layers perpendicular to the z-axis. The focused Li atom (pointed by the yellow circle) exists between two neighboring Ti-O layers in Fig. 1a, while exists within a layer in Fig. 1b. Hereafter, these two types of Li atoms are described as inter-layer-Li and intra-layer Li, respectively.

Figs. 2 show three typical stable sites for sub-H. Each site is characterized by (1) a type of Li vacancy (inter or intra) and (2) H-O-Ti angle (90° or 180°). The combination of (1) intra-layer-Li and (2) 180° does not appear in Li_2TiO_3 due to constraint from the crystalline structure. In any case, O-H bond is formed, which means that sub-H exists as $-\text{OH}^-$.

Fig. 3 shows correlation between the stability and configurational parameters (Ti-H/O-H/Li-H distances) of sub-H in Li_2TiO_3 . It is clear that the stability of sub-H can be categorized by $\alpha/\beta/\gamma$ states in Figs. 2, rather than such inter-atomic distances.



Figs. 1. Two types of different sites for Li atoms in Li_2TiO_3 : (a) inter-layer-Li (pointed by the yellow circle) existing between Ti-O layers, and (b) intra-layer-Li existing in a Ti-O layer.



Figs. 2. Three types of different sites for sub-H in Li_2TiO_3 . Each site is characterized by combination of (1) a type of Li vacancy (inter/intra) and (2) H-O-Ti angle ($90^\circ/180^\circ$).

3.2. Migration paths and barriers for sub-H

The migration paths between two of $\alpha/\beta/\gamma$ states were evaluated, in order to deepen understanding on diffusion mechanisms of hydrogen isotopes (sub-H). Although more than 10 paths are possible, migration motions of sub-H are divided into two types: jump and rotation. Schematic drawings are given in Figs. 4,

together with concrete examples of these motions: from β to β for the jump, and from β to γ for the rotation. In case of the jump motion, Li vacancy attracting H atom is not changed, while O atom to which the H atom is binding is changed. On the other hands, in case of the rotation motion, Li vacancy attracting H atom is changed, while O atom to which the H atom is binding is not changed. Repetition of these two motions results in diffusion of sub-H in Li_2TiO_3 . Note that only one type of motions cannot induce diffusion of sub-H.

Barriers for the jump motions are basically lower than those for the rotation motions: 0.5~1.0 eV and 1.2~1.6 eV, respectively. This is reasonable because jump motions are basically composed by simple movement of sub-H, while the rotation motions require exchange of positions between Li atom and sub-H. As the distance between Li atom and sub-H becomes small during the exchange process, electrostatic repulsive forces between Li and H atoms (Li^+ and H^+ , nominally) would heighten barriers for the rotation motions.

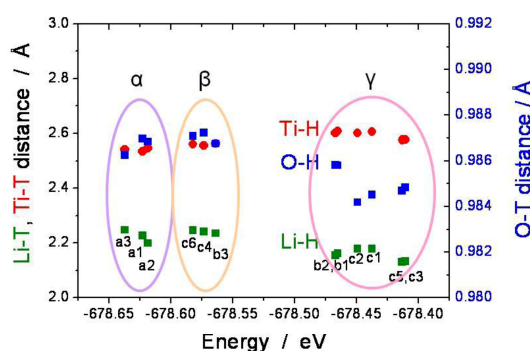
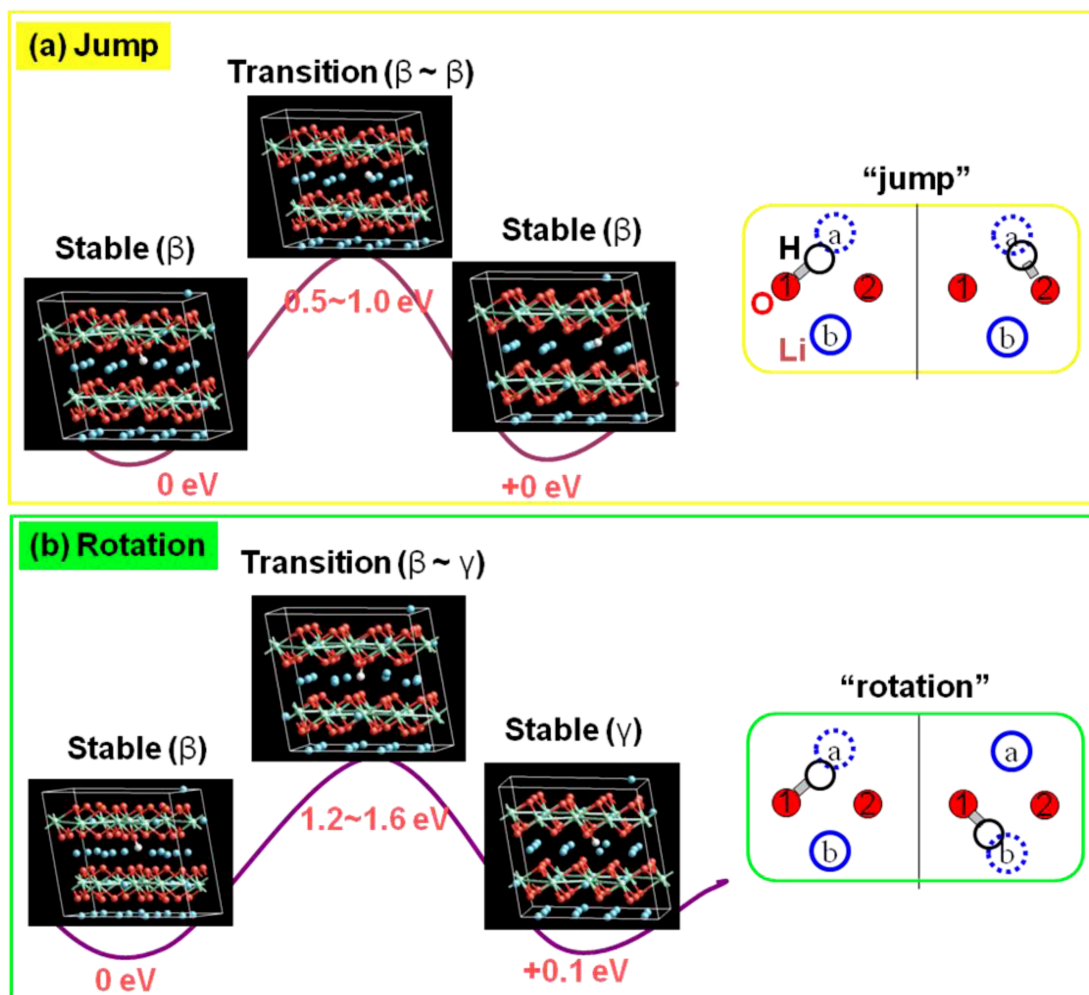


Fig. 3. Correlation between the stability and configurational parameters (Ti-H/O-H/Li-H distances) of sub-H in Li_2TiO_3 .



Figs. 4. Schematic drawing of jump and rotation motions of sub-H. These two motions are needed for diffusion of sub-H in Li_2TiO_3 . Barriers for jump motions are 0.5~1.0 eV, and those for rotation motions are 1.2~1.6 eV.

Based on the evaluated migration paths and migration barriers, we performed a kinetic Monte Carlo simulation [9], in order to obtain diffusion coefficients of H/D/T. The apparent activation energy of tritium diffusion was comparable between the present calculation result and previous experimental result, around 1 eV [10]. However, absolute values of calculated diffusion coefficients were lower than the experimental values by one or two orders of magnitude. There are three possible reasons of this discrepancy:

- (1) Calculation results contain significant errors.
- (2) Role of interstitial H^+ was not taken into account in the present calculation.
- (3) Experimentally determined diffusion coefficients were underestimated.

As for (2), it was shown that interstitial H^+ has much higher diffusivity than sub-H in Li_2O [3]. Hence, consideration of interstitial H^+ would heighten the diffusion coefficients. Regarding (3), in fact, lower diffusion coefficients have been also reported [11]. To conclude these points, further studies are needed for both calculation and experiment.

4. Summary

In order to understand behavior of hydrogen isotopes in Li_2TiO_3 , quantum mechanical calculation based on density functional theory was performed. With focusing on H^+ substitutional for Li^+ in Li_2TiO_3 , the stabilities, migration paths and migration barriers were evaluated. There were several stable sites for the substitutional H^+ in Li_2TiO_3 , and the sites were categorized into three groups by (1) position of Li vacancy and (2) H-O-Ti angle. Migration between two of these three sites was also divided into two types, jump and rotation. The jump has basically a larger barrier than the rotation. Based on obtained atomic-scale information, a kinetic Monte Carlo simulation was conducted to evaluate diffusion coefficients of T. The apparent activation energy for T diffusion was comparable between the present calculation and previous experiment results, although the absolute values were different by one or two orders of magnitude. In order to clarify the reasons of this discrepancy, further studies are needed for both calculation and experiment.

References

- [1] A. Donato, Fusion Eng. Des. 38 (1998) 369.
- [2] H. Tanigawa, S. Tanaka, J. Nucl. Mater. 307-311 (2002) 1446.
- [3] R. Shsh, A.D. Vita, V. Heine, M.C. Payne, Phys. Rev. B 53 (1996) 8257.
- [4] H. Tanigawa, S. Tanaka, Fusion Eng. Des. 61-62 (2002) 789.
- [5] M. Oyaidzu et al., J. Nucl. Mater. 329 (2004) 1313.
- [6] K. Okuno, H. Kuco, J. Nucl. Mater. 138 (1986) 31.
- [7] T. Oda, Y. Oya, S. Tanaka, J. Nucl. Mater. 346 (2005) 306.
- [8] G. Mills, H. Jonsson, G.K. Schenter, Surf. Sci. 324 (1995) 305.
- [9] T. Oda, S. Tanaka, in preparation.
- [10] T. Tanifuji et al., J. Nucl. Mater. 258 (1998) 543.
- [11] T. Kinjyo et al., Fusion Eng. Des. 83 (2008) 580.

**Modeling of tritium behavior in ternary lithium oxides:
in case of lithium titanate**

Takuji Oda, Satoru Tanaka

Department of Nuclear Engineering and Management, The University of Tokyo, Japan

Tritium economy is one of the key issues for realization of commercial fusion reactors. In order to estimate it precisely, tritium inventory in materials should be grasped. In the present paper, we focus on the tritium inventory in solid breeders. In most of the previous works, these subjects were studied by neutron irradiation experiment. However, the reproductivity of results was low due to multiple factors affecting tritium behavior, such as defect density, concentration of other isotopes (H and D), material composition (impurity, non-stoichiometry), etc. For more precise prediction of the inventory, more detailed information about how these factors affect tritium behavior is needed. Hence, we perform atomic-scale modeling about tritium behavior in lithium-containing oxides. Li_2TiO_3 was studied in the present paper, because this material has showed favorable tritium release property and is considered as a promising candidate of tritium breeder.

Quantum mechanical calculation based on density functional theory (DFT) was conducted using *VASP* code. Li_2TiO_3 crystal was modeled by $\text{Li}_{16}\text{Ti}_8\text{O}_{24}$ or $\text{Li}_{32}\text{Ti}_{16}\text{O}_{48}$ supercells with periodic boundary conditions. Stability and diffusion barrier of hydrogen isotopes were evaluated. Then, these results were integrated by Monte Carlo technique in order to evaluate tritium inventory in several systems of different temperatures.

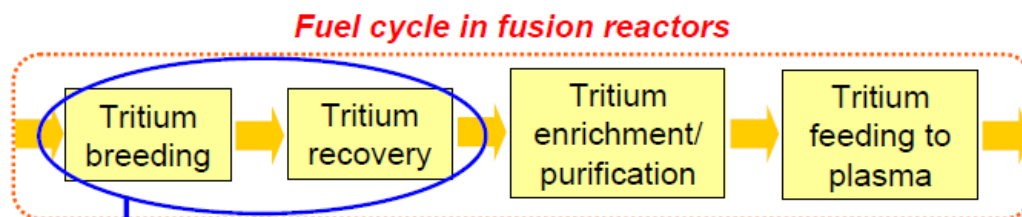
It was indicated by quantum mechanical calculation that Li vacancies trap hydrogen atoms in Li_2TiO_3 . The charge state of tritium trapped by Li vacancy is T^+ , and it binds to a neighboring O^{2-} by forming $-\text{OT}^+$. The diffusion of T^+ trapped by Li vacancy was composed by two kinds of motions: rotation and jump. The rotation has a higher barrier than the jump basically, and thus should be the rate-determining process. T^+ trapped by Li vacancy showed multiple different configurations in Li_2TiO_3 . These configurations were categorized into three groups according to Ti-O-T angle and the position of Li vacancy. These qualitative informations were used to construct a Monte Carlo model, and the quantitative values (frequency, barrier) obtained by quantum mechanical calculation were used as input parameters of the model. In Monte Carlo simulation, it was observed that increase of defect concentration results in high inventory and low diffusivity of tritium.

Modeling of tritium behavior in ternary lithium oxides: in case of Li_2TiO_3

Takuji Oda, Satoru Tanaka

*Department of Nuclear Engineering and Management,
The University of Tokyo*

Background

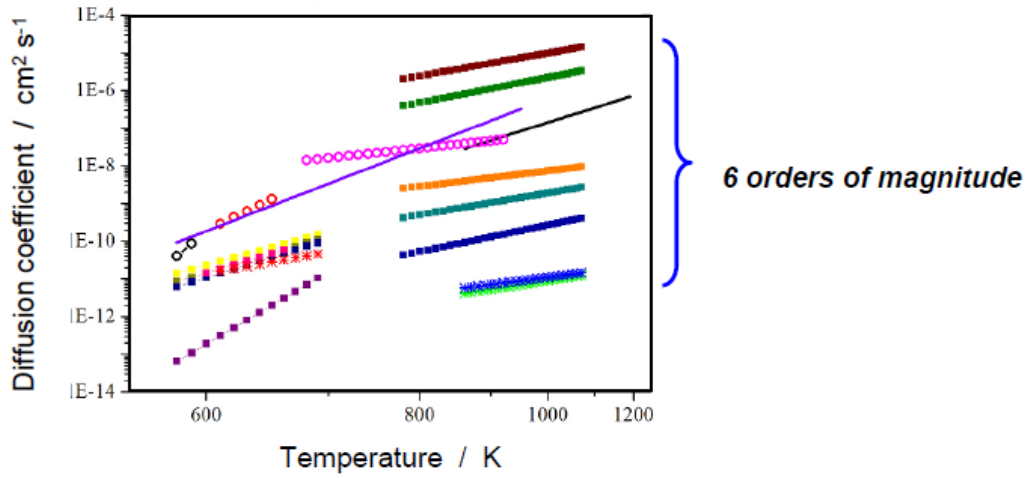


- ◆ Need to breed tritium adequately. (for sustaining a fuel cycle)
- ◆ Need to recover bred tritium thoroughly. (for economy and safety)
- ◆ Need to them reliably. (for commercialization)

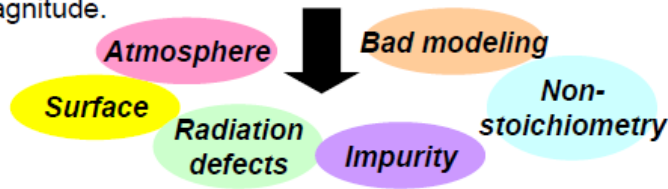
◆ Need to create a model which predicts tritium recovery amount/rate precisely.

>> a model based on short-period experiments is adequate ??

Previous works: Tritium diffusivity in lithium oxides

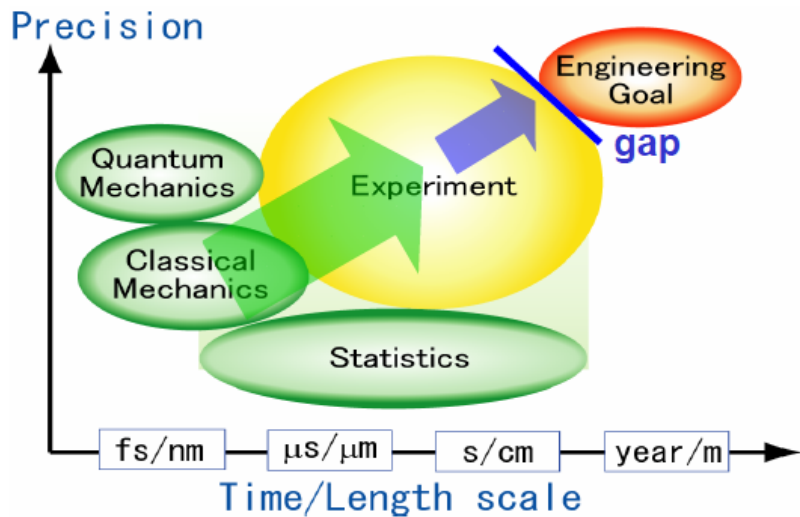


For example, reported diffusion coefficients of tritium in Li_2O are scattered over 6 orders of magnitude.

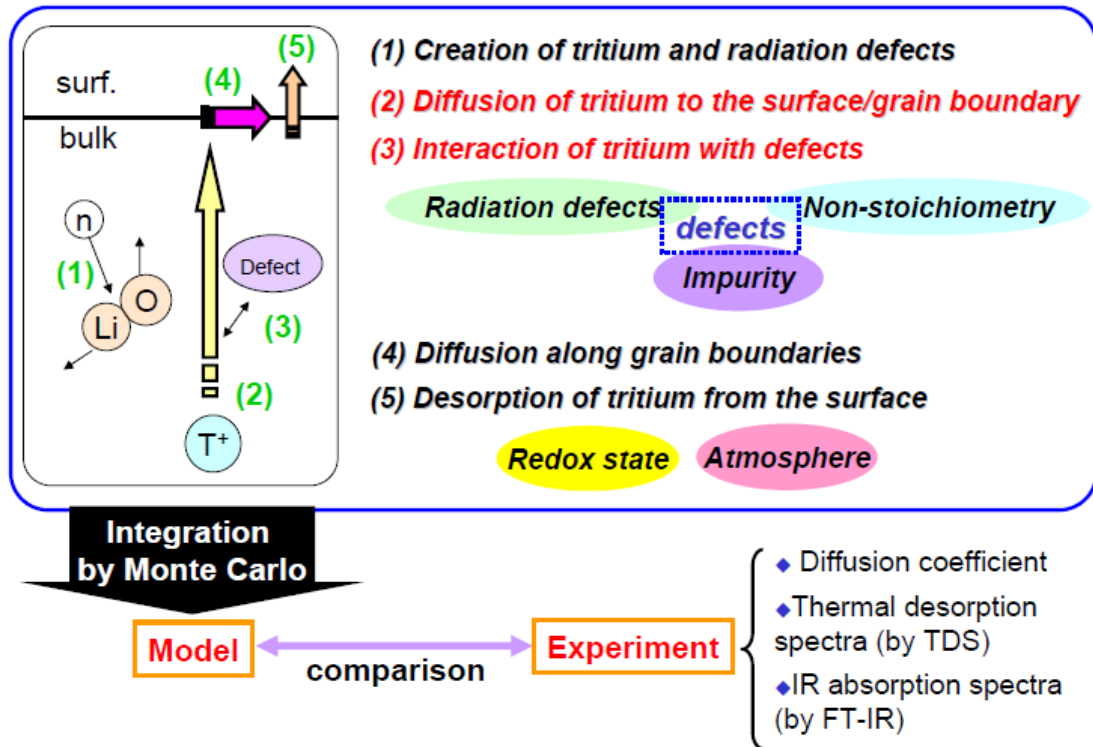


How to approach (1/2) : Multi-scale modeling

<Key points>
 Establish a **chain of knowledge** over microscopic/macrosopic range by **integration of detailed understanding on the mechanisms of fundamental phenomena**.



How to approach (2/2) : fundamental processes



Contents

1. Tritium in Li_2TiO_3 (quantum mechanical calculation: DFT)

- ✓ Stable sites for Tritium in Li_2TiO_3
- ✓ Key parameters to arrange the stability
- ✓ Migration paths from a stable site to another
- ✓ Diffusion mechanism: jump + rotation
- ✓ Calculated T diffusion coefficients with experimental values

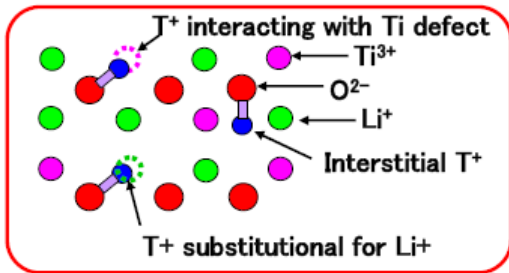
Software: VASP

- ◆ DFT-GGA (Functional: PBE)
- ◆ Plane wave basis set with PAW potential (projector augmented-wave)
- ◆ 3-D periodic boundary condition

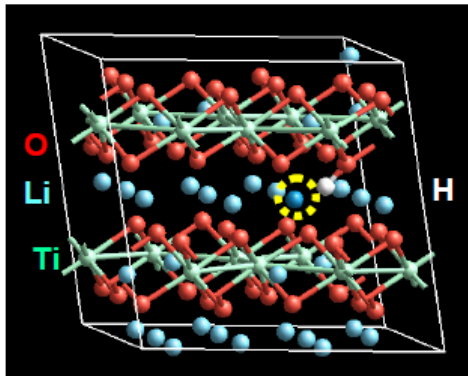
2. Modeling of diffusion of T interacting with defects

- ✓ Influence of defect concentration on T diffusivity
- ✓ Influence of [H+D+T] concentration on T diffusivity
- ✓ Direct comparison with experiment: via TDS spectrum

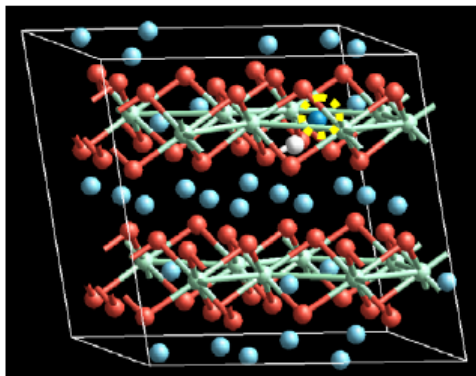
1. Tritium in Li_2TlO_3



Focus on "T⁺ substitutional for Li⁺" due to
 (1) its high stability
 (2) high formation rate of Li vacancy



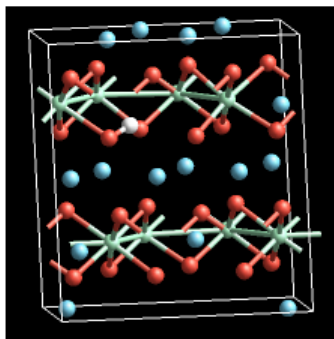
Exist **between layers** (inter-layer)



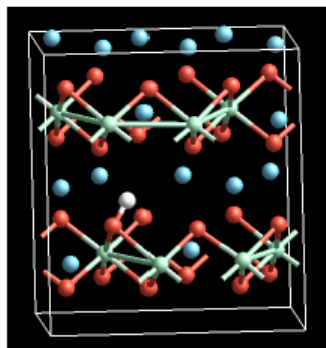
Exist **within a layer** (intra-layer)

1. Key configuration parameters (1/2)

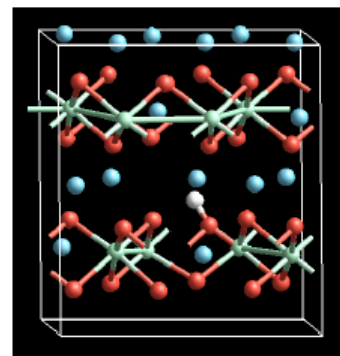
Existence states of T can be categorized into three groups according to
 (1) position of Li vacancy (inter/intra-layer)
 (2) T-O-Ti angle (90° or 180°)



< α state: intra- 90° >
 (1) Li: intra-layer
 (2) T-O-Ti = 90°



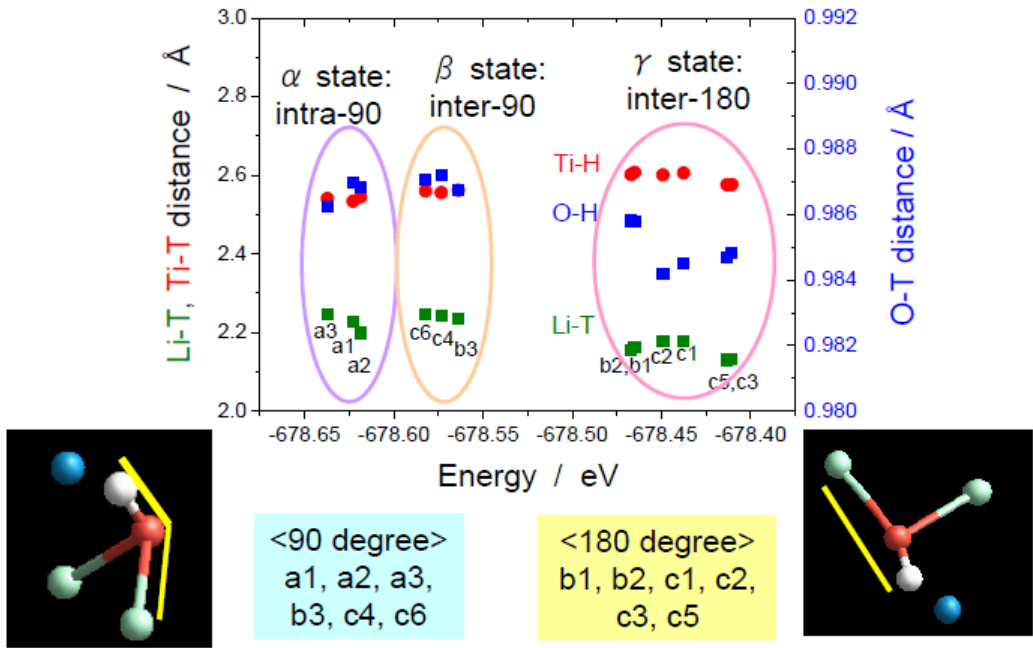
< β state: inter- 90° >
 (1) Li: inter-layer
 (2) T-O-Ti = 90°



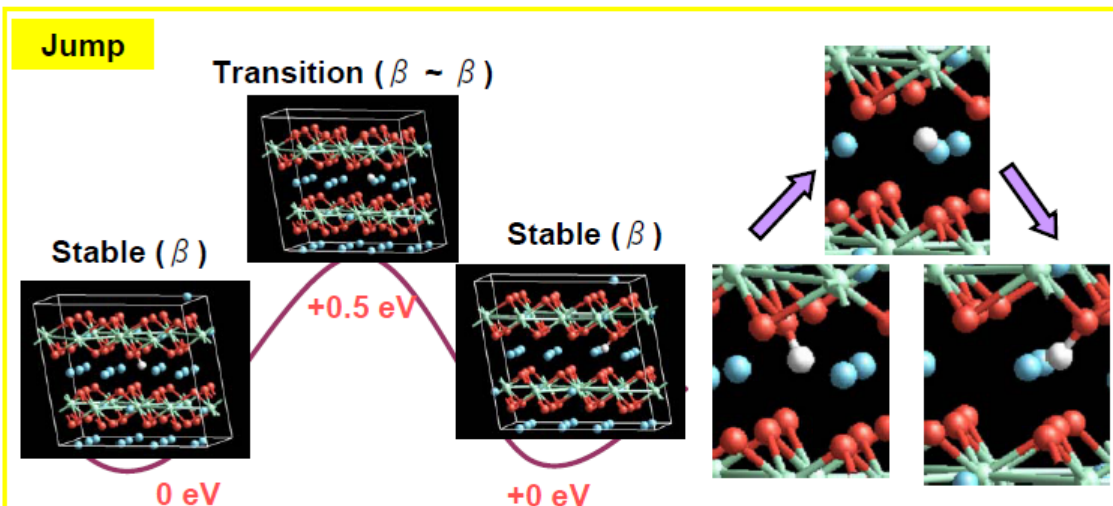
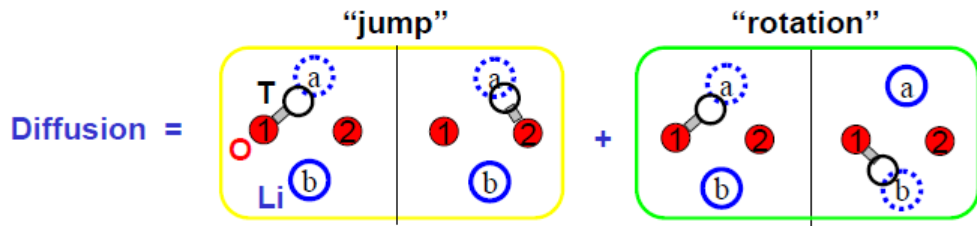
< γ state: inter- 180° >
 (1) Li: inter-layer
 (2) T-O-Ti = 180°

1. Stability and configuration parameters (2/2)

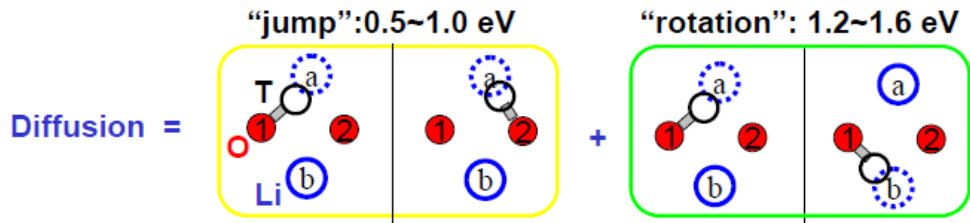
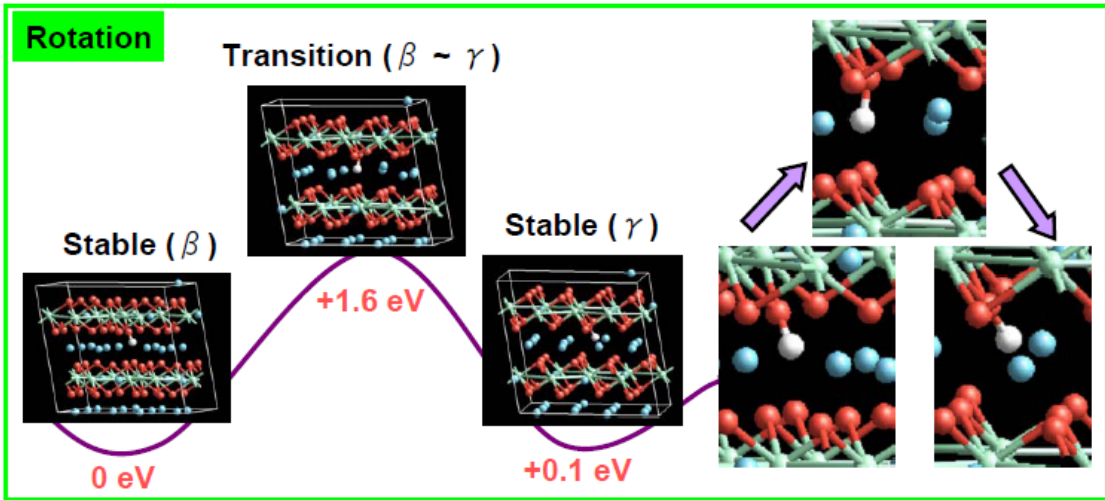
Potential energy comparison of “substitutional T⁺ for Li⁺” in various configurations



1. T diffusion processes (1/2) : “jump”



1. T diffusion processes (2/2) : "rotation"

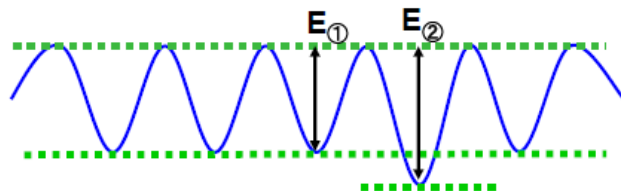


1. Definition of diffusivity in atomic-scale

Classical diffusion theory:

$$D_{CT} = \frac{d^2}{6} \times f \times \left\{ n_{path} \times \nu \times \exp\left(-\frac{E_d}{RT}\right) \right\}$$

- d : jump distance (m)
- f : correlation factor
- n_{path} : the number of equivalent paths
- ν : effective frequency (s^{-1})
- E_d : diffusion barrier (eV)

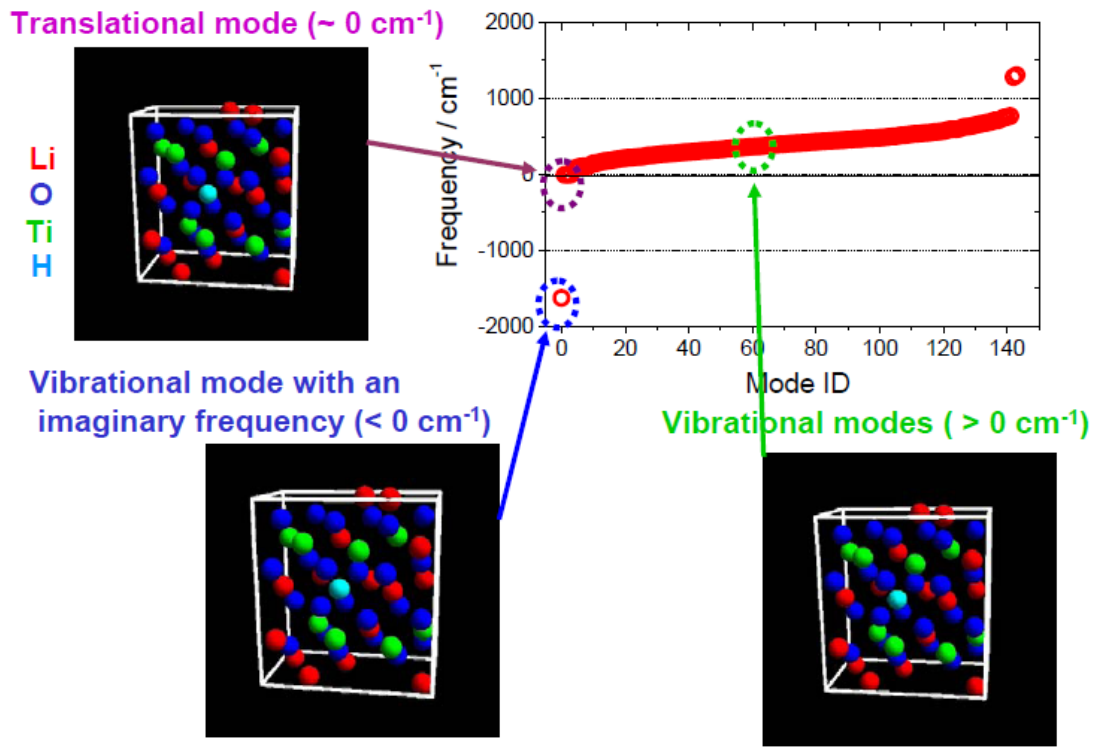


$E_d \gg$ DFT (+ zero-point energy correction)

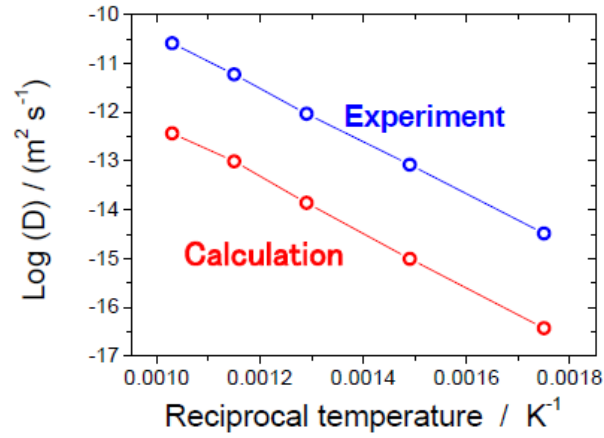
$$\nu = \frac{\left(\prod_{i=1}^N \nu_i \right)}{\left(\prod_{i=1}^{N-1} \nu'_i \right)} \gg \text{DFT (vibration analysis)}$$

The other factors related to crystal structure and path configuration
 \gg MC

1. "Effective frequency" from vibration analysis



1. Comparison of T diffusivity with experiment



<Experiment*>
 $D[\text{m}^2 \text{s}^{-1}] = 1\text{E-}5 \exp(-104 \text{ kJ mol}^{-1} / RT)$

<Calculation>
 $D [\text{m}^2/\text{s}] = 2.5\text{E-}7 \exp(-107 \text{ kJ mol}^{-1} / RT)$

*T. Tanifuji et al., JNM 258 (1998) 543.

The calculation value underestimates the diffusion coefficient by around 2 orders of magnitude at any temperature.

- ◆ Due to diffusion as interstitial T⁺ or along grain boundaries ?
- ◆ But, pre-exponential factor of experiment may be too small...

$$D_{CT} = \frac{d^2}{6} \times f \times \left\{ n_{path} \times v \times \exp\left(-\frac{E_d}{RT}\right) \right\} \quad \left\{ d \sim 2 \text{ \AA} = 2\text{E-}10 \text{ m}, v = 1\text{E}13 \text{ s}^{-1}, f \sim 1, n_{path} \sim 1 \right\} \gg 4\text{E-}7 \text{ m}^2$$

Contents

1. Tritium in Li_2TiO_3 (quantum mechanical calculation: DFT)

- ◆ The stability of T can be arranged by **position of Li vacancy (inter/intra-layer) & T-O-Ti angle (90° or 180°)**.
- ◆ The T diffusion consists of two fundamental motions: **jump & rotation**.
- ◆ The calculated diffusion coefficients were lower than those of experimental values by 2 orders of magnitude.

2. Modeling of diffusion of T interacting with defects

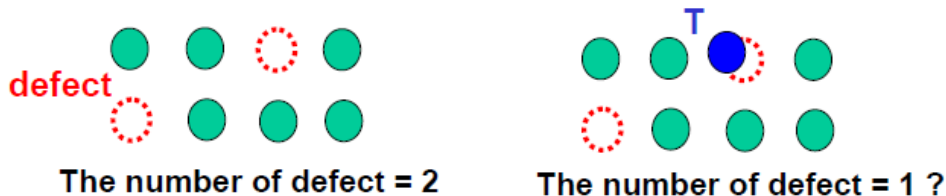
- ✓ Influence of defect concentration on T diffusivity
- ✓ Influence of [H+D+T] concentration on T diffusivity

2. Approach: How to include interaction with defects ?

<Key parameters>

- (i) Tritium concentration
⇒ Change during reactor operation by creation and release.
- (ii) Defect concentration
⇒ Change during reactor operation by creation and recovery.

As tritium cannot interact with defects occupied by the other tritium,



Assumption on “constant defect density” & “rapid equilibration in distribution of T interacting with defects”

We can estimate “*average interaction time*” by means of mean field theory.

12. Integration and Verification of Tritium Release Model in Thermo-hydraulic Analysis Code

Y. Seki¹, T. Hirose¹, H. Tanigawa¹, A. Yoshikawa¹, M. Enoda¹,
S. Fukada², M. Nishikawa², T. Kinjo²

1: *Japan Atomic Energy Agency, Naka-shi, Ibaraki-ken, 311-0193 Japan,*
enoeda.mikio@jaea.go.jp

2: *Kyushu University, Fukuoka-shi, Fukuoka-ken, 812-8581, Japan*

Development of Water Cooled Solid Breeder (WCSB) TBM is being performed as the primary candidate of ITER Test Blanket Module (TBM) of Japan. Prior to the installation of each TBM, it is necessary to develop the capability of the analyses of all essential functions of the blanket, because the validation of the analyses tools by the TBM performance data under the real fusion environment of ITER enables extrapolation of the design and performance analyses to DEMO blanket. Especially the analysis tool of tritium control in the blanket system is one of the most important issues. From this view point, this paper overviews the status of the integration and verification of tritium release model in thermo-hydraulic analysis code.

Tritium behavior in the blanket is a complex phenomenon which consists of tritium generation, tritium release from the breeder pebble, purge gas thermo-hydraulics and tritium permeation. Objective of this study is to construct the total tritium behavior simulation taking into account all essential tritium transfer process.

The effect of thermo-hydraulics of the purge gas in the breeder pebble bed was studied numerically, using 3D thermo-hydraulic analysis code "FLUENT". Taking into account the distribution of the tritium generation rate and nuclear heating rate distribution in the radial direction of the blanket, the purge gas stream and tritium concentration was calculated by the 2D numerical simulation, assuming the tritium release mass transfer conductance is negligible. By the result of tritium concentration distribution in the breeder pebble bed, it was clarified that the concentration near by the cooling panel is two times higher than at the center of the breeder pebble bed.

Tritium release model, developed by Nishikawa et al., was integrated into a commercial "FLUENT". The calculation of the tritium behavior on the first breeder layer of WCCB TBM was performed. Currently, the consistency of the calculated result is being examined.

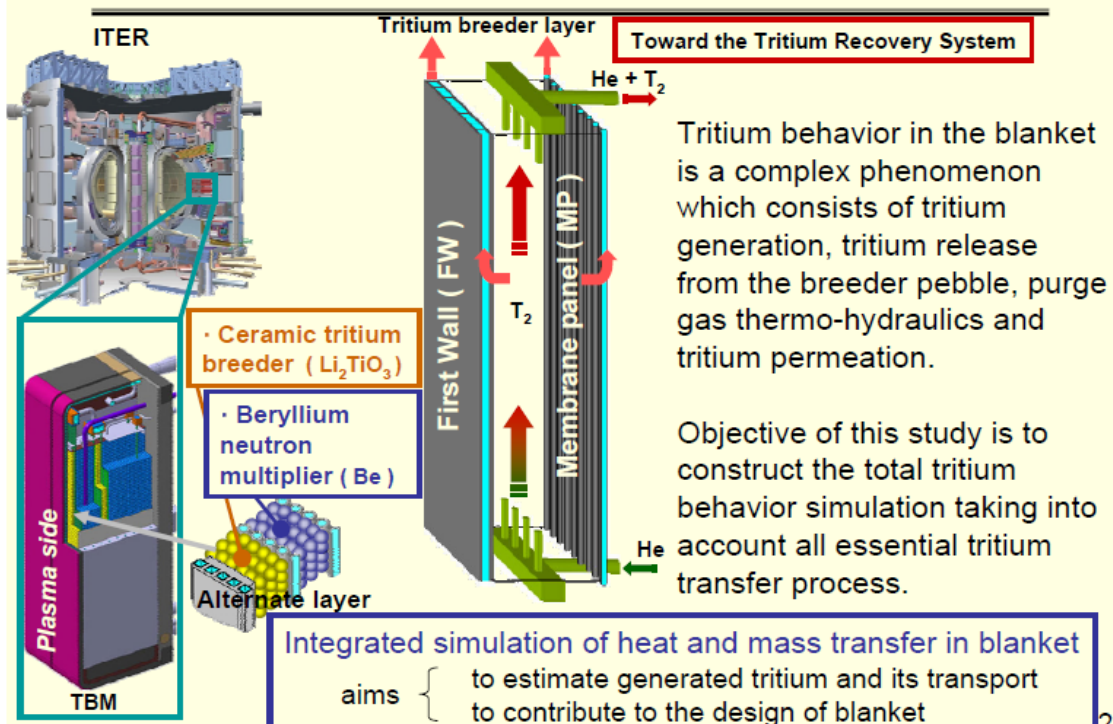
15th International Workshop on CERAMIC BREEDER BLANKET INTERACTIONS (CBBI-15)
Sapporo, Japan, 3 – 5, Sept. 2009

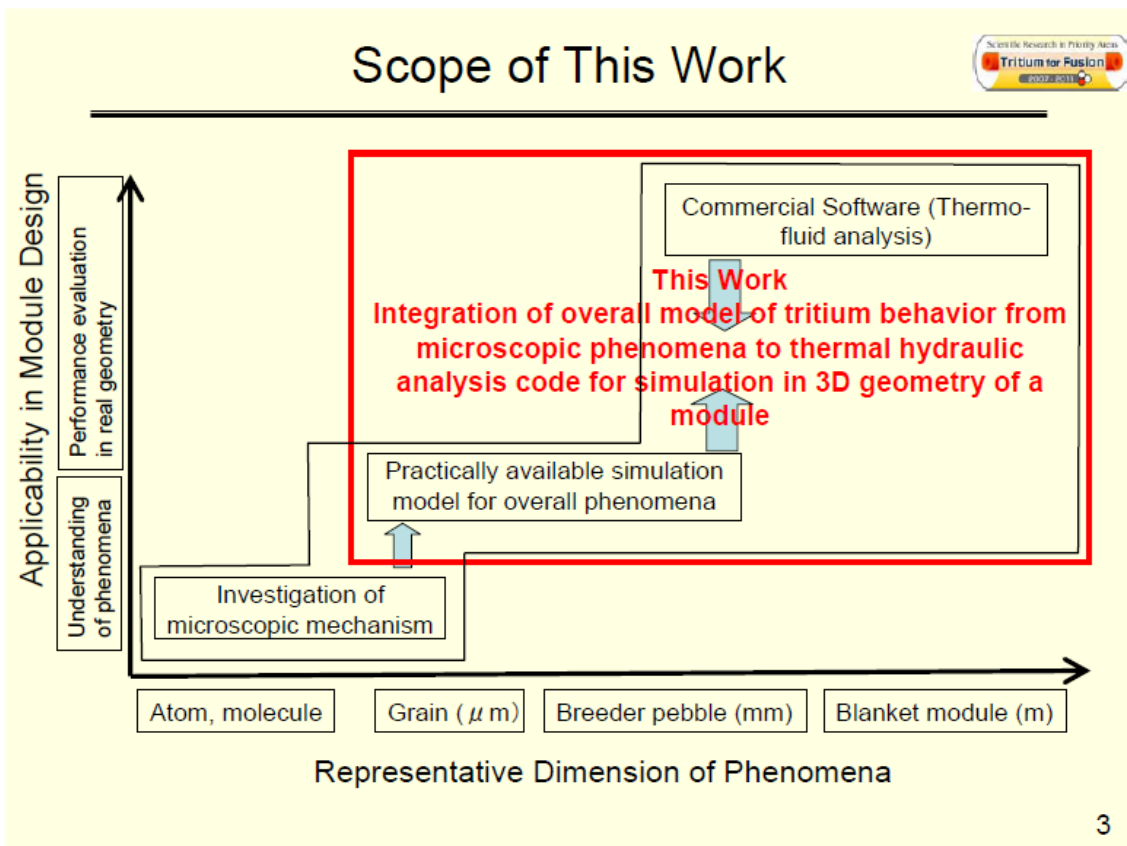
Integration and Verification of Tritium Release Model in Thermo-hydraulic Analysis Code

Y. Seki, T. Hirose, H. Tanigawa, A. Yoshikawa, M. Enoda (JAEA)
and
S. Fukada, M. Nishikawa, T. Kinjo (Kyushu University)



Background and Objective



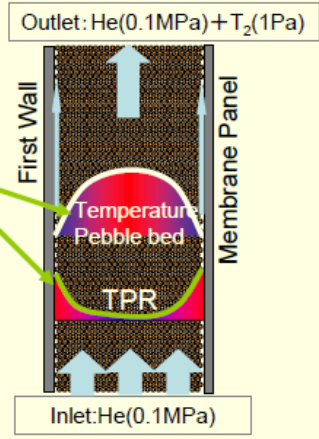
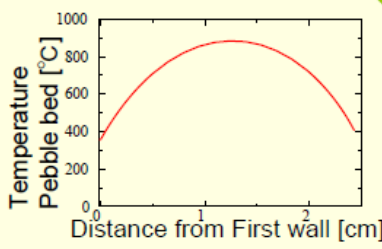
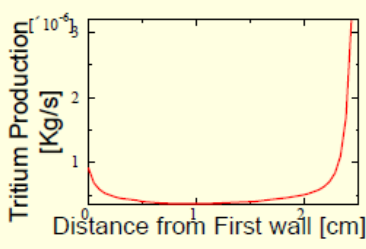


Analysis of behavior of He purge gas in breeder pebble beds

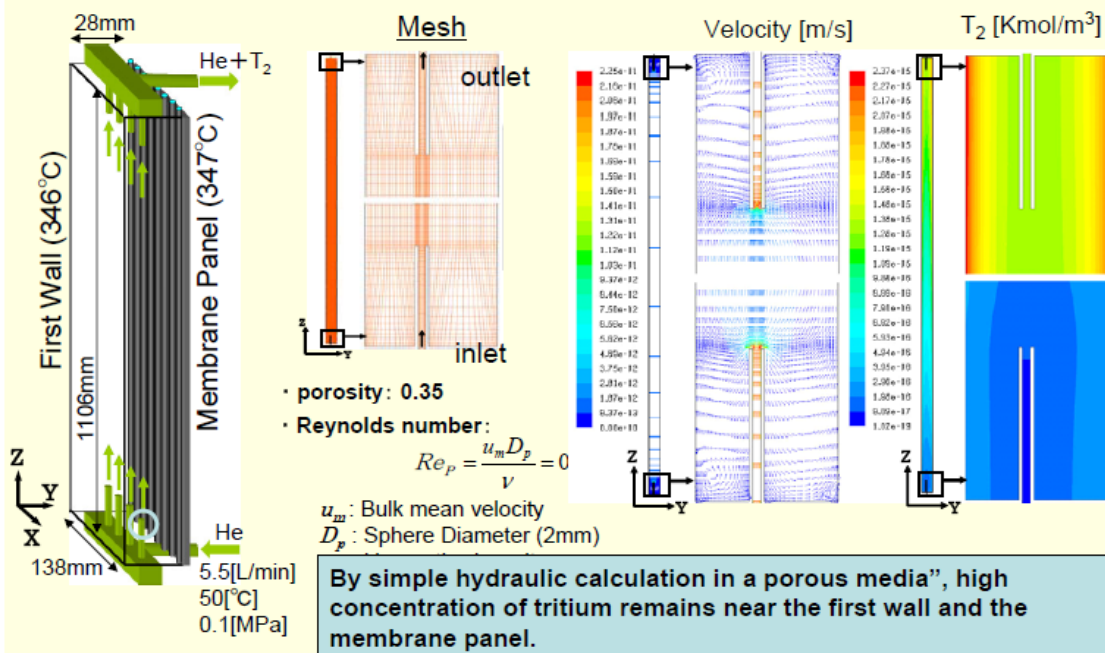
The effect of thermo-hydraulics of the purge gas stream in the breeder pebble bed was studied numerically. For preliminary analysis, the purge gas stream was calculated by 2D thermo-hydraulic simulation code "FLUENT" to examine the effect of distribution of tritium generation in a low flow rate of the purge gas.

Taking into account the distribution of the tritium generation rate and nuclear heating rate distribution in the radial direction of the blanket, the purge gas stream and tritium concentration were calculated by the 2D numerical simulation, assuming the tritium release mass transfer conductance is negligible.

Tritium production and temperature of pebble bed obtained by one-dimensional nuclear and thermal analyses are applied to source terms.



Computational Configuration and Results

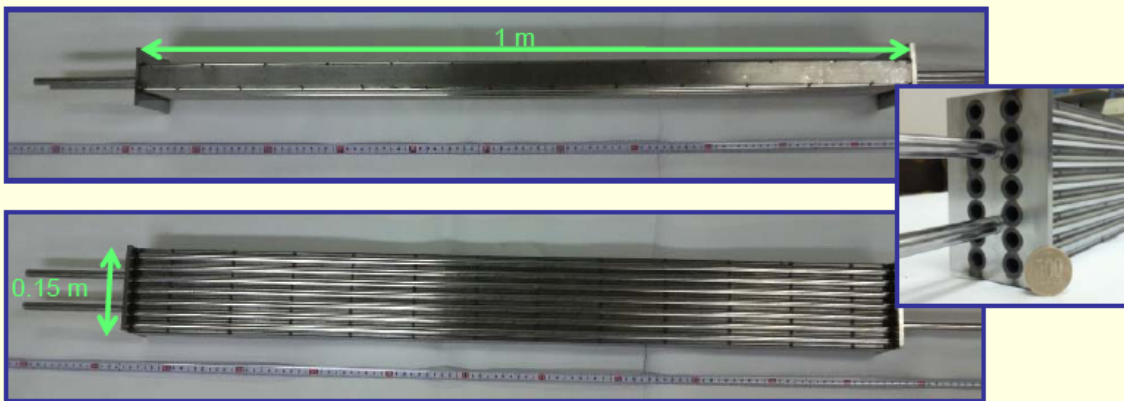


It is necessary to further investigate the flow in the pebble bed. 5

Mockup for Breeder Pebble Packing Test and Purge Gas Flow Test



The mockup represents real structure and dimension of the WCCB TBM, and is made of F82H.



Test Items

- Breeder pebble packing test → Observation of packing fraction
- Purge gas flow test → Measurement of pressure drop



Comparison data of purge gas flow behavior

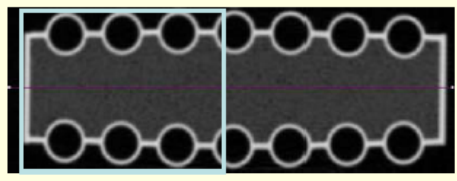
Breeder Pebble Bed Packing Test



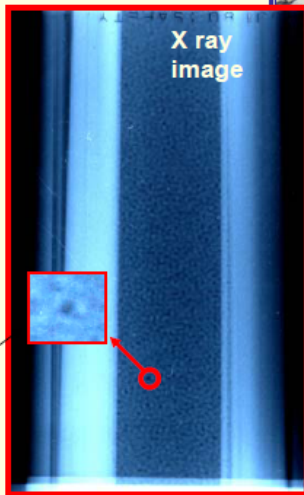
Real breeder pebbles (Li_2TiO_3 1mm dia. Sphere) were packed in the real scale Breeder Pebble Bed Mockup. Overall packing fraction was measured by volume and weight. Also, packing status was observed by X-CT scanning Tomography.



Overall Packing Fraction, P.F. = 64.1% (by volume and weight)

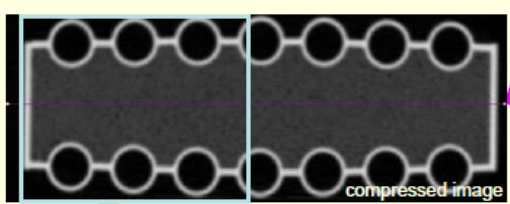


X-CT image

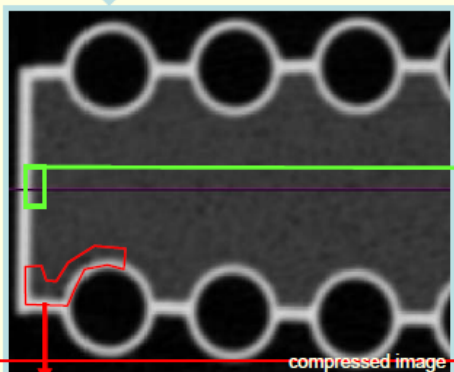


By X-CT, no major void was found. Small voids by bridging was found.

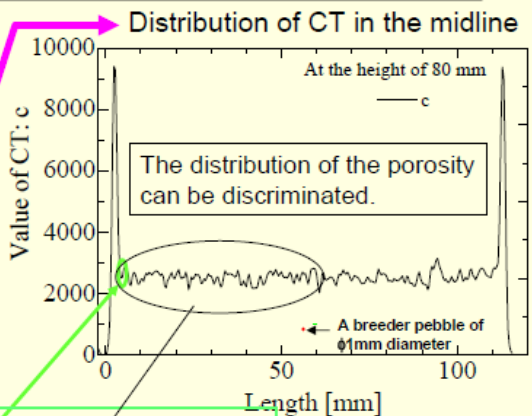
Porosity distribution and values of X-ray computed tomography (CT)



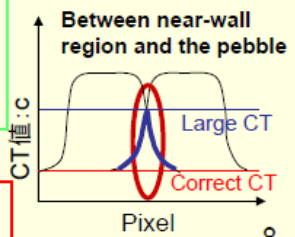
compressed image



compressed image

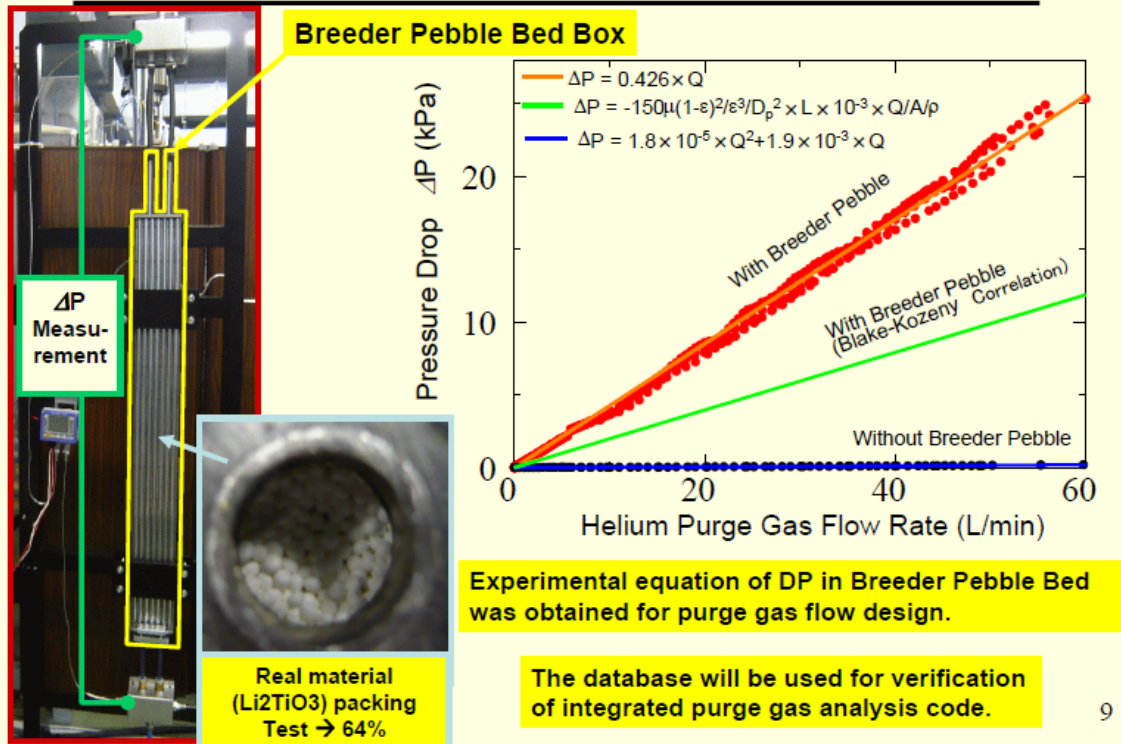


The porosities near the wall are the almost same value around the central region because of producing an image which is blurred around the edges.



The existence of relatively large porosity is confirmed near the narrow walls between the corner and the coolant pipe.

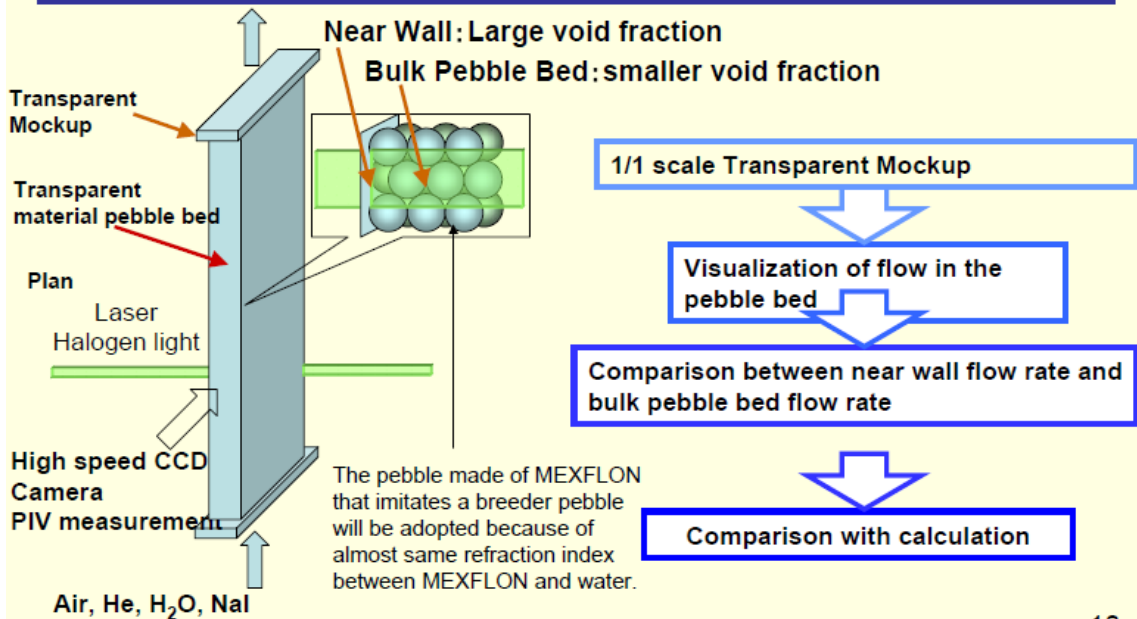
Function Test of Breeder Pebble Bed Box - Packing Test and Purge Gas Pressure Drop Test



Verification Test of Hydraulic Performance of Purge Gas



Flow in the pebble bed is simulated by the flow in the porous media.
→ Difference between porous media and pebble bed is to be clarified.



13. Tritium Inventory of Test Blanket Module in ITER and Blanket of Demonstration Reactor

T. Hino¹, H. Shibata¹, Y. Yamauchi¹, Y. Nobuta¹, S. Suzuki² and M. Akiba²

¹Laboratory of Plasma Physics and Engineering, Hokkaido University, Sapporo, Japan

²Naka Fusion Institute, Japan Atomic Energy Agency, Naka, Japan

Abstract

The tritium produced in the tritium breeder has to be desorbed under the temperature distribution to reduce the tritium inventory. Lithium titanate pebbles were irradiated by deuterium ions with different temperatures and ion fluences. The deuterium retained in the pebbles desorbed in forms of HD, D₂, HDO and D₂O. The amount of retained deuterium rapidly decreased for the temperature higher than 473 K, and became to zero for the temperature higher than 773 K. If the temperature range is from 573 to 1173 K in the TBM, the tritium inventory is less than 1 gram. However, in the demonstration reactor, the total tritium inventory of blankets becomes a few kilograms. For the reduction of the tritium inventory, the region with the low temperature region has to be significantly reduced.

1. Introduction

In-vessel tritium inventory in ITER is limited below a few hundreds grams from view points of safety and regulation. It is pointed out that the tritium inventory of co-deposited carbon dust/flake may become significantly large. However, the tritium inventory of Test Blanket Modules (TBMs) [1] may become large if the design for TBM is not suitable. The tritium inventory of TBM has not been investigated so far. In the fusion demonstration reactor, the in-vessel tritium inventory might be limited owing to the same reasons. The tritium inventory of blankets in the fusion demonstration reactor becomes extremely large, so that the reduction of this inventory is required. In the present

study, the tritium inventories of TBM and blanket in the demonstration reactor are estimated based on the results of the deuterium ion irradiation experiment, and the condition required for the reduction of the tritium inventory is suggested. The present approach for evaluation of tritium inventory can be applied for the different types of blankets.

In the water cooled solid breeder TBM, lithium titanate pebbles (Li_2TiO_3) are employed as the tritium breeder. As the solid breeder material, Li_2TiO_3 shows good chemical stability and tritium (T) release by thermal desorption [2, 3]. In the blanket of fusion reactors, the pebbles are irradiated by fusion neutrons and then tritium is produced by nuclear reactions of ${}^6\text{Li} (n, \alpha) \text{T}$ or ${}^7\text{Li} (n, n \alpha) \text{T}$. The temperature distribution of the solid breeding material in TBM has been estimated with taking account of nuclear heating to be in the range from 573 K to 1173 K [4]. Although it is desired for the tritium to be recovered completely in whole region of blanket during ITER operation, a small fraction of the tritium remains in low temperature region [5]. Therefore, in order to estimate the tritium inventory in Li_2TiO_3 pebbles in the TBM of ITER and the blanket of the demonstration reactors, the retention and desorption behavior of the tritium in the lithium titanate has to be investigated.

In the present study, the deuterium ion irradiation experiment was conducted for in Li_2TiO_3 pebbles to simulate the tritium retention and desorption behavior. The pebbles were irradiated by deuterium ions with energy of 1.7 keV at various irradiation temperatures (RT, 473 K, 573 K, 673 K, 773 K), and after that the retention and desorption behavior of retained deuterium was investigated by using a technique of thermal desorption spectroscopy (TDS). Based upon the obtained results, the tritium inventory in the TBM and the blanket of the demonstration reactor was estimated.

2. Experiments

Totally 18 Li_2TiO_3 pebbles with diameter of 2 mm ϕ [6] were used for the deuterium ion irradiation. These pebbles were heated at 973 K for an hour in a vacuum chamber to remove

impurities, such as hydroxides and carbon oxides [6]. After the heating, the pebbles were installed to a sample holder in an electron cyclotron resonance heating (ECR) ion source (Fig.1) and irradiated by deuterium ions. The sample holder made of Ta plate and Mo mesh was used to fix these pebbles, and the sample was heated by indirect resistive heating during the ion irradiation. The irradiation temperature (surface temperature of the pebbles) was changed from RT to 773 K. The surface temperature of the pebble and the temperature of the sample holder were measured up to 1000 K, by using a thermocouple. The temperature difference between the surface of the pebble and the sample holder was approximately 100 - 200 K at each irradiation temperature.

The deuterium ion energy was 1.7 keV and the ion flux was approximately 9×10^{14} D/cm²·s. The deuterium retention saturate at the fluence of approximately 1×10^{18} D/cm². Then, the ion fluence was taken 5×10^{18} D/cm². After the ion irradiation, the pebbles were transferred to the TDS chamber. Then, the sample was heated by an infrared light furnace from RT to 973 K with a heating rate of 10 K/min. At the highest temperature, 973 K, the heating was conducted for 1h. The ultimate pressure before the TDS analysis was approximately 10^{-8} Pa. The change of the surface morphology and the atomic composition were also investigated. The lithium titanate is electrically insulator, so that the surface has to be changed to electrically conductive for scanning electron microscope (SEM) and Auger electron spectroscopy (AES). For this purpose, the platinum coating was carried out on the surface of the lithium titanate.

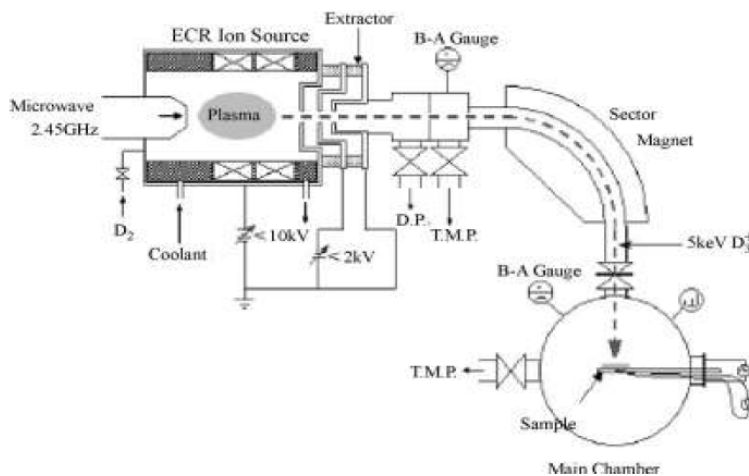


Fig. 1 ECR ion source apparatus.

3. Results

Figure 2 shows the thermal desorption spectra of gases containing the deuterium in the deuterium-irradiated Li_2TiO_3 pebbles with the irradiation temperatures of (a) RT, (b) 573 K and (c) 773 K. In these figures, the horizontal axis is the temperature of the lithium titanate pebbles. The deuterium retained in these pebbles desorbed in forms of HD, D_2 , HDO and D_2O . In our previous study, the deuterium desorption behavior of the Li_2TiO_3 pebbles was very similar with that of the Li film, therefore most of retained deuterium is trapped in forms of Li-D and Li-O-D [5]. The deuterium retention saturated at the ion fluence of approximately 1×10^{18} D/cm², and the deuterium concentration at RT in the atomic ratio became D/Li \sim 0.5 [5].

The desorption rates of these gases decreased with increase of the irradiation temperature. At the irradiation temperature of 773 K, the retained deuterium completely desorbed during the irradiation. This result suggests that the tritium produced in Li_2TiO_3 pebbles at the temperature higher than 773 K completely desorbs during the blanket operation. Figure 3 shows the amounts of gases containing the deuterium and total amount of deuterium desorbed from the pebbles as a function of the irradiation temperature. In the cases of HD and D_2 , the amounts of desorbed gases decreased with increase of the irradiation temperature. On the other hand, in the cases of HDO and D_2O , the amounts of desorbed gases did not decrease with the increase of the irradiation temperature in the range lower than 473 K, but decreased in the range higher than 473 K. This behavior in the irradiation temperature dependence of the desorption occurs due to the different desorption peak temperatures of these gas species. The amount of deuterium desorbed in form of HDO was largest in these gases at every irradiation temperature. The total amount of retained deuterium was almost the same in the temperature range lower than 473 K, while the total amount decreased sharply with increase of the irradiation temperature in the range higher than 473 K. At the temperature higher than 773 K, the desorption was not observed.

Figure 4 shows the desorption spectra of HD, D_2 , HDO and D_2O after the irradiation at RT. In the spectra of HD and D_2 , two peaks appeared at 500 K and 700 K. In the spectra of HDO and D_2O ,

three peaks appeared at 500 K, 600 K and 700 K. In our previous experiment for the Li film [5], two dominant peaks appeared at 500 K and 600 K. In addition, most of D was trapped by Li. Thus, it is presumed that the peaks at 500 K and 600 K are due to de-trapping from bonds of Li-D and Li-OD. In the case that the ion fluence increased, the peak intensity at 700 K relatively increased in the spectra of HD and D₂. Since the lithium content decreases by the selective sputtering, the titanium content relatively increases as shown later. Then, the desorption at 700 K may be due to de-trapping from bonds of Ti-D and Ti-OD.

Figure 5 shows the atomic composition of the lithium titanate before and after the ion irradiation. The lithium content was high before the irradiation, but significantly decreased after the irradiation. The major contents at the surface were titanium and oxygen. Figure 6 shows the surface morphologies before and after the ion irradiation. After the ion irradiation, the surface was eroded by the irradiation and the structure clearly changed. The surface structure consisted with the particles with a micron meter. The atomic concentration suggests that the major content of the particle is titanium oxide, TiO₂.

Figure 7 shows the amount of retained deuterium (total amount of retained deuterium) versus the temperature of lithium titanate. In the design of water cooling solid breeder TBM, the tritium breeder (Li₂TiO₃) has a temperature range from 573 K to 1173 K. The dashed lines in Fig.7 show this temperature range. The retained deuterium completely desorbes in the region with temperature higher than 773 K, while a small fraction of the deuterium is retained in the region with temperature lower than 773 K. In the TBM, the region with temperature lower than 773 K exists. The amount of retained tritium in this region becomes the tritium inventory. Namely, the tritium is retained in the region with temperature of 573-773 K (shown as dot region in Fig.7). The amount of retained tritium in the TBM can be estimated using the present result. The amount of lithium in the TBM is approximately 7 kg [8]. The tritium produced in the TBM becomes 3000 g x burn up ratio. The ratio of the low temperature region (573-773 K) is 10 % of the entire region of the breeder [8]. In this low temperature region, approximately 10 % of the tritium produced remains in the blanket.

Thus, the tritium inventory becomes 30 g x burn up ratio. The burn up ratio in ITER is very small, 0.01 [7], so that the tritium inventory becomes negligible small, 0.3 gram. However, in the case of the demonstration reactor, the tritium inventory becomes 6 g per blanket module if the burn up ratio is 0.2. The tritium inventory becomes approximately 3 kg if the number of blanket module is 500. Therefore, the tritium inventory has to be decreased by reducing the low temperature region in the tritium breeding region.

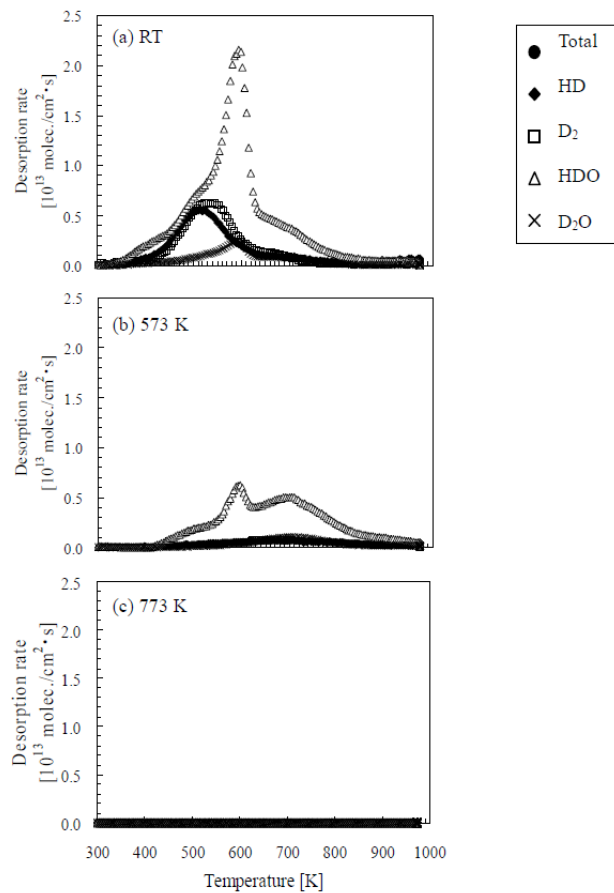


Fig. 2 Thermal desorption spectra of gases containing deuterium for deuterium ion irradiated Li_2TiO_3 pebbles at the irradiation temperatures of (a)RT, (b)573 K and (c)773 K.

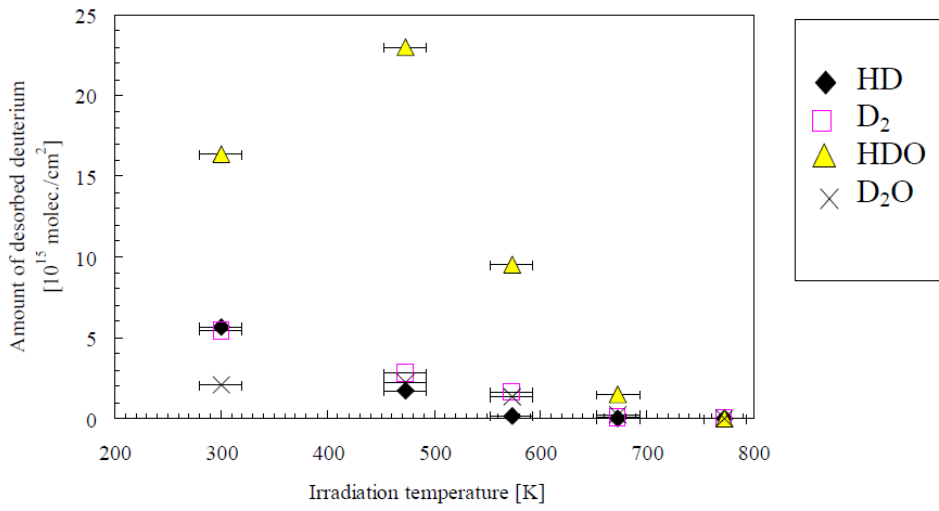


Fig. 3 Amounts of gases containing deuterium desorbed from Li₂TiO₃ pebbles as a function of irradiation temperature.

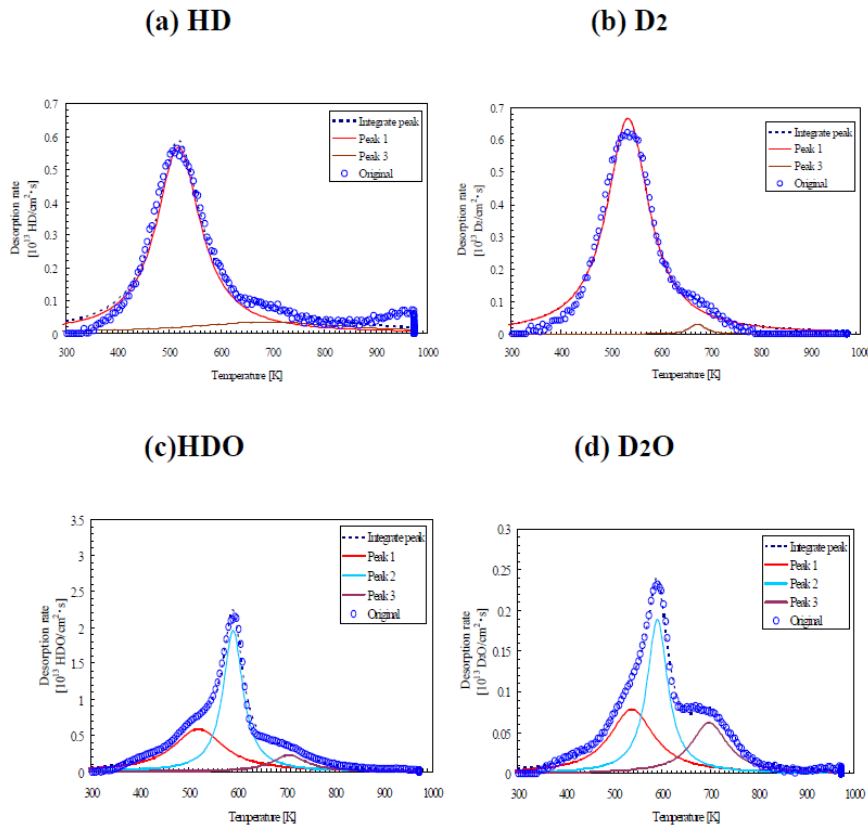


Fig. 4 Desorption spectra at RT with peak separation for HD (a), D₂ (b), HDO (c) and D₂O (d).

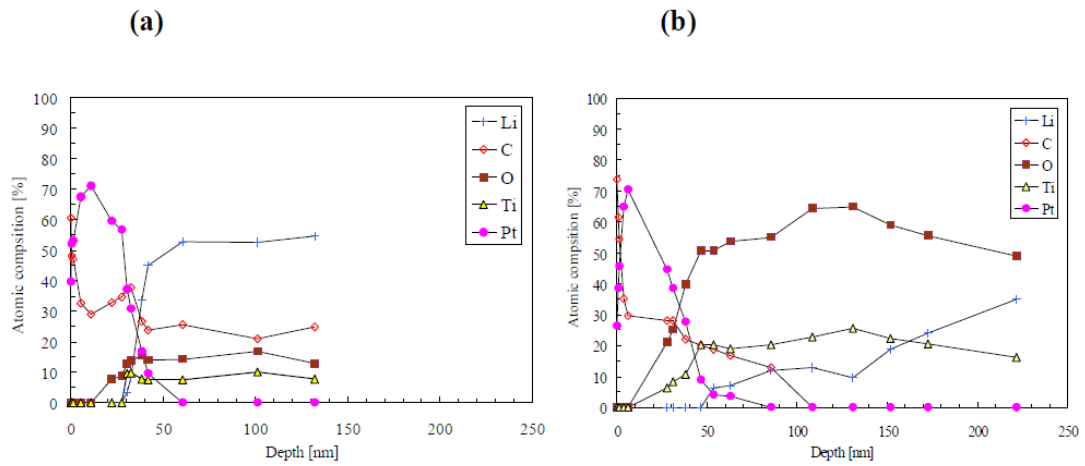


Fig.5 Depth profiles of atomic composition of lithium titanate before irradiation (a) and after irradiation (b).

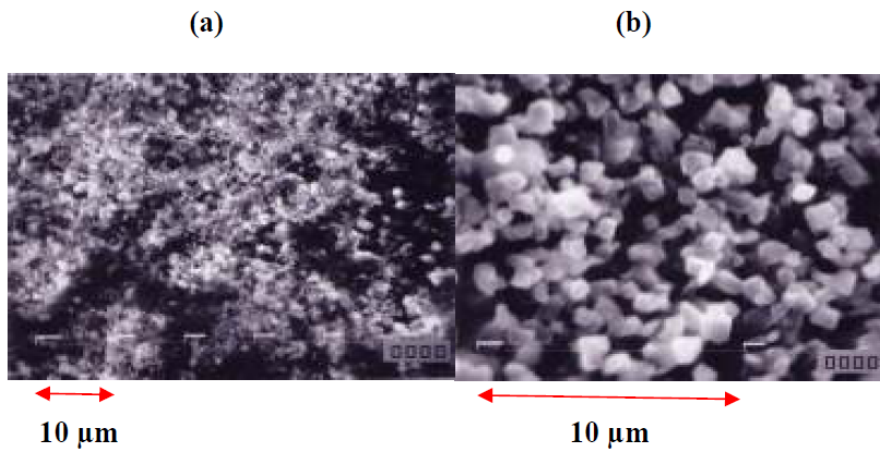


Fig. 6 Surface morphologies of lithium titanate before irradiation (a) and after irradiation (b).

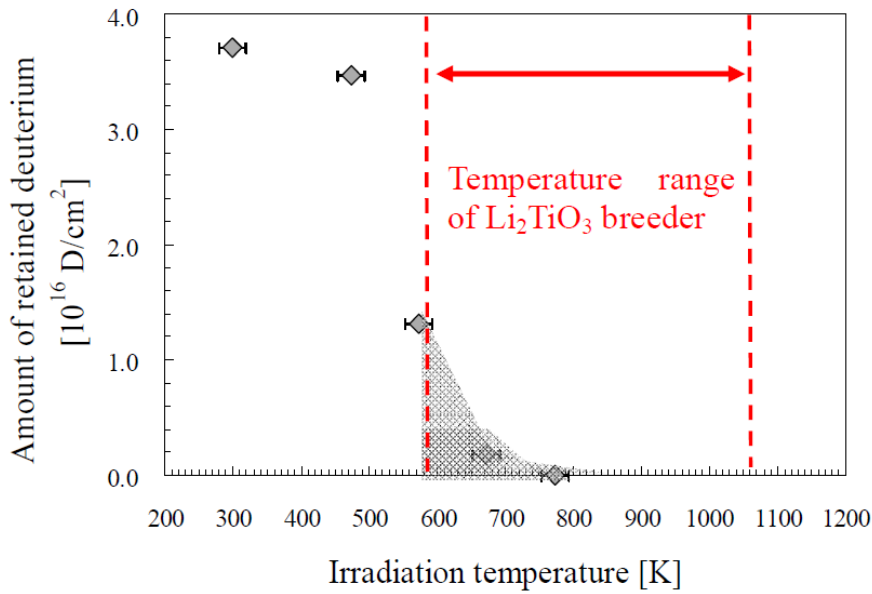


Fig. 7 Amounts of retained deuterium in Li_2TiO_3 pebbles as a function of irradiation.

4. Conclusions

In the current design of the blanket including the TBM, the tritium breeder region has a temperature distribution. In order to evaluate the tritium inventory and quickly recover the tritium produced in the tritium breeder, the tritium has to be desorbed completely under the temperature distribution. In order to simulate this behavior, the pebbles of lithium titanate were irradiated by deuterium ions (1.7keV D^+) with different temperatures (RT-773 K). After the irradiation, the retention and desorption behavior of retained deuterium was investigated using a thermal desorption spectroscopy.

The deuterium retained in the lithium titanate pebbles desorbed in forms of HD, D_2 , HDO and D_2O . The amount of desorbed deuterium in form of HDO was largest in these gases at any irradiation temperatures. When the irradiation temperature was higher than 473K, the amount of retained deuterium decreased, and became to zero for the temperature higher than 773K. The spectra of HD and D_2 have two peaks at 500 K and 700 K. The spectra of HDO and D_2O have three peaks at 500 K, 600 K and 700 K. The peaks at 500 K and 600 K are owing to the bonds of Li-D

and Li-OD. The peak at 700 K may be owing to the bonds of Ti-D and Ti-OD. After the irradiation, the atomic composition and the surface morphology were examined. The lithium at the surface disappeared owing to the selective sputtering.

Based on these data including the design parameters, the tritium inventory was estimated. If the ratio of low temperature region is 0.1 and the burn up ratio is 0.01, the tritium inventory may become lower than 1 g. However, in the demonstration reactor, the burn up ratio is high, 0.2, so that the inventory per blanket becomes a few grams. The total in-vessel inventory of blanket modules becomes a few kilograms. Thus, the low temperature region in the tritium breeding region has to be decreased by a suitable design for the temperature profile.

Acknowledgements

This work was supported by the Grant-in-Aid for Scientific Research (No. 18360439) from the Ministry of Education, Science, Sports and Culture in Japan, and partly supported by the JAEA Collaboration Research Program.

References

- [1] A. Ying et al, *J. Nucl. Mater.*, 367-370 (2007) 1281.
- [2] Japan Atomic Energy Research Institute Report, "JAERI-Review 2005-011", (2005).
- [3] N. Roux et al, *J. Nucl. Mater.*, 233-237 (1996)1431.
- [4] S. Tanaka et al, *J. Plasma Fusion Res.*, 81 (2005)434.
- [5] T. Hino et al, "Deuterium retention and desorption behavior of lithium titanate", 8th International Symposium on Fusion Nuclear Technology (ISFNT-8), Heidelberg, Germany, (2007).
- [6] K. Tsuchiya et al, *J. Nucl. Mater.*, 258-263 (1998)1985.
- [7] M. Enoeda, "Development of blanket materials in JAEA", 2nd Roadmap Meeting for Development of Fusion Reactor, Fusion Forum in Japan, Tokyo, (2006).
- [8] T. Hino et al, "Deuterium retention and desorption behavior of lithium titanate", Advanced Blanket Meeting at National Institute of Fusion Science (NIFS), July 1, (2008).

Deuterium Retention and Desorption Behavior of Li_2TiO_3 after Deuterium Ion Irradiations with Different Temperatures

T. HINO, H. SHIBATA, Y. NOBUTA, Y. YAMAUCHI

Laboratory of Plasma Physics and Engineering, Hokkaido University, Kita-13, Nishi-8, Kita-ku, Sapporo, 060-8628 Japan

M. AKIBA and S. SUZUKI

Naka Fusion Institute, Japan Atomic Energy Agency, Naka-shi, Ibaraki-ken, 311-0193 Japan

Lithium Titanate (Li_2TiO_3) pebbles were irradiated by deuterium ion (D^+ , 1.7 keV) under different irradiation temperatures (RT, 473 K, 573 K, 673 K and 773 K), and the amount of retained deuterium and the desorption behavior were investigated by using a technique of thermal desorption spectroscopy (TDS). The amount of retained deuterium was almost the same with the irradiation temperature up to 473 K, while the amount decreased sharply with increase of irradiation temperature in the range higher than 473 K. The amount of retained deuterium at the irradiation temperature of 773 K became almost zero. This result suggests that the tritium produced in Li_2TiO_3 pebbles in the region with temperature higher than 773 K completely desorbs during the operation, although a small fraction of the tritium remains in the pebbles in the region with temperature lower than 773 K. Figure 1 shows the amount of retained deuterium as a function of irradiation temperature.

The present result is useful to evaluate the tritium inventory of blanket, and to design the temperature profile of the tritium breeding material.

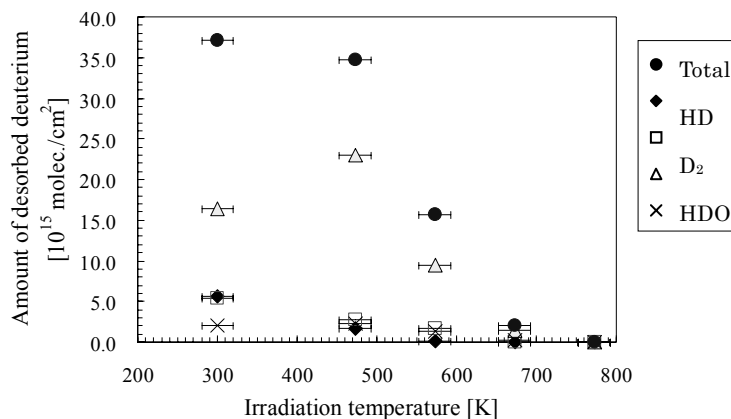


Fig.1 Amounts of gases containing deuterium desorbed from Li_2TiO_3 pebbles as a function of irradiation temperature.

This work was supported by the Grant-in-Aid for Scientific Research from the Ministry of Education, Science, Sports and Culture in Japan, and partly supported by the JAEA Collaboration Research Program.

CBBI-15, 9:00-, Sept. 4, 2009, Convention Centre, Sapporo

Tritium Inventory of Blanket Module in ITER and Demonstration Reactor

T. Hino, H. Shibata, Y. Yamauchi, Y. Nobuta

Laboratory of Plasma Physics and Engineering, Hokkaido University, Sapporo, Japan

S. Suzuki and M. Akiba

Naka Fusion Institute, Japan Atomic Energy Agency, Naka, Japan

1. Introduction

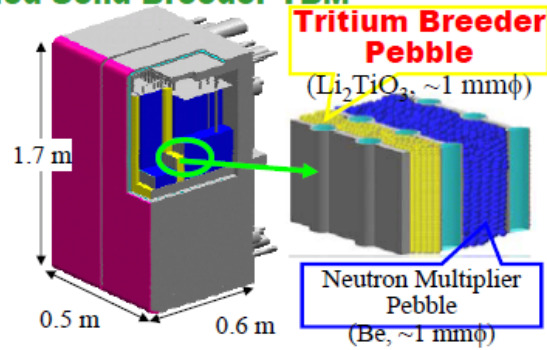
In-vessel tritium inventory in ITER is limited below a few hundreds grams.

Tritium inventory of Test Blanket Modules (TBMs) has not been estimated.

Tritium inventory in demo reactor becomes extremely large but has not been estimated.

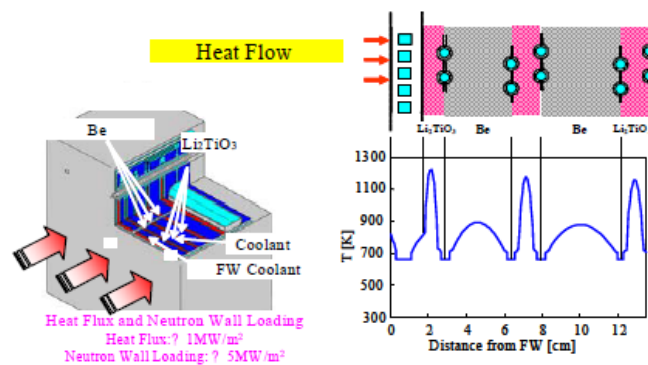
For example, temperature of tritium breeding material, lithium titanate (Li_2TiO_3) in water cooled solid breeder TBM has a range from 573 K to 1173 K.

JA Water-Cooled Solid Breeder TBM



Temperature Profile of JA TBM (Example)

Average Temperature in Lithium Titanate: 900K



Questions:

Tritium is retained in the tritium breeder during the operation?

What is the retained amount of tritium if so? → tritium inventory

How we can reduce the inventory?

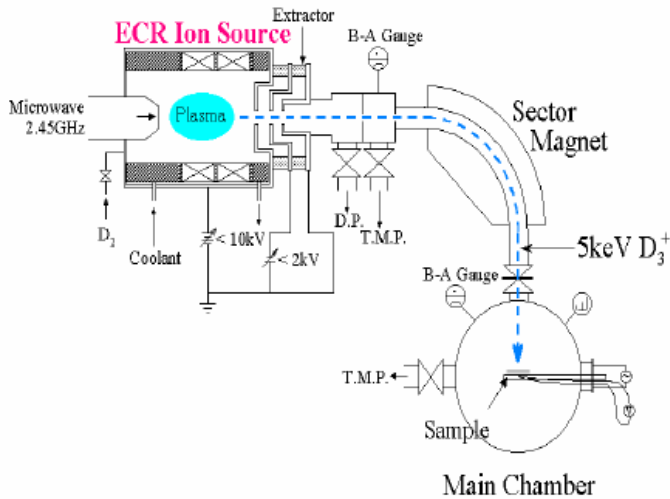
In this study:

Tritium inventory of TBM and blanket in demo reactor : estimated based on deuterium ion irradiation

Condition required for reduction of tritium inventory : suggested

2. Experiments

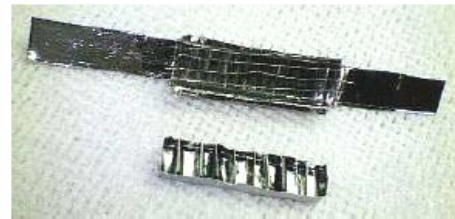
ECR ion source



**Lithium titanate pebbles
1hr pre-heating (1000K)**

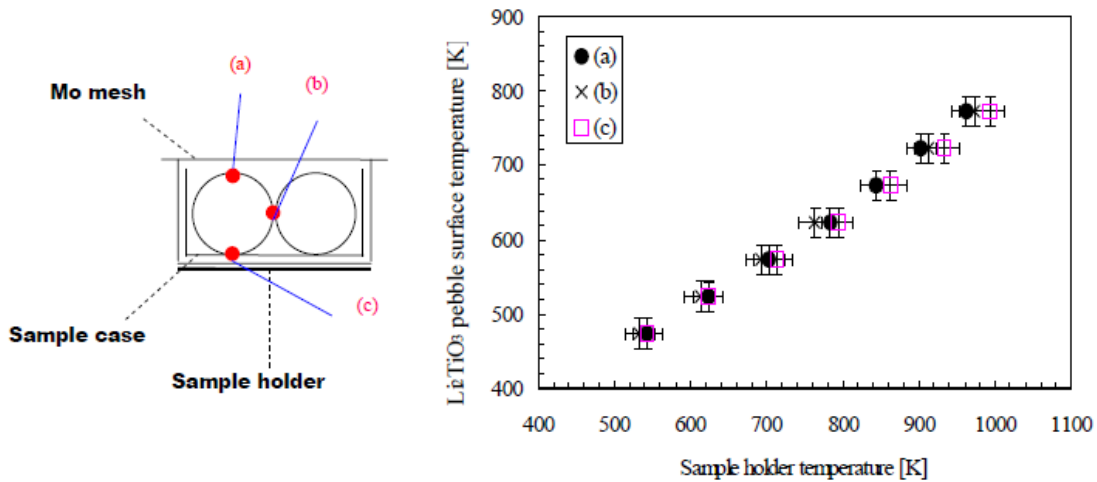


Sample holder



**Irradiation temperature: RT-773K
D ion fluence: $5 \times 10^{18} \text{D/cm}^2$
D ion energy :1.7keV**

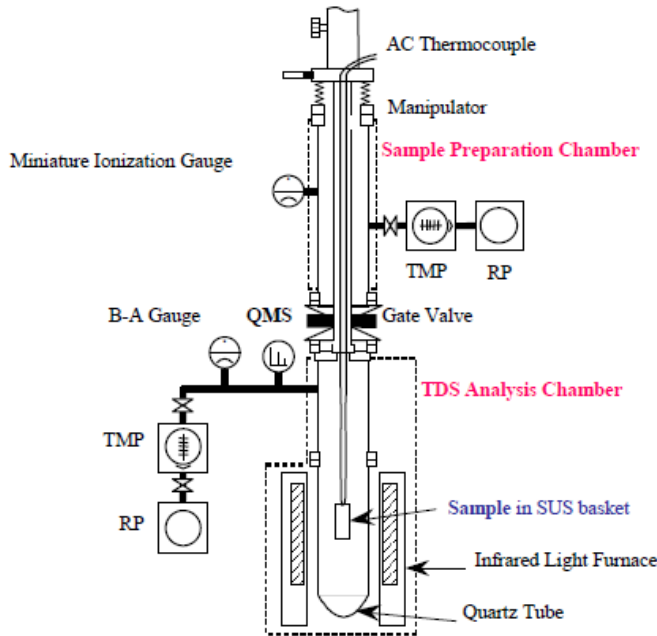
Temperature measurement during irradiation



Sample holder temperature → Pebble temperature

Thermal desorption

RT-1073K, 10K/min



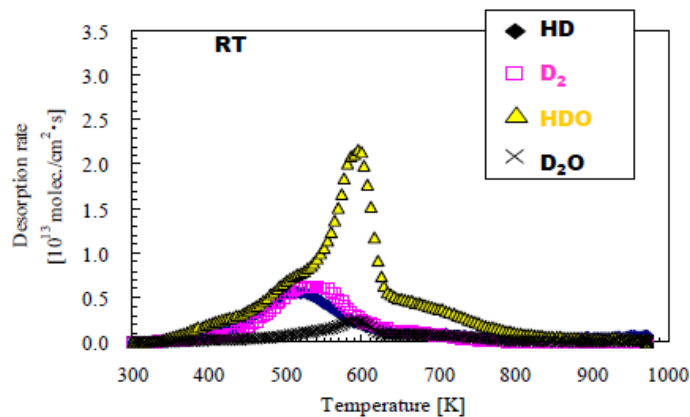
Ta sample holder



3. Results

(1) Deuterium thermal desorption spectrum at different temperature

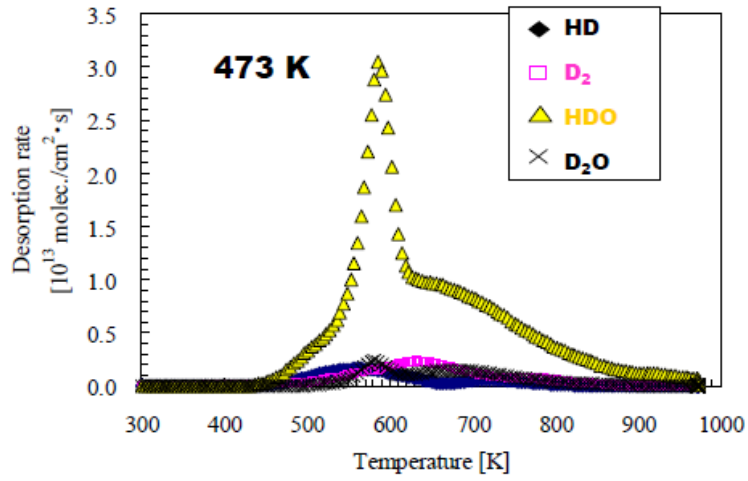
Thermal desorption spectra of gases containing deuterium, RT



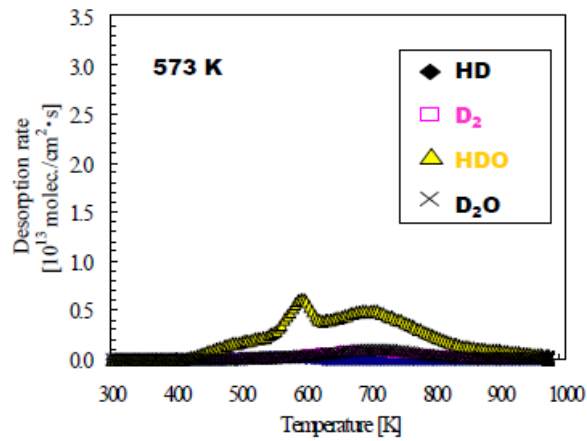
Outgas species: HDO, D₂, HD, D₂O

Major peaks: 500K for hydrogen gas, and 600K for water

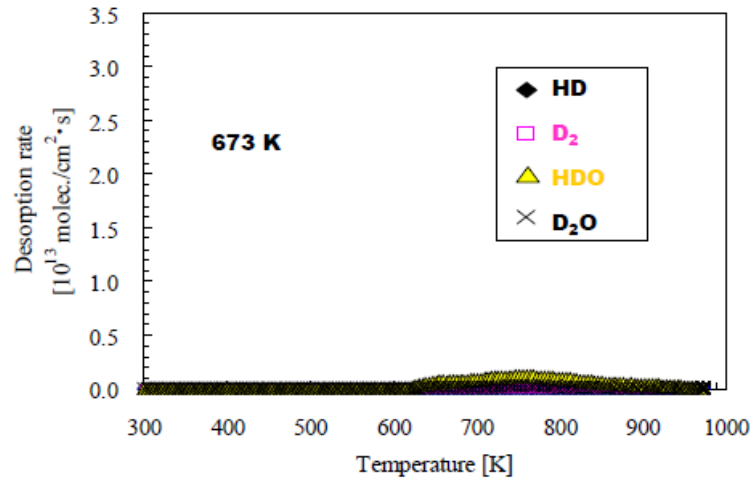
Thermal desorption spectra, 473 K



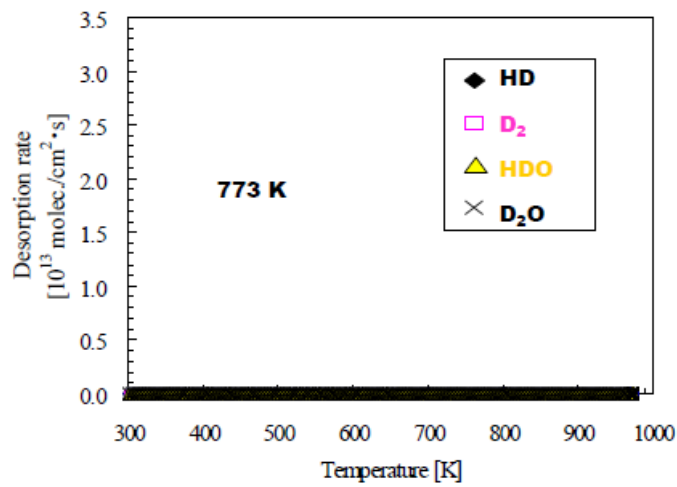
Thermal desorption spectra, 573 K



Thermal desorption spectra, 673 K

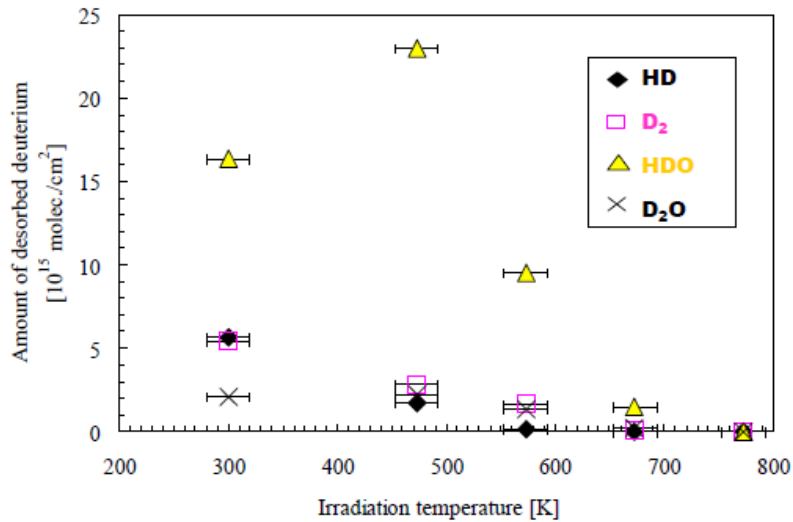


Thermal desorption spectra, 773 K



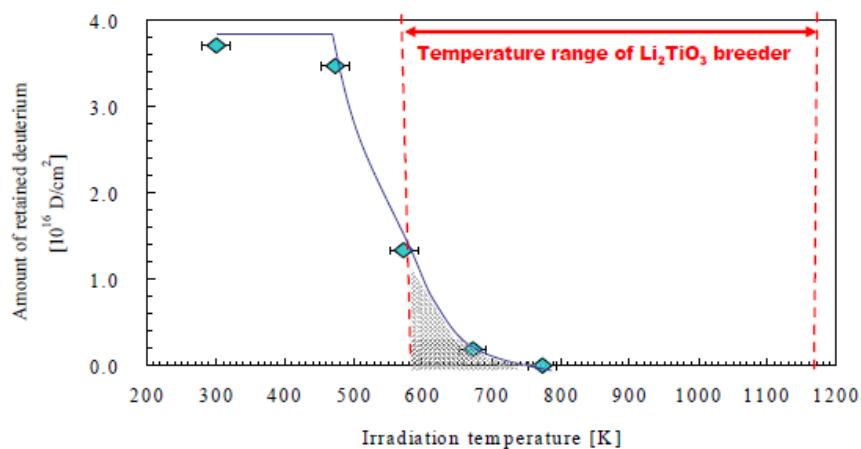
At temperature higher than 773K, no deuterium retention was observed.

(2) Amounts of gases containing deuterium as a function of irradiation temperature



Deuterium retention is constant up to 473K, and drops from 473K.

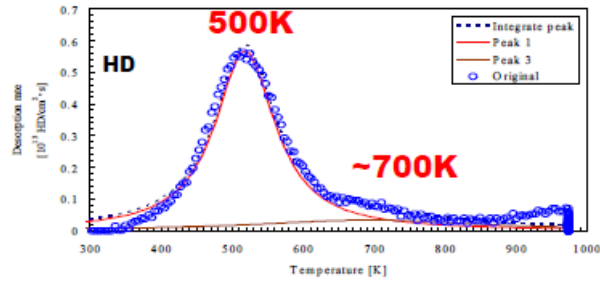
Amounts of retained deuterium as a function of irradiation temperature



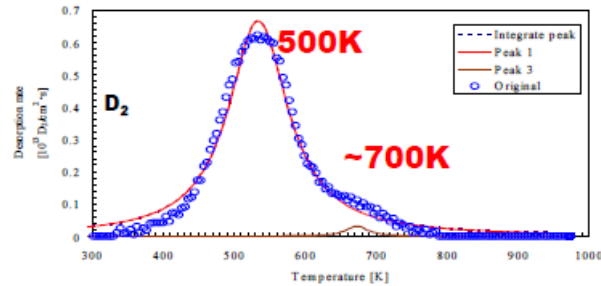
At 573-773K, the ratio of retained D is 1/10 of that at RT.

(3) Desorption peak separation → Binding state

Peak fitting for **HD** at RT



Peak fitting for **D₂** at RT



HD and D₂ have 2 peaks at 500K, and ~700K.

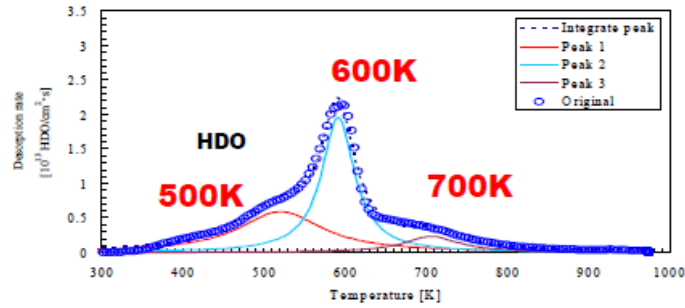
In our previous experiment for Li

Spectral pattern of Li was very similar with Li₂TiO₃ → Most of D is trapped by Li .

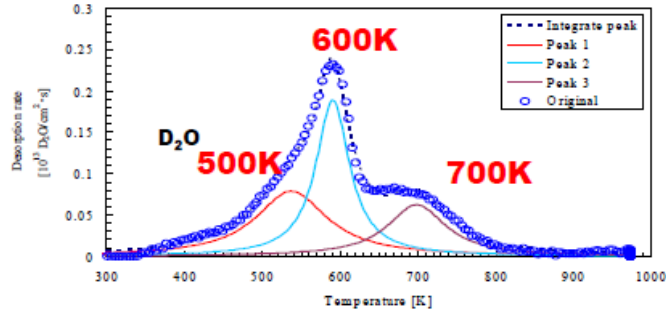
Sharpe peaks at 500K and ~700K

→ **Li-D** and/or partly **Li-OD**

Peak fitting for **HDO** at RT



Peak fitting for **D₂O** at RT



HDO and D₂O have 3 peaks at 500K, 600K and 700K.

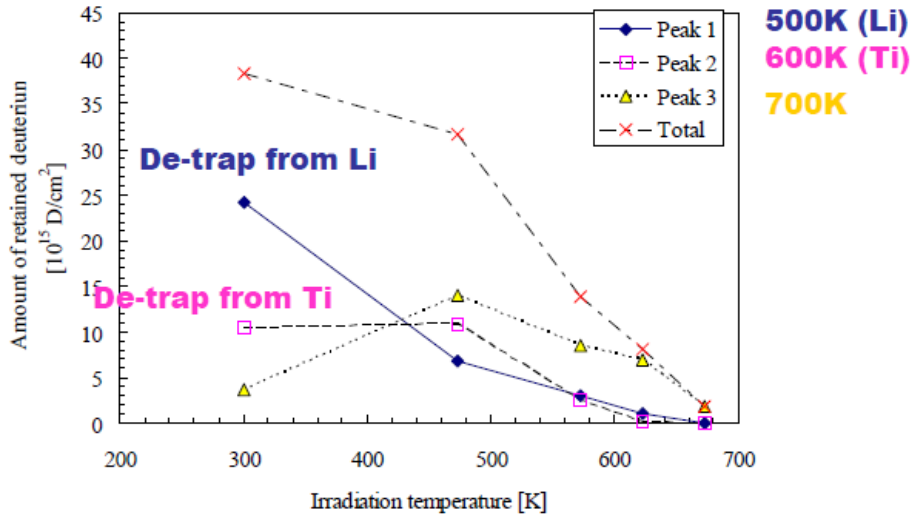
In our previous experiment for Ti

D ion irradiation for Ti

Sharpe peak at 600K appeared.

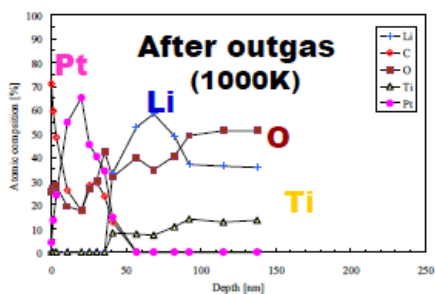
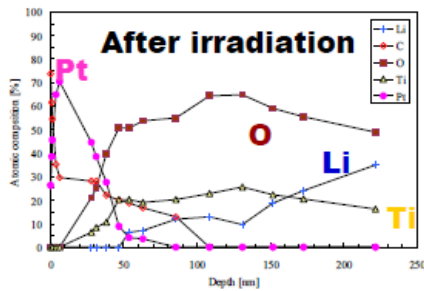
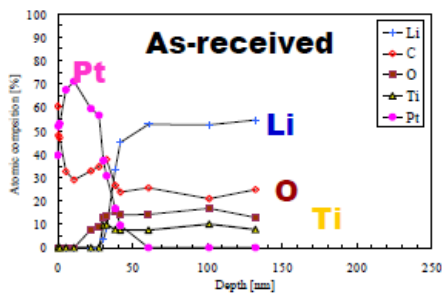
→ **600K peak: Ti-D and/or partly Ti-OD**

Change of peak fraction vs irradiation temperature



**Lower irradiation temp: D is trapped mainly by Li.
High irradiation temp: D is trapped mainly by Ti.**

(4) Change of atomic composition (Pt coating for the surface to be electrically conductive)

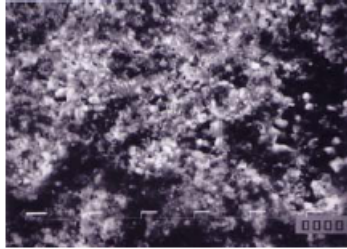


Li content decreased by selective sputtering.

As increase of ion fluence, D is trapped mainly by Ti.

(5) Change of surface morphology

As-received



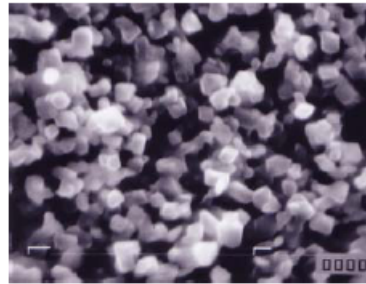
10 μm

After outgas(1000K)



10 μm

After irradiation



10 μm

TiO₂ particles

4. Tritium inventory of TBM and blanket of demo reactor

Temperature of tritium breeder region : 573-1173K

No tritium retention for temperature >773K

(Tritium is retained in the region with temperature 573-773K)

Ratio of the low temperature region : 0.1

Most of tritium is trapped by Li. \rightarrow Li-T

Ratio of retained tritium in the region with temperature 573-773K : 0.1

Assume Li amount of TBM or blanket = 7000g

Tritium amount at the low temp. region:

**=maximum tritium amount (7000 x 3/7)
x burn up ratio
x residual ratio (1/10 x1/10)
= 30 x burn up ratio**

ITER TBM, burn up ratio ~1% → 0.3g/TBM

Demo reactor, burn up ratio ~20%→6g/blanket

→Total tritium inventory :3kg

**Low temperature region has to be reduced by
suitable design.**

Higher inlet temperature

**Steep temperature gradient between coolant and
tritium breeder**

5. Conclusion

Retained deuterium : desorption in forms of HDO, HD, D₂, D₂O.

Most of deuterium : trapped by Li

Peak temperatures: 500K for HD and D₂ (De-trap from Li)

600K for HDO and D₂O (De-trap from Ti)

Perfect desorption : at temperature > 773K

Atomic composition

: lithium content reduced by selective sputtering

Surface morphology after irradiation: TiO₂ particles

Tritium inventory < 1g for ITER TBM

Tritium inventory ~ 6g for Demo blanket (Total inventory ~ 3kg)

Low temperature region has to be reduced by the design !

14. Study on hydroxyl desorption from F82H oxidized surface by FT-IR

*Daisuke Masuyama, Takuji Oda, Satoru Tanaka
The University of Tokyo, 7-3-1 Hongo, Bunkyo-ku, Tokyo 113-8656, Japan
E-mail: masuyama@flanker.q.t.u-tokyo.ac.jp*

Abstract

The reaction between water vapor and surface hydroxyls on F82H oxidized surfaces was studied using FT-IR. After D₂O vapor exposure, an IR absorption peak related to O-D stretching vibration was observed in a F82H as-received plate, which means that surface hydroxyls OH⁻ was replaced with OD⁻ by isotope exchange reaction between surface hydroxyls OH and D₂O vapor. On the other hand, no absorption peak was observed in F82H powders oxidized at various temperatures in the air. XRD analysis showed existence of Fe₂O₃ in all the samples. IR analysis indicated that Cr₂O₃ mainly existed on the outermost surface of the F82H as-received plate, and oxidation states other than Fe₂O₃ coexisted with Fe₂O₃ on that of the F82H oxidized powders. It was suggested that the reactivity between water vapor and surface hydroxyls on F82H surfaces is strongly affected by the oxidation state of the outermost surface.

Keywords:

F82H, surface hydroxyls, isotope exchange, FT-IR, oxidation, adsorption/desorption

1. Introduction

Tritium adsorbs on the surface of structural materials in nuclear fusion reactors when tritium contacts with it [1]. Because tritium is a radioactive isotope, tritium accumulation on material surfaces leads to contamination. In practice, metal/alloy surfaces are naturally oxidized, and tritium generally exists as hydroxyls on the surfaces [2]. High stability of surface hydroxyls makes decontamination difficult, which causes problems in repair of equipment or waste management. Therefore, it is important to understand the nature of hydroxyls on material surfaces.

Surface hydroxyls OT⁻ can be eliminated from material surfaces by heat treatment or isotope exchange reaction with OH⁻ or OD⁻ [3, 4]. The surface hydroxyls existing on metal surfaces have been widely studied, e.g. steel, aluminum, and copper [5-8]. It is clear that the stability and adsorption/desorption behaviors of surface hydroxyls depend on material and the surface conditions.

In Japan, low activation ferritic steel F82H is planned to use as the structural material of ITER test blanket module (TBM) [9]. Nevertheless, knowledge about surface hydroxyls on F82H is limited. It has been reported that the HDO gas release from F82H irradiated with D⁺ was observed by thermal desorption method [10]. However, surface hydroxyls were not focused in this work. As far as we know, no work has reported about the behavior of surface hydroxyls on F82H. In the present paper, therefore, we study the nature of surface hydroxyls on F82H using

Fourier transform infrared absorption spectroscopy (FT-IR) and X-ray diffraction (XRD), especially with focusing on reactions with water vapor.

2. Experiment

2.1. Sample preparation

A plate (10×10 mm²) and powder were fabricated from a F82H block provided by Japan Atomic Energy Agency, and then were used as samples. The plate had a heavily oxidized surface in as-received state, and it was analyzed. The average grain size of the powder was 22.9 μm. As oxidation treatments, the powder was heated at 473, 673, and 1073 K in the air under atmospheric pressure for twelve hours.

Additionally, powders of iron and chromium oxides, which are oxides of the main component of F82H alloy, were also tested for comparison: Fe₂O₃ (average grain size 0.4 μm, purity 95 %, Wako Pure Chemical Industries Ltd.), Fe₃O₄

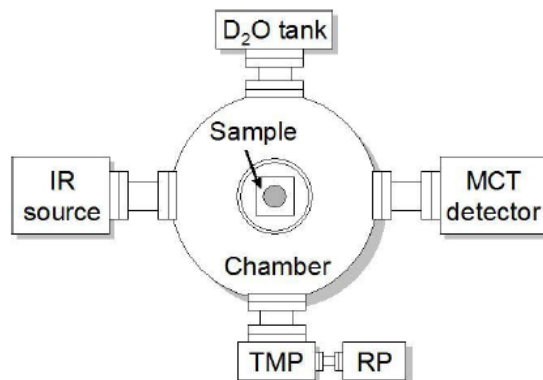


Fig. 1 Schematic drawing of the diffuse-reflectance FT-IR experimental system

Cr₂O₃ (average grain size 3 μm, purity 99.9 %, Soekawa Chemical Co Ltd.).

Due to heavy oxidation, the surface of the F82H as-received plate was rough and was colored brown. The F82H powders were black in independent of the oxidation conditions. The Fe₂O₃ powder was red-brown, Fe₃O₄ black, and Cr₂O₃ green.

2.2. FT-IR measurement

Diffuse reflectance spectroscopy, which has a high sensitivity to surface analysis, was adopted for FT-IR measurement. The schematic drawing of the experimental system is shown in Fig. 1. The experimental system was composed of FT-IR (Mattson, Infinity Gold), external MCT detector, vacuum chamber, diffuse reflectance mirror system, sample holder of molybdenum, and D₂O tank.

After introduction of the sample, the vacuum chamber was evacuated to about 5.0×10^{-6} Pa. Subsequently, the sample was exposed to 1.0×10^{-3} Pa D₂O vapor for one hour at room temperature. For distinction from OH⁻ that had already adsorbed on the samples at the start of the experiment, D₂O was used as exposure gas. If D₂O adsorption was not observed by this exposure, the sample was further exposed to 1.0 Pa D₂O vapor for one hour. The number of scans was set to 500 for achieving an adequate S/N ratio. The required time for one spectrum was five minutes.

2.3. XRD analysis

The crystalline structures of the F82H samples were analyzed by XRD. Cu Kα was used for the X-ray source. Diffraction patterns were recorded from 20° to 90° (2θ angle) with the resolution of 0.02°.

3. Results

3.1. OD⁻ formation by D₂O exposure

The F82H as-received plate and the F82H oxidized powders were exposed to 1.0×10^{-3} Pa D₂O vapor at room temperature. After one-hour exposure, the absorption spectra of them were obtained by FT-IR. No absorption peak related to O-D stretching vibration was observed from all of the spectra. By the further 1.0 Pa D₂O vapor exposure, formation of surface OD⁻ was indicated by a broad peak at 2400 cm⁻¹ in the F82H as-received plate, while not in the F82H oxidized powders.

The acquired IR spectrum is shown in Fig. 2, together with that of Fe₂O₃, Fe₃O₄ and Cr₂O₃ powders subjected to the same D₂O vapor exposure experiment. In the case of the Fe₂O₃ and Cr₂O₃ powders, by 1.0×10^{-3} Pa D₂O vapor exposure, O-D absorption peaks were observed mainly at 2680 cm⁻¹ and 2550 cm⁻¹ in Fe₂O₃, and at 2420 cm⁻¹ in Cr₂O₃. Contrastively, no peak was observed in Fe₃O₄ even after the further 1.0 Pa D₂O vapor exposure.

The sensitivity of diffusion reflectance FT-IR becomes more sensitive as the grain size becomes smaller. The grain sizes of the F82H powders (22.9 μm) are larger than those of Fe₂O₃ powder (0.4 μm) and Cr₂O₃ powder (3 μm), in which absorption peaks were observed. Therefore, no existence of absorption peaks in the F82H powders might be attributed to their large grain size. The further D₂O exposure experiment would be produced with the smaller-grain-size F82H powders in our future work.

3.2. Oxidation states of the F82H samples

3.2.1. FT-IR analysis

In order to analyze the surface oxidation state of each sample, IR spectra before the D₂O exposure

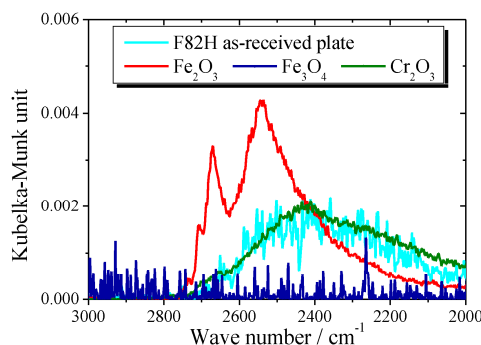


Fig. 2 Absorption spectra of the F82H as-received plate, and the Fe₂O₃/Fe₃O₄/Cr₂O₃ powders

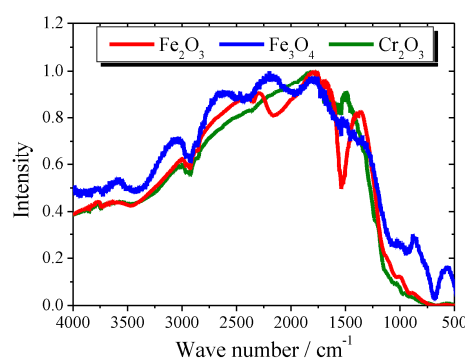


Fig. 3 IR power spectra of the Fe₂O₃/Fe₃O₄/Cr₂O₃ powders

were compared. The spectra of the Fe_2O_3 , Fe_3O_4 , and Cr_2O_3 powders are shown in Fig. 3, and the spectra of the F82H as-received plate, the powder before the oxidation, and the powder oxidized at 1073 K are shown in Fig. 4. The peak intensities are normalized for easy comparison. Note that a peak at 2800 cm^{-1} was excluded from the further discussion, because it was observed in all the spectra, and thus was regarded as a peak derived from the experimental equipment.

In the spectrum of the F82H as-received plate, a negative peak corresponding to IR absorption by the sample was observed at 1700 cm^{-1} . This peak was also observed in the spectrum of the Cr_2O_3 powder. In the region of wave number higher than 1700 cm^{-1} , the shape of the spectrum of the F82H as-received plate was similar to that of the Cr_2O_3 powder. In addition, IR was sufficiently detected even at $1000\sim 700\text{ cm}^{-1}$, as the same with the F82H powder before the oxidation treatments and the Fe_3O_4 powder. No clear resemblance was observed between the F82H as-received plate and the Fe_2O_3 powder.

In the case of the F82H powder samples, the IR detection at $1000\sim 700\text{ cm}^{-1}$ was diminished by the oxidation treatments. Instead, negative peaks emerged at 2150 cm^{-1} and 1500 cm^{-1} by the oxidation at 1073 K. These peaks were observed also in the Fe_2O_3 powder. The overall shape of the spectrum of the F82H powder oxidized at 1073 K was similar to that of the Fe_2O_3 powder, although the negative peaks at 2150 cm^{-1} and 1500 cm^{-1} were larger and IR intensities at $1000\sim 700\text{ cm}^{-1}$ were higher in the F82H powder than those in the Fe_2O_3 powder.

Table 1 summarizes the characteristic peaks observed in each sample.

3.2.2 XRD data

The results of XRD analysis on the various F82H samples were shown in Fig. 5. In the F82H as-received plate, Fe-Cr peaks were mainly observed. Small peaks related to Fe_2O_3 were also observed at 33.06° and 35.50° . On the other hand, in the F82H powder oxidized at 1073 K, only Fe_2O_3 -related peaks were detected.

4. Discussion

The result of F82H is discussed together with the surface oxidation state of F82H analyzed by FT-IR and XRD.

First, the surface states of the F82H samples are discussed. The IR spectrum of the F82H as-received plate was similar to that of Cr_2O_3 as shown in section 3.2. Therefore, it is thought that Cr_2O_3 mainly existed on the surface of the F82H as-received plate. Peaks related to Fe_2O_3 , however, were observed by XRD analysis, while peaks related to Cr_2O_3 were not. Additionally, a part of the surface of the F82H as-received plate was colored brown like Fe_2O_3 . Because diffuse reflectance FT-IR should give information about more outer surfaces than XRD, it is considered that Cr_2O_3 mainly existed on a surface region including the outermost surface, while Fe_2O_3 separated out at a deeper region than Cr_2O_3 . This consideration is supported by the fact that the shape of O-D stretching vibration peaks in the F82H

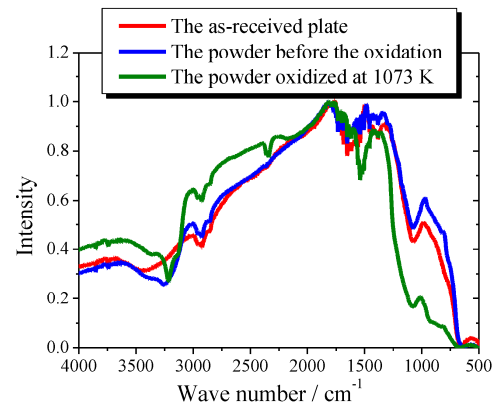


Fig. 4 IR power spectra of the F82H samples

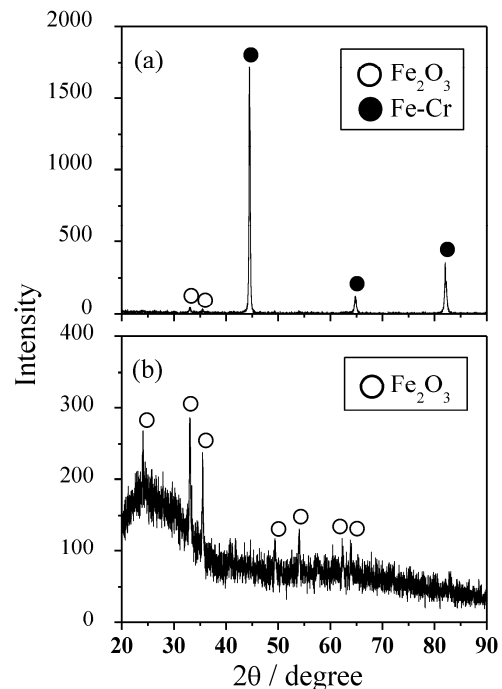


Fig. 5 XRD patterns of the F82H samples: (a) the as-received plate and (b) the powder heated at 1073 K

as-received plate resembled to that in Cr₂O₃ rather than that in Fe₂O₃ as seen in Fig. 2.

In the case of the F82H powder oxidized at 1073 K, the XRD and FT-IR measurement indicated that Fe₂O₃ was dominant from the outermost surface to the bulk. However, it should be noted that the peaks related to Fe₂O₃ (2150 cm⁻¹ and 1500 cm⁻¹) in the F82H oxidized powder were weaker than that in Fe₂O₃, although only Fe₂O₃ crystalline peaks were detected in XRD pattern. These facts imply that there was a region where crystalline Fe₂O₃ are not well formed, probably a surface region including the outermost surface. This could be the reason why OD⁻ was not detected in the F82H oxidized powder, although existence of Fe₂O₃ were confirmed by XRD and FT-IR.

From the results, it is indicated that reactivity between water vapor and surface hydroxyls on F82H surface depends strongly on the oxidation state of the outermost surface, which is difficult to evaluate by XRD. Hence, in order to conduct decontamination thoroughly and effectively, careful analysis of the outermost surface is necessary in the future works.

5. Conclusion

The adsorption/desorption behaviors of surface hydroxyls by isotope exchange reaction with D₂O vapor on the F82H as-received plate and the powders oxidized at 473 K, 673 K, and 1073 K in the air for twelve hours were observed using FT-IR. The results were compared with those of Fe₂O₃, Fe₃O₄, and Cr₂O₃ powders. IR absorption peaks related to O-D stretching vibration was observed in the spectrum of the F82H as-received plate, which means that the surface hydroxyls OH⁻ were replaced with OD⁻ by isotope exchange reaction with D₂O vapor even at room temperature. On the other hand, no O-D vibration peak was observed from the F82H oxidized powders. FT-IR analysis showed that Cr₂O₃ mainly existed on the outermost surface of the F82H as-received plate, and oxidation states other than Fe₂O₃ coexisted with Fe₂O₃ on the oxidized powders, although XRD detected Fe₂O₃ in the both samples. It was indicated that the reactivity between water vapor and surface hydroxyls on F82H surface is strongly affected by the oxidation state of the outermost surface.

References

- [1] K.D. Rendulic., Surface Science. 272 (1992) 34.
- [2] T. Hirabayashi, M. Saeki, Journal of Nuclear Materials. 120 (1984) 309.
- [3] T. Hirabayashi, M. Saeki, E. Tachikawa, Journal of Nuclear Materials. 126 (1984) 38.
- [4] M. Nishikawa, N. Nakashio, T. Shiraishi, S. Odoi, T. Takeishi, K. Kamimae., Journal of Nuclear Materials. 277 (2000) 99.
- [5] T. Hirabayashi, M. Saeki, E. Tachikawa., Journal of Nuclear Materials. 136 (1985) 179.
- [6] R. Ohmori, T. Yoneoka, M. Taniguchi, S. Tanaka., Journal of Nuclear Materials. 258 (1998) 474.
- [7] Y. Oya, K. Kobayashi, W. Shu, T. Hayashi, S. O'hira, H. Nakamura, Y. Iwai, M. Nishi, T. Higashijima, K. Obara, K. Shibanuma, K. Koizumi., Fusion Technology. 39 (2001) 1023.
- [8] T. Higashijima, K. Obara, K. Shibanuma, K. Koizumi, K. Kobayashi, Y. Oya, W. Shu, T. Hayashi, M. Nishi., Fusion Science and Technology. 41 (2002) 731.
- [9] M. Enoeda, M. Akiba, S. Tanaka, A. Shimizu, A. Hasegawa, S. Konishi, A. Kimura, A. Kohyama, A. Sagara, T. Muroga., Fusion Engineering and Design. 81 (2006) 415.
- [10] Y. Yamauchi, Y. Hirohata, T. Hino., Journal of Nuclear Materials. 363 (2007) 984

Table 1 Summary of characteristic IR absorption observed in the powder spectra: (a) the as-received plate; (b) the powder before the oxidation; (c) the powder after the oxidation at 1073 K.

	1000~ 700 cm ⁻¹	1500 cm ⁻¹	1700 cm ⁻¹	2150 cm ⁻¹
F82H (a)	○		○	
F82H (b)	○			
F82H (c)		○		○
Fe ₂ O ₃		○		○
Fe ₃ O ₄	○			
Cr ₂ O ₃			○	

FT-IR analysis on removal of surface hydroxyls from F82H oxidized surface using isotope exchange method

Daisuke Masuyama, Takuji Oda and Satoru Tanaka

Department of Nuclear Engineering and Management: The University of Tokyo

Material contamination due to tritium accumulation in structural materials of nuclear fusion reactors is a problem in repair of equipment or waste management. Hence, it is important to build up decontamination technique of tritium on the surface in the sight of safety. In practice, metal surface is oxidized, and hydrogen isotopes generally exist as hydroxyl. High stability of surface hydroxyl makes decontamination difficult. In order to perform decontamination effectively, therefore, it is necessary to understand the stability and desorption behavior of hydroxyls on the oxidized surface of structural materials. In the present work, we aim to quantify removal rates of hydroxyls from F82H surface by isotope exchange method.

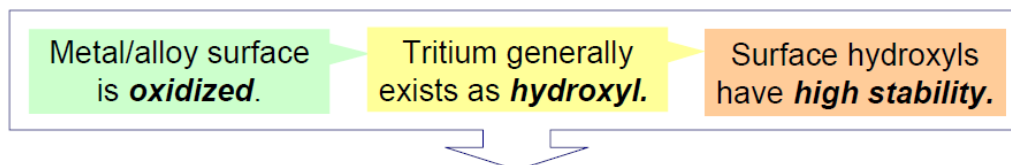
In experiment, deuterium was employed instead of tritium. For comparison, Fe, which is the main component of F82H, was also tested. After oxidation treatment, a specimen (powder of Fe_2O_3 , Fe_3O_4 or F82H) was exposed to deuterium water vapor (D_2O). Hydroxyl (-OD) formed on the surface was detected using Fourier transform infrared spectroscopy (FT-IR) of diffuse reflection method, which is effective for surface analysis. Then, exposure experiment to H_2O gas was performed, and hydroxyl removal rates by isotope exchange were quantified from variation of O-D vibration peaks.

In Fe_2O_3 powder exposed to D_2O atmosphere, five IR absorption peaks (2744 cm^{-1} , 2708 cm^{-1} , 2680 cm^{-1} , 2650 cm^{-1} , 2550 cm^{-1}) were observed in a typical region of O-D stretching vibration modes. This result indicates that hydroxyl has multiple different forms on oxidized surface. Then, with performing exposure experiment to H_2O gas, the intensity of these peaks was decreased corresponding to removal of -OD from the surface. Decreases of three sharp peaks (2708 , 2680 , and 2650 cm^{-1}) were first-order reactions with respect to the concentration of -OD on the surface. On the other hand, decrease of 2550 cm^{-1} peak, which is a peak of hydroxyls interacting with each other by hydrogen bonding, was not fit to first-order kinetics. 2744 cm^{-1} peak almost did not change during H_2O gas exposure experiment, which indicates that this -OD is hardly influenced by isotope exchange reactions. In comparison with results of Fe_3O_4 and F82H, the mechanism of hydroxyl removal from F82H surface by isotope exchange reactions was discussed.

FT-IR analysis on removal of surface hydroxyls from F82H oxidized surface using isotope exchange method

*Department of Nuclear Engineering and Management,
The University of Tokyo*
Daisuke Masuyama, Takuji Oda, Satoru Tanaka

Introduction / Aim of this study

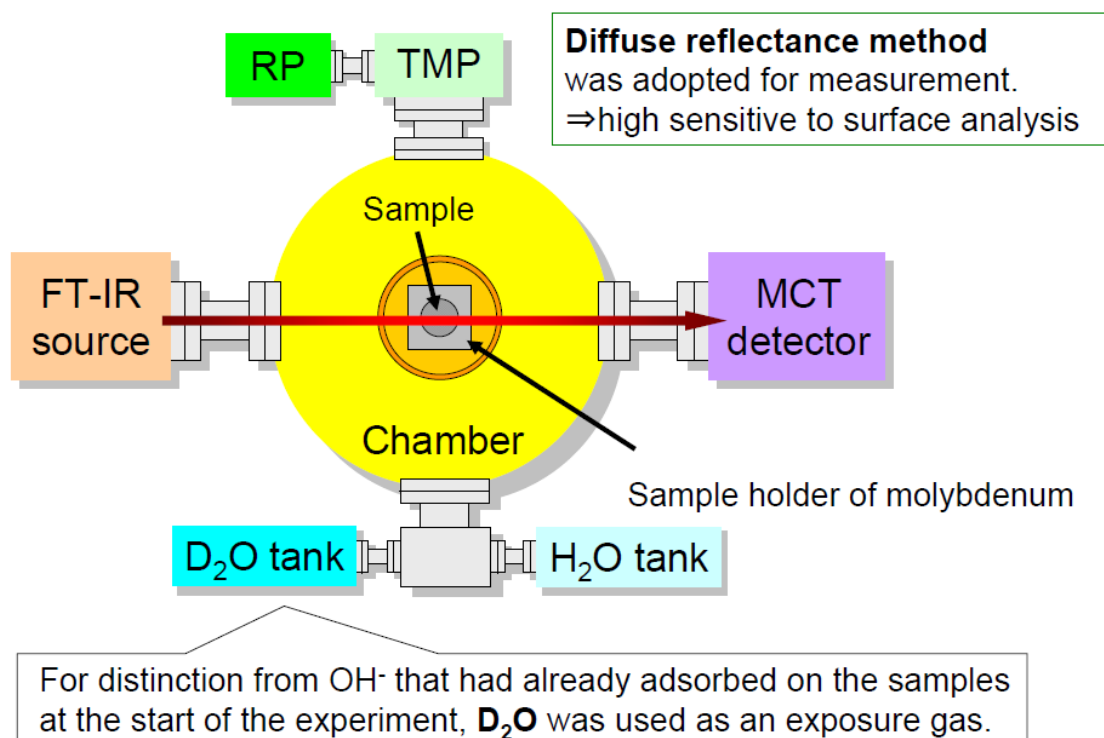


This causes problems in repair of equipment or waste management. It is important to understand **the nature of hydroxyls on material surfaces**.

- The surface hydroxyls existing on metal surfaces have been widely studied. (e.g. steel, aluminum, and copper)
- Nevertheless, no work has reported about the behavior of surface hydroxyls on **low activation ferritic steel F82H**,
 - ※A candidate of the structural material of ITER-TBM in Japan

In the present work, we study the nature of surface hydroxyls on F82H using FT-IR and XRD, especially with focusing on reactions with water vapor.

Experimental system

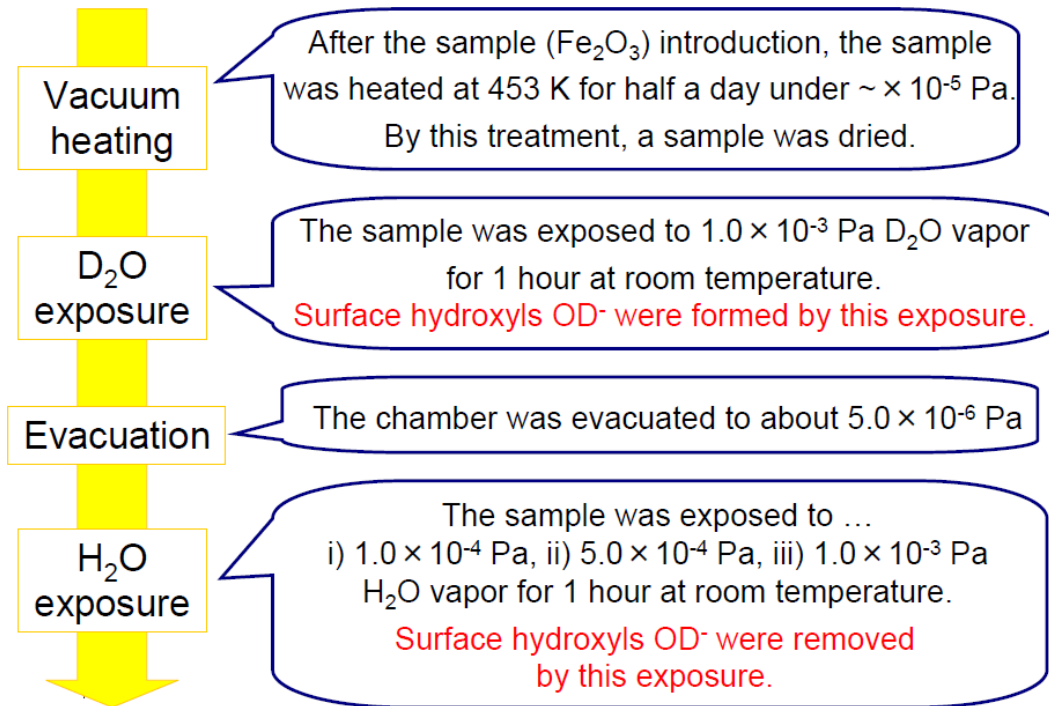


Contents

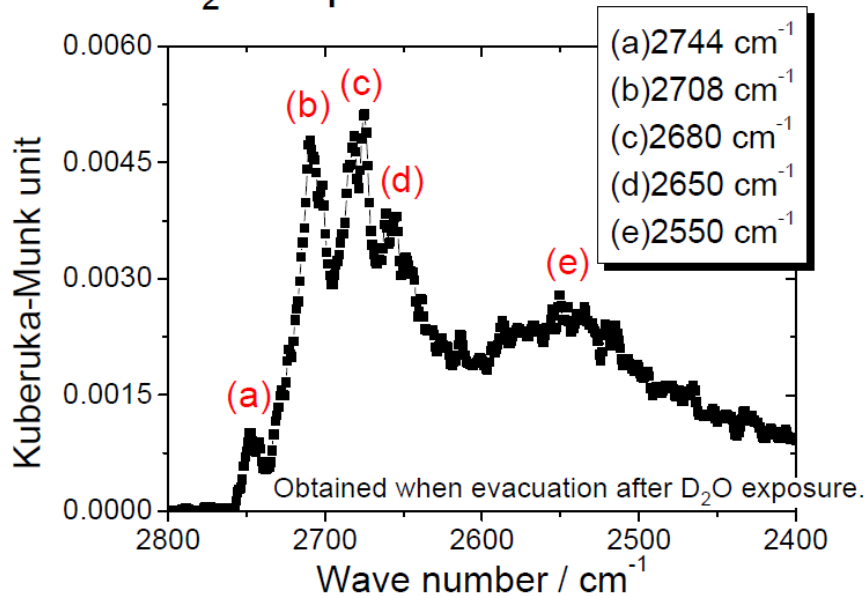
- **Surface hydroxyls on Fe₂O₃** (confirmatory experiment)
 - The removal rates of isotope exchange reaction
 - The apparent activation energy of isotope exchange reaction

- **Surface hydroxyls on F82H**
 - The reactivity with water vapor
 - The surface states of F82H samples

Experimental Procedure



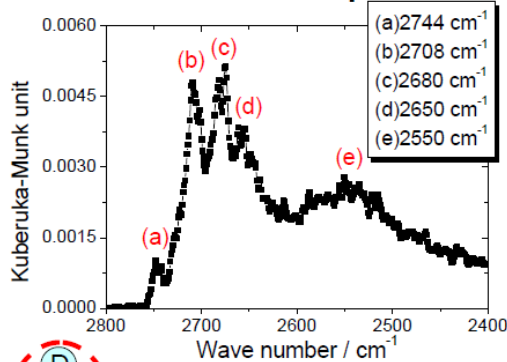
Result of D_2O exposure



Five IR absorption peaks related to O-D stretching vibration were observed.

This indicates that surface hydroxyls have multiple different forms on Fe_2O_3 .

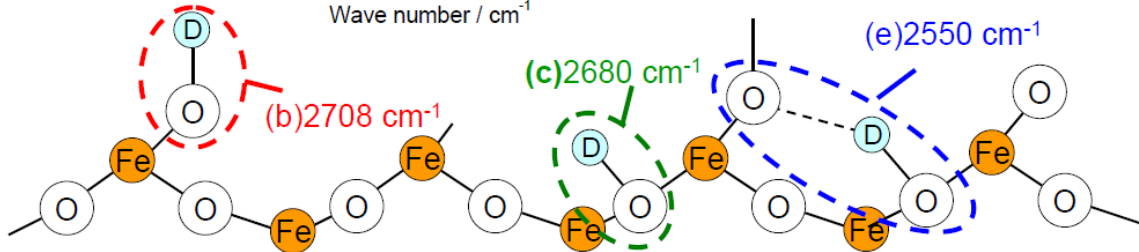
Attribution of O-D peaks



Some of the chemical forms of surface hydroxyls on Fe_2O_3 have been elucidated.

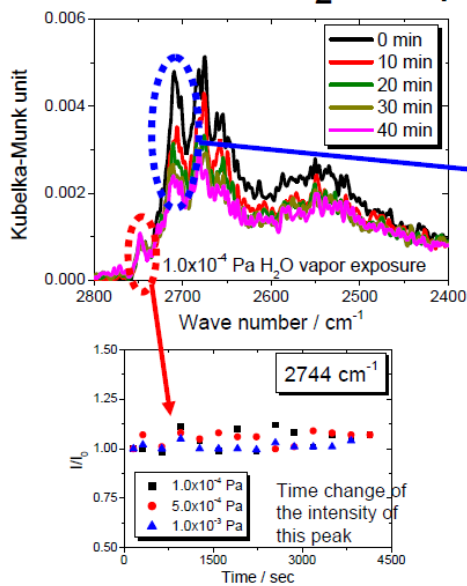
- [1]K.Chiba (2004)
- [2]M.A.Henderson (2000)
- [3]T.Ichikawa (1993)
- [4,5]G.Buska (1980,1983)

(※(a), (d) are unknown.)

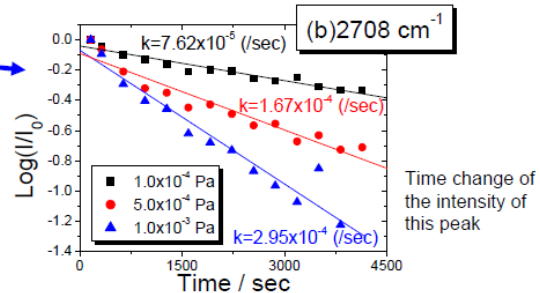


- 2708 cm^{-1} is attributed to the isolated OD^- coordinating to one Fe^{3+} .
- 2680 cm^{-1} is attributed to the isolated OD^- coordinating to two Fe^{3+} .
- 2550 cm^{-1} is attributed to the OD^- interacted with each other by hydrogen bonding.

Results of H_2O exposure



The intensity of O-D vibration peaks decreased with time, which is corresponding to removal of surface OD^- .



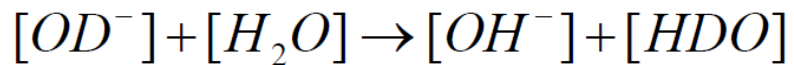
The removal rates increase with H_2O vapor pressure. Decreases of this peak are first-order reactions.

2744 cm^{-1} peak almost did not change during H_2O exposure, which indicates that this OD^- is hardly influenced by isotope exchange reactions.

The desorption behavior of this hydroxyl is discussed.

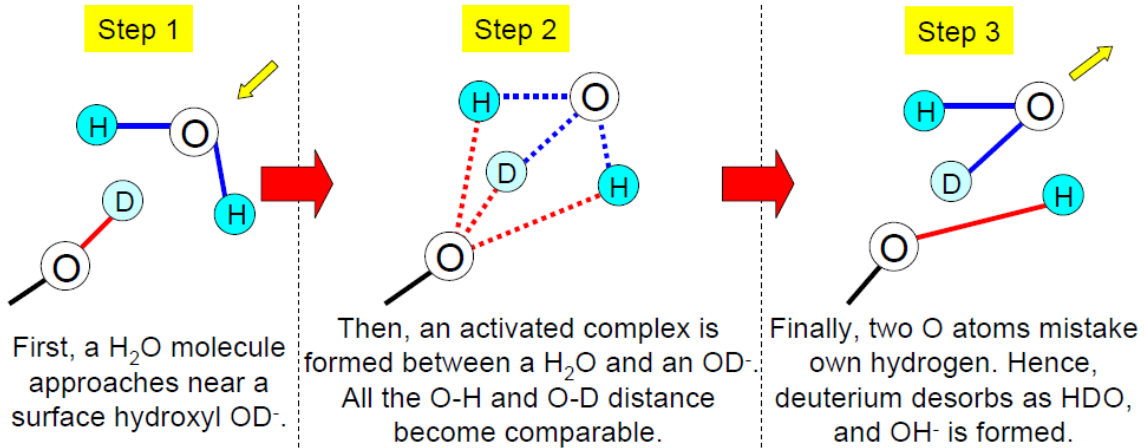
Estimation of desorption reaction model

Reaction formula of this hydroxyl desorption



In the present condition, H₂O pressure was kept constant.

The decrease of 2708 cm⁻¹ is a first-order reaction with respect to [OD⁻].



The apparent activation energy of this reaction is estimated about 24 kJ/mol, which is less than that of recombinative desorption reaction (120 kJ/mol). It is reasonable that OD⁻ was removed mainly by isotope exchange reaction.

Summary of Fe₂O₃

Desorption rate of hydroxyl from Fe₂O₃ surface by isotope exchange method was estimated, and desorption mechanism was suggested.

- ✓Five absorption peaks were observed, which indicates that surface hydroxyls have multiple chemical forms.
- ✓The desorption of surface hydroxyls have the pressure dependency.
- ✓The desorption of hydroxyls of 2708 cm⁻¹ peak is a first-order reaction with respect to [OD⁻], and this is easily removed by isotope exchange reaction.
- ✓Hydroxyls of 2744 cm⁻¹ peak are hardly influenced by isotope exchange reactions.
- ✓The apparent activation energy of isotope exchange reaction is estimated about 24 kJ/mol.

Contents

- **Surface hydroxyls on Fe_2O_3** (pre-experiment)

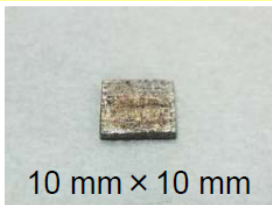
- The removal rates of isotope exchange reaction
- The apparent activation energy of isotope exchange reaction

- **Surface hydroxyls on F82H**

- The reactivity with water vapor
- The surface states of F82H samples

Sample preparation

F82H as-received plate



10 mm × 10 mm

Colored brown.

F82H powder



grain size: 23 μm

The plate and powder were fabricated from a F82H block provided by JAEA.

As oxidation treatment, this powder was heated at 473 K, 673 K, and 1073 K in the air for 12 hours.

The oxides of the main component of F82H alloy were also tested for comparison.

Fe_2O_3 powder



grain size: 0.40 μm

Fe_3O_4 powder



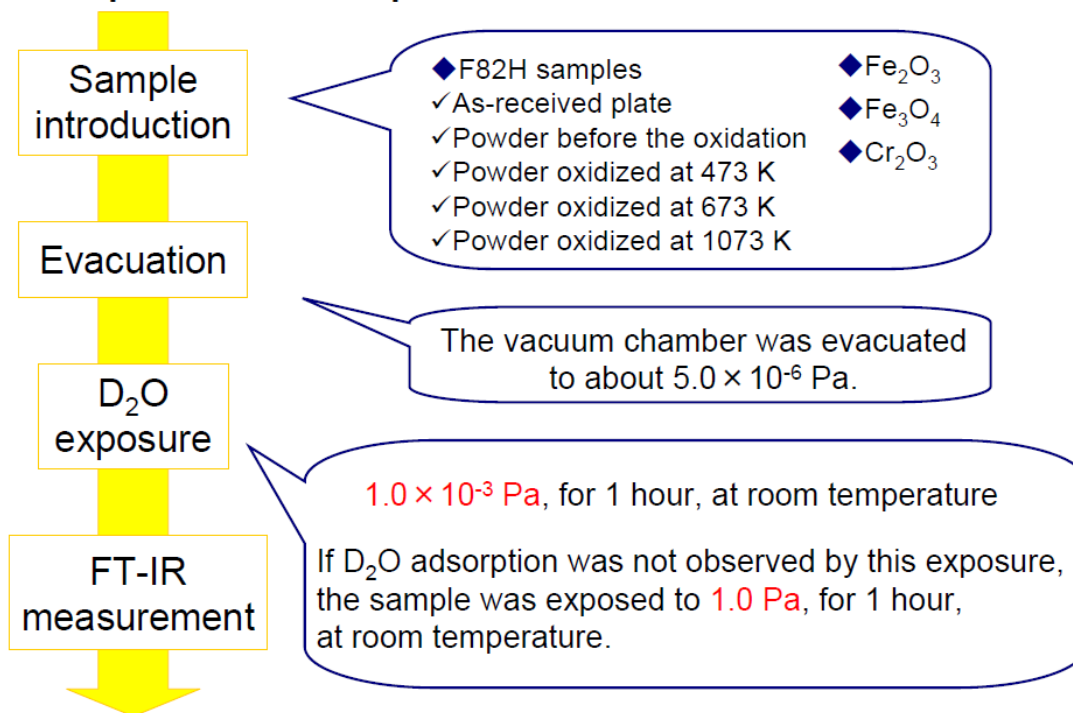
grain size: 2.0 μm

Cr_2O_3 powder



grain size: 3.0 μm

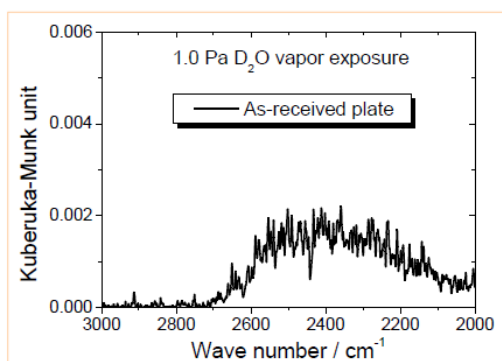
Experimental procedure



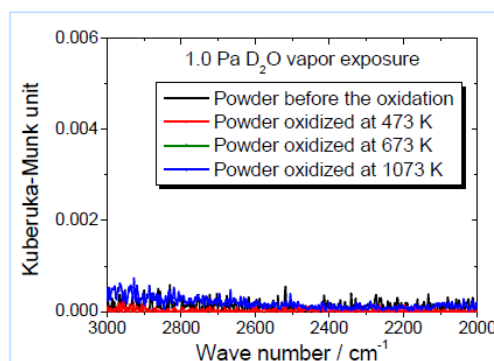
Results of F82H samples

1.0×10^{-3} Pa D_2O exposure

⇒ No absorption peak related to O-D stretching vibration was observed from all the spectra.

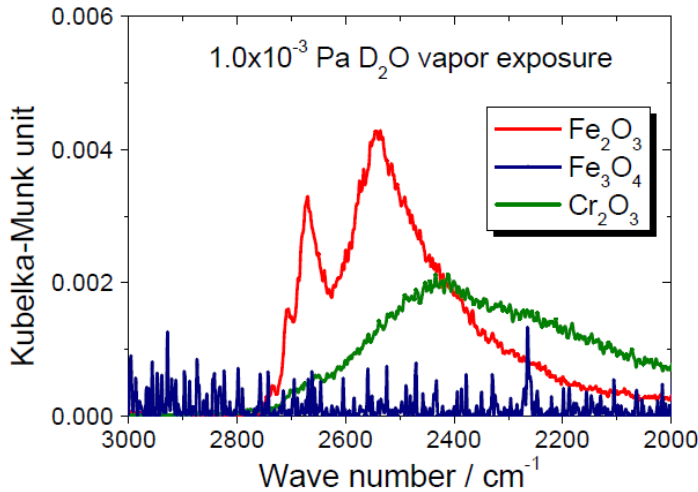


- A broad peak was observed at 2400 cm^{-1} .
- This indicates the formation of surface hydroxyls OD^- .



- In all the powders, no absorption peak was observed even by 1.0 Pa D_2O vapor exposure.

Results of Fe₂O₃, Fe₃O₄, and Cr₂O₃



Fe₂O₃ powder

O-D absorption peaks were observed mainly at **2680 cm⁻¹** and **2550 cm⁻¹**.

Cr₂O₃ powder

A O-D absorption peak was observed mainly at **2420 cm⁻¹**.

Fe₃O₄ powder

No peak was observed even after the further 1.0 Pa D₂O vapor exposure.

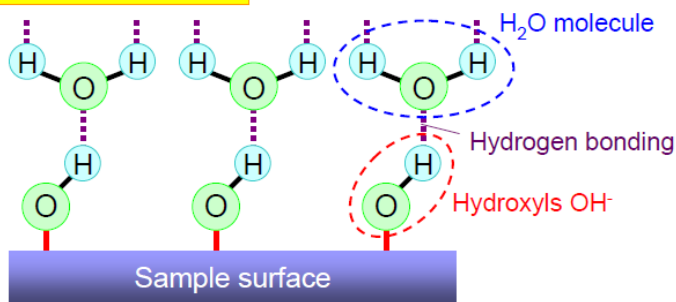
■ Absorption peaks related to O-D stretching vibration were observed in the spectra of the F82H as-received plate, and the Fe₂O₃ and Cr₂O₃ powders.

First, the mechanism of surface hydroxyls OD⁻ formation is considered.

Surface OD⁻ formation 1/2

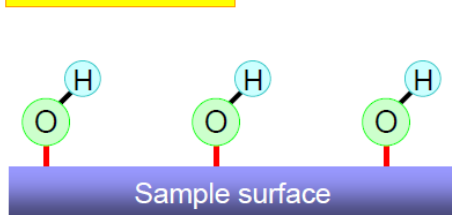
The surface oxidation state before the D₂O vapor exposure is discussed.

Before evacuation



Samples had contact with H₂O vapor contained in air.
 ⇒ It is thought that ...
 ➢ the **surface hydroxyls OH⁻** were formed on the sample surface, and
 ➢ **H₂O molecule** existed on the upper layer by the hydrogen bonding with the surface hydroxyls.

After evacuation



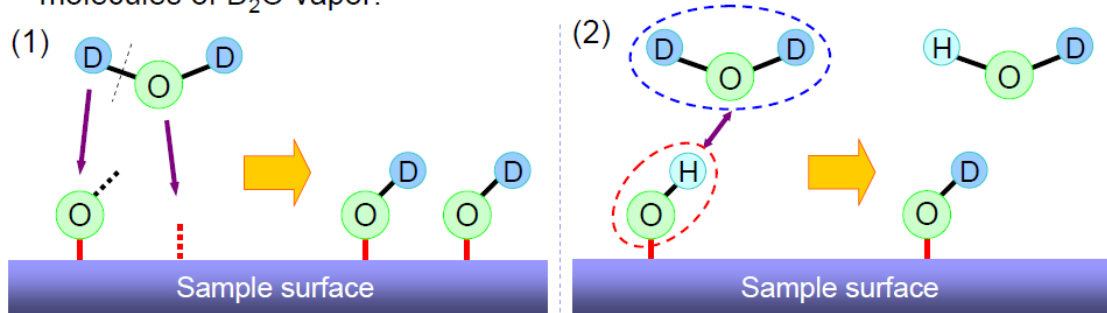
➢ H₂O molecules are removed by evacuation.
 ⇒ The **hydrogen bonding is comparatively weak**.
 ➢ The surface hydroxyls are hardly removed by evacuation at room temperature.
 ⇒ They are **chemisorbed on the surface**.

It is reasonable to consider that the surfaces were **fully covered with surface hydroxyls OH⁻** before the D₂O vapor exposure.

Surface OD⁻ formation 2/2

Formation of surface hydroxyls OD⁻ can be induced by ...

- (1) dissociative adsorption of D₂O molecule on the surface
- (2) isotope exchange reaction between surface hydroxyls OH⁻ and D₂O molecules of D₂O vapor.



➤ In the present experimental condition, sites where dissociative adsorption of D₂O molecules can take place should have been filled with OH⁻ as previously mentioned.

➤ It is suggested that the absorption peaks of the O-D stretching vibration were formed **mainly by the isotope exchange reaction**.

Summary of D₂O vapor exposure experiment

Formation of surface hydroxyls OD⁻ was ...

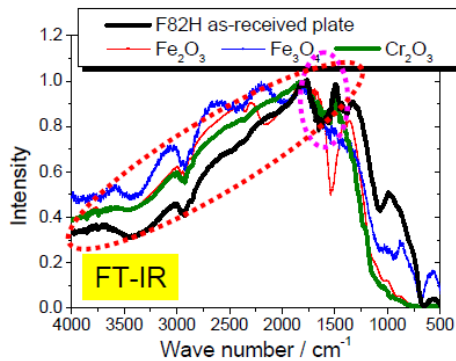
○ observed	× NOT observed
<ul style="list-style-type: none"> ● F82H as-received plate (1.0 Pa) ● Fe₂O₃ powder (1.0 × 10⁻³ Pa) ● Cr₂O₃ powder (1.0 × 10⁻³ Pa) 	<ul style="list-style-type: none"> ● F82H powders (regardless of oxidation condition) ● Fe₃O₄ powder

These results mean that the surface hydroxyls OH⁻ on Fe₂O₃, Cr₂O₃ and the F82H as-received plate were easily replaced by OD⁻ through reaction with D₂O vapor, while not on the others.

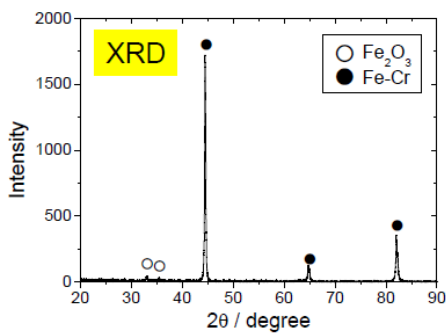
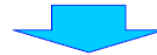


The result of F82H is discussed, together with the surface oxidation state of F82H analyzed by FT-IR and XRD.

About the as-received plate 1/2



- The IR power spectrum of the F82H as-received plate was similar to that of Cr_2O_3 .
- ✓ The peak at 1700 cm^{-1}
- ✓ The shape in the region of wave number higher than 1500 cm^{-1}
- No clear resemblance was observed between the F82H as-received plate and the Fe_2O_3 powder.



Cr_2O_3 mainly existed on the surface of the F82H as-received plate.

- Peaks related to Fe_2O_3 were observed by XRD analysis, while peaks related to Cr_2O_3 were not.
- Fe-Cr peaks were mainly observed.

(Cu $K\alpha$ source was used for the X-ray source)

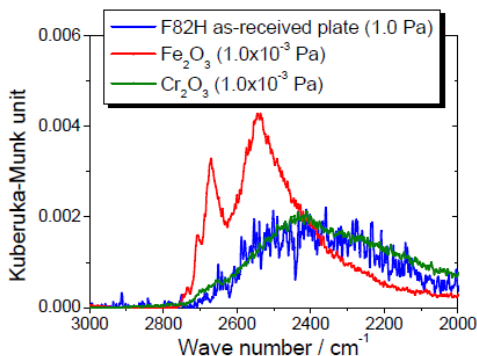
About the as-received plate 2/2

- ✓ FT-IR analysis \Rightarrow Cr_2O_3 mainly existed.
- ✓ XRD analysis \Rightarrow Fe_2O_3 existed. Cr_2O_3 did NOT.

Diffuse reflectance FT-IR should give information about more outer surfaces than XRD.

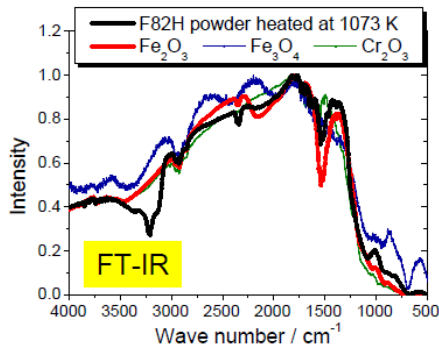


It is considered that ...
 Cr_2O_3 mainly existed on a surface region including the outermost surface, while Fe_2O_3 separated out at a deeper region than Cr_2O_3 .



This consideration is supported by the fact that the shape of O-D stretching vibration peaks in the F82H as-received plate resembled to that in Cr_2O_3 rather than that in Fe_2O_3 .

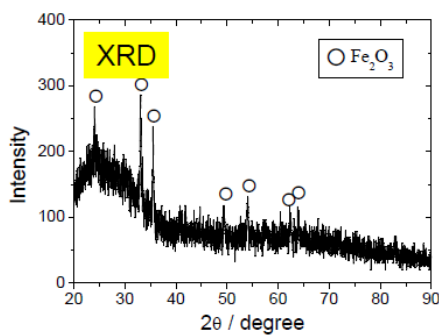
About the powder oxidized at 1073 K 1/2



➤ Negative peaks were observed at 2200 cm^{-1} and 1500 cm^{-1} .
(observed also in the Fe_2O_3 powder)

➤ The overall shape of the spectrum of the F82H powder oxidized at 1073 K was similar to that of the Fe_2O_3 powder.

➤ Only Fe_2O_3 -related peaks were detected by XRD analysis.



These results indicates that Fe_2O_3 was dominant from the outermost surface to the bulk.

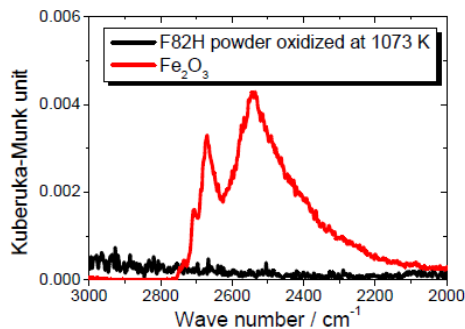
About the powder oxidized at 1073 K 2/2

It should be noted that ...

the peaks related to Fe_2O_3 (2300 cm^{-1} and 1500 cm^{-1}) in the F82H oxidized powder were weaker than that in Fe_2O_3 , although only Fe_2O_3 crystalline peaks were detected in XRD pattern.



These facts imply that ...
there was a region where crystalline Fe_2O_3 are not well formed, probably a surface region including the outermost surface.



This could be the reason why OD⁻ was not detected in the F82H oxidized powder, although existence of Fe_2O_3 were confirmed by XRD and FT-IR.

Summary of the surface states

	XRD analysis	FT-IR analysis (more outer surfaces than XRD)	O-D absorption peak
F82H as-received plate	Fe_2O_3	Cr_2O_3	observed (similar to Cr_2O_3)
F82H powder oxidized at 1073 K	Fe_2O_3	Fe_2O_3 (Crystalline Fe_2O_3 are not well formed.)	NOT observed

From the results, it is indicated that reactivity between water vapor and surface hydroxyls on F82H surface depends on the oxidation state of the outermost surface, which is difficult to evaluate by XRD.

In order to conduct decontamination thoroughly and effectively, careful analysis of the outermost surface is necessary in the future works.

Summary of F82H

The behaviors of surface hydroxyls OH^- on the F82H oxidized surface by isotope exchange reaction with D_2O vapor were observed using FT-IR.

- An O-D absorption peak was observed in the spectrum of the F82H as-received plate, which means that the surface hydroxyls OH^- were replaced with OD^- by isotope exchange reaction with D_2O vapor even at room temperature.
- No O-D peak was observed from the F82H powders before the oxidation, oxidized at 473 K, 673 K, and 1073 K.
- It was indicated that the reactivity between water vapor and surface hydroxyls on F82H surface is affected by the oxidation state of the outermost surface.
- By analyzing the outermost surface of F82H by Raman spectroscopy, the relation between the surface states of F82H and the nature of surface hydroxyls will be studied in the future.